

Air Force Institute of Technology

**AFIT Scholar**

---

Theses and Dissertations

Student Graduate Works

---

12-1997

## Orbit Estimation Using Track Compression and Least Squares Differential Correction

Vincent J. Chioma

Follow this and additional works at: <https://scholar.afit.edu/etd>



Part of the [Astrodynamics Commons](#)

---

### Recommended Citation

Chioma, Vincent J., "Orbit Estimation Using Track Compression and Least Squares Differential Correction" (1997). *Theses and Dissertations*. 5597.

<https://scholar.afit.edu/etd/5597>

This Thesis is brought to you for free and open access by the Student Graduate Works at AFIT Scholar. It has been accepted for inclusion in Theses and Dissertations by an authorized administrator of AFIT Scholar. For more information, please contact [AFIT.ENWL.Repository@us.af.mil](mailto:AFIT.ENWL.Repository@us.af.mil).

AFIT/GA/ENY/97D-1

ORBIT ESTIMATION USING TRACK COMPRESSION AND  
LEAST SQUARES DIFFERENTIAL CORRECTION

THESIS

Vincent J. Chioma, Captain, USAF

AFIT/GA/ENY/97D-1

**DTIC QUALITY INSPECTED 3**

Approved for public release; distribution unlimited

19980127 022

The views expressed in this thesis are those of the author and do not reflect the official policy or position of the Department of Defense or the U.S. Government.

**ORBIT ESTIMATION USING TRACK COMPRESSION AND  
LEAST SQUARES DIFFERENTIAL CORRECTION**

**THESIS**

**Presented to the Faculty of the Graduate School of Engineering  
of the Air Force Institute of Technology  
Air University  
Air Education and Training Command  
In Partial Fulfillment of the Requirements for the  
Degree of Master of Science in Astronautical Engineering**

**Vincent J. Chioma, Captain, USAF**

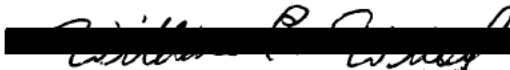
**December 1997**

**Approved for public release; distribution unlimited**

ORBIT ESTIMATION USING TRACK COMPRESSION AND  
LEAST SQUARES DIFFERENTIAL CORRECTION

Vincent J. Chioma  
Captain, USAF

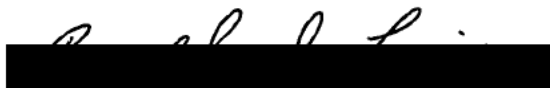
Approved:

  
William E. Wiesel, Jr.

20 NOV 97  
date

  
Sharon A. Heise

20 NOV 97  
date

  
Bradley S. Liebst

20 NOV 97  
date

## *Acknowledgments*

I would like to express my sincere appreciation to my thesis advisor, Dr. William Wiesel, for his guidance and many hours of assistance. His boundless knowledge of and insight into orbital mechanics has assisted a long line of Air Force officers through the astronautical engineering program at AFIT. I am humbled to see my name among those of his former students -- among the most significant contributors to the field of astronautical engineering in the Air Force.

I owe a debt of gratitude to Dr. Shankar Mall for allowing me the opportunity to pursue a graduate degree at AFIT, to my fellow classmates who helped make this an enjoyable experience, and to the readers for their valuable comments.

Most importantly, I would like to thank my wife, Kristin, (the hardest working officer in the Air Force) and my son, Alex. Without your love, patience, understanding and many sacrifices, this would not have been possible.

Vincent J. Chioma

## *Table of Contents*

	Page
Approval .....	ii
Acknowledgments .....	iii
Table of Contents .....	iv
List of Figures .....	ix
List of Tables .....	xii
Abstract .....	xiv
1. Introduction .....	1-1
1.1 Background .....	1-1
1.2 Problem Statement .....	1-1
1.3 Method of Solution .....	1-2
1.4 Thesis Description .....	1-3
2. Theoretical Background .....	2-1
2.1 Introduction .....	2-1
2.2 Orbit Determination .....	2-1
2.3 Probability .....	2-2
2.4 Central Limit Theorem .....	2-5
2.5 Least Squares .....	2-6
2.5.1 One-Dimensional Least Squares .....	2-6
2.5.2 Multi-Dimensional, Linear Least Squares .....	2-7
2.5.3 Non-Linear Least Squares .....	2-9
2.5.4 Computer Implementation .....	2-11
2.6 Sequential Estimation .....	2-11
2.7 Summary .....	2-13

	Page
3. Taylor Series Track Compression.....	3-1
3.1 Introduction.....	3-1
3.1.1 Notation .....	3-1
3.1.2 Units .....	3-1
3.2 Truth Model .....	3-2
3.2.1 State Vector .....	3-2
3.2.2 Equations of Motion .....	3-2
3.2.3 Reference Frames .....	3-4
3.2.4 Observation Data.....	3-4
3.2.4.1 Radar Locations .....	3-5
3.2.4.2 Radar Capabilities .....	3-5
3.2.4.3 ECR Site Vector Calculation .....	3-6
3.2.4.4 Observation Geometry.....	3-7
3.2.5 Noise .....	3-8
3.3 General Description of Track Compression .....	3-10
3.4 Detailed Taylor Series Track Compression Development .....	3-12
3.4.1 Initial Reference State .....	3-12
3.4.2 Dynamics Model .....	3-13
3.4.2.1 Order of Terms .....	3-14
3.4.2.2 Reference Trajectory .....	3-15
3.4.2.3 State Transition Matrix.....	3-17
3.4.3 Observation Relation .....	3-17
3.4.3.1 Determining the RhoIJK Vector .....	3-18
3.4.3.2 Determining the RhoSEZ Vector.....	3-19
3.4.3.3 Final Observation Relation Determination .....	3-19



	Page
3.4.4 Observation Matrix.....	3-20
3.4.5 Instrument Covariance Matrix .....	3-21
3.4.6 Convergence Criteria .....	3-21
3.4.7 Summary.....	3-22
3.5 Results .....	3-22
3.6 Summary .....	3-29
4. Integrator Track Compression.....	4-1
4.1 Introduction.....	4-1
4.2 Detailed Integrator Track Compression Development .....	4-1
4.2.1 Comparison .....	4-1
4.2.2 Initial Reference State .....	4-1
4.2.3 Dynamics Model .....	4-2
4.2.3.1 Reference Trajectory .....	4-2
4.2.3.2 State Transition Matrix.....	4-2
4.2.4 Taylor Series Similarities.....	4-3
4.2.5 Summary.....	4-3
4.3 Results .....	4-3
4.4 Summary .....	4-9
5. Global Estimate .....	5-1
5.1 Introduction.....	5-1
5.2 Detailed Global Estimate Development.....	5-2
5.2.1 Truth Model.....	5-2
5.2.1.1 State Vector.....	5-2
5.2.1.2 Equations of Motion.....	5-2
5.2.1.3 Observation Data .....	5-4

	Page
5.2.2 Initial Reference State .....	5-4
5.2.3 Dynamics Model .....	5-4
5.2.4 Observation Relation .....	5-5
5.2.5 Observation Matrix.....	5-5
5.2.6 Instrument Covariance Matrix .....	5-5
5.2.7 Convergence Criteria .....	5-6
5.2.8 Summary.....	5-6
5.3 Results .....	5-6
5.4 Summary .....	5-11
6. Simulation.....	6-1
6.1 Introduction.....	6-1
6.2 Phase One .....	6-2
6.2.1 Orbits Modeled .....	6-2
6.2.2 Propagation .....	6-6
6.2.3 Track Compression.....	6-7
6.2.4 Global Estimate.....	6-7
6.2.5 Bayes Filter.....	6-7
6.2.6 Update Satellite.....	6-7
6.2.7 Truth Catalog Comparison .....	6-8
6.2.8 Prioritize.....	6-8
6.2.9 Output.....	6-8
6.2.10 Simulation Robustness.....	6-8
6.3 Phase One Results .....	6-9
6.4 Phase Two.....	6-15
6.5 Phase Two Results.....	6-16

	Page
6.6 Phase Three.....	6-21
6.7 Phase Three Results.....	6-23
6.8 Summary .....	6-30
7. Conclusions and Recommendations.....	7-1
7.1 Summary .....	7-1
7.2 Conclusions.....	7-1
7.3 Recommendations .....	7-2
Appendix A Atmospheric Model .....	A-1
Appendix B Geopotential and the Equations of Motion .....	B-1
Appendix C Taylor Series Track Compression State Transition Matrix .....	C-1
Appendix D Track Compression <b>H</b> Matrix .....	D-1
Appendix E Integrator Track Compression Equations of Variation .....	E-1
Appendix F Global Estimate Equations of Variation.....	F-1
Appendix G Orbital Elements.....	G-1
Appendix H Bibliography Cross Reference .....	H-1
Bibliography .....	BIB-1
Vita.....	I-1

## *List of Figures*

Figure	Page
2-1 Density Distribution Number One .....	2-3
2-2 Density Distribution Number Two .....	2-4
2-3 Density Distribution Number Three .....	2-4
3-1 Radar Sites of the SSN .....	3-5
3-2 Geodetic and Geocentric Latitudes .....	3-6
3-3 Observation Geometry .....	3-8
3-4 Gaussian Random Number Distribution .....	3-9
3-5 Random Range Noise .....	3-9
3-6 Random Azimuth Noise .....	3-10
3-7 Random Elevation Noise .....	3-10
3-8 Contribution of Taylor Series Terms .....	3-14
3-9 First Pass Range Residuals .....	3-23
3-10 First Pass Azimuth Residuals .....	3-24
3-11 First Pass Elevation Residuals .....	3-24
3-12 Last Pass Range Residuals .....	3-25
3-13 Last Pass Azimuth Residuals .....	3-25
3-14 Last Pass Elevation Residuals .....	3-26
4-1 First Pass Range Residuals .....	4-4
4-2 First Pass Azimuth Residuals .....	4-5
4-3 First Pass Elevation Residuals .....	4-5
4-4 Last Pass Range Residuals .....	4-6
4-5 Last Pass Azimuth Residuals .....	4-6

	Page
4-6 Last Pass Elevation Residuals .....	4-7
6-1 Semi-Major Axis .....	6-3
6-2 Radius of Apogee .....	6-4
6-3 Radius of Perigee .....	6-4
6-4 Eccentricity .....	6-4
6-5 Inclination .....	6-5
6-6 Longitude of Ascending Node .....	6-5
6-7 Argument of Perigee .....	6-5
6-8 True Anomaly .....	6-6
6-9 Ballistic Coefficient .....	6-6
6-10 Simulation One Results .....	6-10
6-11 Altitude of Perigee – Simulation Two .....	6-11
6-12 Ballistic Coefficient – Simulation Two .....	6-11
6-13 Simulation Two Results .....	6-12
6-14 Altitude of Perigee – Simulation Three .....	6-13
6-15 Simulation Three Results .....	6-13
6-16 Simulation Four Results .....	6-14
6-17 Altitude of Perigee – Simulation Five .....	6-14
6-18 Simulation Five Results .....	6-15
6-19 Simulation Six Results .....	6-16
6-20 Simulation Seven Results .....	6-17
6-21 Simulation Eight Results .....	6-17
6-22 Simulation Nine Results .....	6-18
6-23 In-Track Error Components .....	6-19
6-24 Radial Error Components .....	6-19

	Page
6-25 Out-of-Plane Error Components .....	6-20
6-26 Simulation Ten Results. ....	6-20
6-27 Phase Three Altitude Distribution .....	6-23
6-28 Simulation Eleven Results .....	6-24
6-29 Individual Satellite Estimation Errors .....	6-25
6-30 Low-Altitude Satellite Errors. ....	6-26
6-31 Simulation Twelve Results. ....	6-27
6-32 Simulation Twelve Error Trends. ....	6-27
6-33 Simulation Thirteen Results. ....	6-28
6-34 Atmospheric Density Variations. ....	6-29
6-35 Simulation Fourteen Results .....	6-30

## *List of Tables*

Table	Page
3-1 Notation .....	3-1
3-2 Radar Sites of the SSN .....	3-5
3-3 Orbit Number One .....	3-22
3-4 Orbit One Track Compression Results .....	3-26
3-5 Orbit Number Two .....	3-27
3-6 Orbit Two Track Compression Results .....	3-27
3-7 Orbit Number Three .....	3-28
3-8 Orbit Three Track Compression Results .....	3-28
3-9 Orbit Number Four .....	3-29
3-10 Orbit Four Track Compression Results .....	3-29
4-1 Orbit Number One .....	4-4
4-2 Orbit One Track Compression Results .....	4-7
4-3 Orbit Number Two .....	4-8
4-4 Orbit Two Track Compression Results .....	4-8
4-5 Orbit Number Three .....	4-8
4-6 Orbit Three Track Compression Results .....	4-8
4-7 Orbit Number Four .....	4-9
4-8 Orbit Four Track Compression Results .....	4-9
5-1 Orbit Number One .....	5-7
5-2 Orbit One State Vectors .....	5-7
5-3 Orbit One Covariance Statistics .....	5-8
5-4 Orbit Number Two .....	5-8
5-5 Orbit Two State Vectors .....	5-8

	Page
5-6 Orbit Two Covariance Statistics .....	5-9
5-7 Orbit Number Three .....	5-9
5-8 Orbit Three State Vectors .....	5-9
5-9 Orbit Three Covariance Statistics .....	5-10
5-10 Orbit Number Four .....	5-10
5-11 Orbit Four State Vectors .....	5-10
5-12 Orbit Four Covariance Statistics .....	5-11
A-1 Atmospheric Constants .....	A-2
A-2 1976 Standard Atmosphere .....	A-2
A-3 1962 Standard Atmosphere .....	A-3
B-1 Coefficients of Gravitational Harmonics .....	B-2
G-1 Orbital Elements .....	G-1
H-1 Bibliography Cross Reference .....	H-1



## *Abstract*

This thesis develops two methods of compressing a track of radar observations of a satellite into a single state vector and associated covariance matrix, and a method of estimating orbits using results from multiple tracks. The track compression uses least squares differential correction to determine a state vector at the central observation time. One method uses a Taylor series expansion in time, modeling first and second order two-body effects and first order  $J_2$  zonal harmonic effects to represent the system dynamics. The second method uses numerical integration of the equations of motion using two-body and  $J_2$  effects to represent the system dynamics.

The resulting state vectors and covariance matrices are then used to estimate the satellite's orbit, also using least squares differential correction. Numerical integration using two-body,  $J_2$  and an atmospheric drag model is used to represent the dynamics. This orbit estimation produces a state vector which includes the ballistic coefficient, as well as an associated covariance matrix.

Finally, a one-fiftieth scale demonstration of the full AFSPC catalog of satellites and debris is conducted to demonstrate the improvement in accuracy over current practice which results. The truth model includes  $J_2$  zonal harmonic effects and an atmospheric drag model. This demonstration shows that the orbits of 90% of the entire catalog of objects can be estimated with sufficient accuracy to allow position determination within one kilometer after only two days of tracking. Within four days, most satellite positions are determined within fifty meters.

This improvement in catalog accuracy would result in a reduced routine radar tracking workload, fewer collision-avoidance maneuvers for manned space flights, more accurate over-flight predictions, faster acquisition for ground-based observation or targeting of satellites and smaller rendezvous fuel budgets, to name just a few advantages.

# ORBIT ESTIMATION USING TRACK COMPRESSION AND LEAST SQUARES DIFFERENTIAL CORRECTION

## *1. Introduction*

### *1.1 Background [4]*

Air Force Space Command (AFSPC) is tasked with the mission of tracking all satellites and debris in orbit about the Earth. This mission is executed by the Space Control Center (SCC), located in Cheyenne Mountain, which operates the Space Surveillance Network (SSN). The SSN is a world-wide network of radar sites and optical tracking cameras which track satellites as they pass overhead. (Throughout this thesis, the term *satellite* is used in its broader sense, to denote any object orbiting the Earth, whether debris or functioning equipment.) The sites then send their information to the SCC where it is centrally-processed using least squares algorithms to estimate the satellites' orbits.

The radar sites of the SSN have the capability of producing 50 to 100 observations of a satellite per second. Thus a single track of data, from rise to set, can consist of over 100,000 observations – for a single pass of a single satellite over a single site. When this is factored by the number of objects in the catalog, and the number of sites in the SSN, the enormous amount of data required for this mission becomes evident.

### *1.2 Problem Statement*

Currently, the SCC does not possess the computing resources to process all of this data. Current practice consists of the radar sites reducing the size of their observation tracks by throwing away all but three observations. These three observations, one near the beginning of the track, one at the middle, and one near the end, are then sent to the SCC for processing. This reduced workload allows the SCC to keep

up with the incoming data at the expense of estimating orbits with far less accuracy than was available from the original track of data.

Numerous benefits would result from a more accurate method of orbit estimation. Also, as radar capabilities improve and space access eases, the SCC workload will undoubtedly increase. For both of these reasons, a method of orbit estimation which allows for some distributed data processing (at the sites) and an increase in catalog accuracy is desirable.

### *1.3 Method of Solution*

The purpose of this thesis is to develop a means of compressing the data in a track of observations while retaining the majority of accuracy available in the track. Specifically, least squares differential correction is used to determine a state vector and associated covariance matrix which very efficiently describes all of the data in the original track. This technique is applied using two dynamics models for comparison. One model uses a Taylor series expansion of the position vector which allows direct calculation of the position and state transition matrix at each observation time. This expansion includes first and second order two-body acceleration as well as first order  $J_2$  zonal harmonic acceleration. The second model uses numerical integration of the equations of motion (EOMs) and the equations of variation accounting for two-body and  $J_2$  accelerations.

To demonstrate the accuracy retained from this procedure, the scope of the thesis was extended to include orbit estimation using state vectors and covariance matrices from multiple tracks of data, simulating the combination of inputs from multiple sites of the SSN. This estimation was again accomplished using least squares differential correction. The dynamics model consisted of numerical integration of the EOMs. This time, the EOMs included acceleration due to air drag using an atmospheric density model. The state vector determined included a ballistic coefficient, and is thus termed orbit estimation. The associated covariance matrix was calculated as an indication of the accuracy of the estimate.

In order to show the applicability of this technique to the mission of tracking an entire catalog of thousands of objects, the scope of the thesis was again broadened to include a one-fiftieth scale simulation of the tracking and orbit estimation of the entire catalog. The justification for this scale will be discussed in the sixth chapter, Simulation. This simulation included the satellite scheduling, observation, track compression, orbit estimation and catalog maintenance required for the SCC mission as well as the propagation of the truth model needed to generate the raw data used as input observations.

#### *1.4 Thesis Description*

This thesis is divided into seven chapters. The first chapter gives the background, problem description and solution. The second discusses the relevant literature and the theoretical background. The third chapter details the solution methodology and results of the Taylor series method of track compression portion of the thesis. Chapter four details the solution methodology and results of the integrator method of track compression. Chapter five does the same for the *Global Estimate* effort. Chapter six does the same for the three phases of the simulation. Finally, chapter seven concludes with recommendations. To allow for continuity of the report, several detailed derivations are removed from the chapters and presented as appendices.

## *II. Theoretical Background*

### *2.1 Introduction*

This chapter is intended to provide the reader with the background in the area of batch and sequential non-linear least squares orbit determination necessary for a thorough understanding of the remainder of the thesis. The chapter begins with a brief history of orbit determination and progresses through the development of the method of least squares. The chapter concludes with a description of modifications to the method of least squares required for sequential estimation.

### *2.2 Orbit Determination*

The science of determining the orbit of an object using observations began in 1609 with Johannes Kepler. He determined planetary orbits using observations made by the Danish astronomer Tycho Brahe. Kepler determined the orbits of the known planets while formulating his three laws of planetary motion. However, it was not until Isaac Newton published *The Mathematical Principles of Natural Philosophy* (the Principia) in 1687 that the forces behind Kepler's three laws were explained. This began a deterministic age in which the motion of moons, planets, and comets could be predicted. These predictions were based on orbits determined using observation data consisting of angular measurements in the sky. Boulet and Herget describe three methods of orbit determination using angles-only data developed by Laplace, Gauss and Olbers. [2, 8] Escobal describes an additional angles-only method and five methods using two position vectors as well as several mixed data techniques. [5] Depending on the assumptions made as to the type of orbit involved, these methods require up to six independent pieces of information, corresponding to the six constants of integration obtained from the combination of Newton's laws of acceleration and universal gravitation.

If these independent pieces of information, or data, were perfectly accurate, and the dynamics were perfectly known, no new observations would be required. However, in some cases, there are forces acting on an orbiting body, such as air drag, which cannot be exactly predicted. In all cases, observational

data contain errors. Thus, there is always a need for more than the minimum set of observations. It is the optimal combination of these imperfect observations which launched Karl Frederick Gauss into the history books.

In 1801, Gauss developed the method of least squares while attempting to determine the orbit of the first minor planet to be discovered, Ceres. [5, 13, 20] He later perfected this method and published it in 1809. This method forms the basis for modern estimation theory. It assumes that all observations contain regular or constant errors and irregular errors. Gauss states, "it is up to the observer to ferret out all sources of constant error and remove them." [6: 5] "Irregular errors are essentially different...we have to put up with them in the observations themselves; however, we should reduce their effects on derived quantities as far as possible by using judicious combinations of the observations." [6: 5] The selection of this judicious combination is rooted in the fundamentals of probability, the topic of the next section.

### 2.3 Probability [6, 17]

Gauss described a continuous density probability function as a means of explaining observational errors. The probability of a particular instrument producing an error between  $x_1$  and  $x_2$  on a particular observation is obtained by integrating the instrument's continuous density probability function,  $f(e)$ , over the range of  $x_1$  to  $x_2$ .

$$P(x_1 < e < x_2) = \int_{x_1}^{x_2} f(e) de \quad (2.1)$$

A continuous density probability function is normalized.

$$P(-\infty < e < \infty) = \int_{-\infty}^{\infty} f(e) de = 1 \quad (2.2)$$

Gauss described three such density functions which will be repeated here. The first function has  $-a$  and  $+a$  as the limits of all possible errors, with all errors between these limits being equally probable. In this case,  $f(e)$  would be described as

$$f(e) = \begin{cases} 0 & e < -a \\ \frac{1}{2a} & -a \leq e \leq a \\ 0 & a < e \end{cases} \quad (2.3)$$

This density function is shown in Figure 2-1.

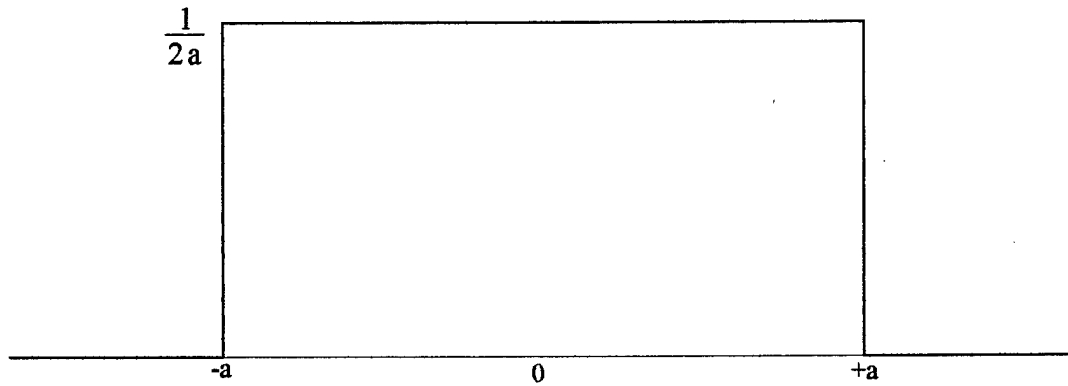


Figure 2-1 Density Distribution Number One

In this case, the mean error, standard deviation and variance are given below.

$$\bar{x} = 0 \quad \sigma = a \sqrt{\frac{1}{3}} \quad \sigma^2 = \frac{a^2}{3}$$

Gauss's second density function is described as

$$f(e) = \begin{cases} 0 & e < -a \\ \frac{a+x}{aa} & -a \leq e \leq 0 \\ \frac{a-x}{aa} & 0 < e \leq +a \\ 0 & a < e \end{cases} \quad (2.4)$$

This density function is shown in Figure 2-2.

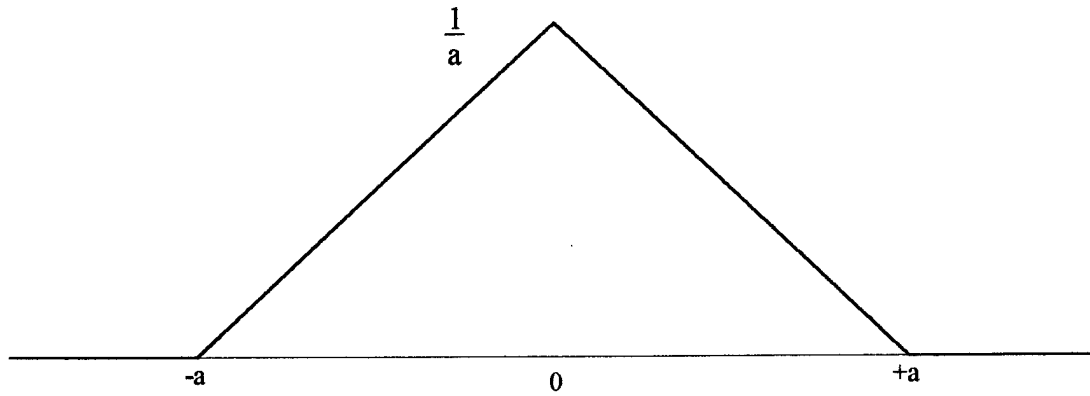


Figure 2-2 Density Distribution Number Two

In this case, the mean error, standard deviation and variance are given below.

$$\bar{x} = 0 \qquad \sigma = a \sqrt{\frac{1}{6}} \qquad \sigma^2 = \frac{a^2}{6}$$

Gauss's third density function is described as

$$f(e) = \frac{\exp\left(\frac{-e^2}{h^2}\right)}{h\sqrt{\pi}} \qquad (2.5)$$

This density function is shown in Figure 2-3.

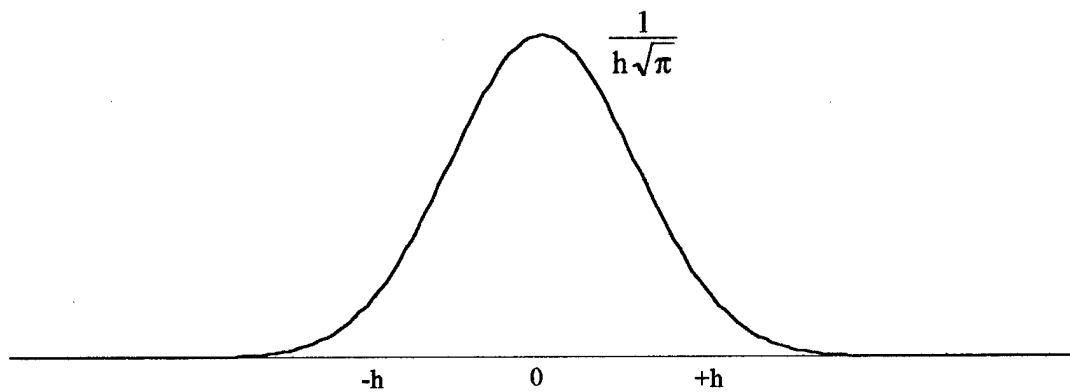


Figure 2-3 Density Distribution Number Three

In this case, the mean error, standard deviation and variance are given as



$$\bar{x} = 0 \qquad \sigma = h \sqrt{\frac{1}{2}} \qquad \sigma^2 = \frac{h^2}{2}$$

Substituting  $h = \sigma\sqrt{2}$  into equation ( 2.5 ) returns the more familiar form of the Gaussian or normal distribution.

$$f(e) = \frac{1}{\sqrt{2\pi}\sigma} \exp\left(\frac{-e^2}{2\sigma^2}\right) \qquad (2.6)$$

#### 2.4 Central Limit Theorem

Equation ( 2.6 ) is remarkable for its frequent occurrence in nature. One of the primary reasons for this is described by the Central Limit Theorem. The Central Limit Theorem is stated as follows.

If random samples of  $n$  observations are drawn from a population with finite mean,  $\mu$ , and standard deviation,  $\sigma$ , then, when  $n$  is large, the sample mean will be approximately normally distributed with mean equal to  $\mu$  and standard deviation  $\sigma / \sqrt{n}$ . The approximation will become more and more accurate as  $n$  becomes large. [12: 153]

The Central Limit Theorem has many applications to the field of estimation theory. One of these is the error probability density function for an instrument. If the instrument is well designed, no single source of error will dominate the results. Instead, the irregular errors which Gauss described will result from the summation of many small errors, none of which dominate. The Central Limit Theorem states why such instruments exhibit errors which follow a normal distribution. This is quite significant because we will not, in general, know the density functions of the individual sources of errors. The Central Limit Theorem states that the resulting combination will be normal regardless of the shape of the contributing error density functions. The only requirement is that the individual distributions each contribute an infinitesimal standard deviation, and that many different sources are combined.

The Central Limit Theorem allowed Gauss to develop the method of least squares by enabling him to mathematically describe the shape of the error curves without actually knowing all of the sources. Thus, it is a cornerstone for this thesis. A second area of this thesis where the Central Limit Theorem is used comes in the random number generator used to add noise to the observational data. A random

number generator which produces random numbers with a distribution similar to Figure 2-1 is called multiple times, and the results are summed. By the Central Limit Theorem, this results in the generation of random numbers with a distribution approximating a normal distribution, as do the real-world observations.

## 2.5 Least Squares

The Central Limit Theorem and equation ( 2.6 ), the normal distribution (also known as the Gaussian distribution), are both fundamental to Gauss's method of least squares. To understand the development of Gauss's method, we must first describe the problem that was at hand. The minor planet Ceres had been discovered and then lost. There were more than enough observations before it was lost to provide the six pieces of information necessary for orbit determination. Astronomers attempted to reacquire the object by fitting orbits to the observational data, but this data was not of sufficient accuracy. Gauss theorized that the best orbit to be calculated would not necessary agree precisely with any one piece of data, but would instead disagree as little as possible with all of the data. To calculate this orbit, Gauss developed the method of least squares in its multi-dimensional, non-linear form. Here, we will develop it in a single dimensional form, expand it to its multi-dimensional, linear form and finally to its full non-linear form.

**2.5.1 One-Dimensional Least Squares.** If  $n$  independent observations of a single quantity,  $x$ , are taken (call this data  $z_1, z_2, \dots z_n$ ) with instruments with standard deviations of  $\sigma_1, \sigma_2, \dots \sigma_n$ , these will form a set of errors of  $e_1, e_2, \dots e_n$  where  $e_i = x - z_i$ . We can determine the joint probability of having obtained this particular set of data which we will call  $f(z)$ , as

$$f(z) = \prod_i \left( \frac{1}{\sqrt{2\pi} \sigma_i} \exp \left( \frac{-(x - z_i)^2}{2 \sigma_i^2} \right) \right) \quad (2.7)$$

where we could solve for this probability if we knew the actual value of  $x$ . But this value is unknown. This is where Gauss applies the fundamental Principle of Maximum Likelihood. Instead of knowing the true value of  $x$ , and using equation ( 2.7 ) to determine the probability of having gotten this set of data,

Gauss assumes that, because we have already gotten this set, the true value of  $x$  must be that value which maximizes the probability of having gotten that set. Thus, a value of  $x$  is determined which drives equation ( 2.7 ) to a maximum. This occurs when the terms inside the exponentials are driven to a maximum. At a glance, one can tell this equates to finding the value of  $x$  which is closest to all of the  $z_i$  with the errors being squared, thus the description, the method of least squares. The problem has thus become one of finding a value for  $x$  (we will call this value  $\bar{x}$  ) which minimizes the following sum

$$\sum_i \frac{(x - z_i)^2}{2\sigma_i^2} \quad (2.8)$$

for given values of  $z_i$  and  $\sigma_i$ . The value of  $\bar{x}$  is obtained by differentiating equation ( 2.8 ) with respect to  $x$  and setting the result equal to zero.

$$\sum_i \frac{x - z_i}{\sigma_i^2} = 0$$

or

$$\bar{x} = \frac{\sum_i \frac{z_i}{\sigma_i^2}}{\sum_i \frac{1}{\sigma_i^2}} \quad (2.9)$$

The denominator of equation ( 2.9 ) provides a measure of the relative weight of the estimate. In fact, the variance of this estimate is given by [20]

$$\sigma_{\bar{x}}^2 = \frac{1}{\sum_i \frac{1}{\sigma_i^2}} \quad (2.10)$$

Thus, equations ( 2.9 ) and ( 2.10 ) provide the best fit estimate of the true value of  $x$  and a statistical measure of the reliability of this estimate,  $\sigma_{\bar{x}}^2$ .

*2.5.2 Multi-Dimensional, Linear Least Squares.* [3, 7, 20] To extend the results of the previous section to a multi-dimensional case, the value to be estimated must be redefined as a state vector,  $\mathbf{x}$ . The individual pieces of data are now typically vectors as well. These will be denoted as  $\mathbf{z}_i$ . These vectors are

not necessarily of the same order as the state vector because, in the linear least squares development, we no longer assume that the instrument directly measures the values of the state. In fact, the instrument is not required to measure its quantities at the time of interest. Instead, a relationship is developed between the state vector at the time of interest, which we will call the reference time, and the state vector at any other time. This relationship is based on the state transition matrix. The state transition matrix allows us to determine the value of the state vector at any time based on the value of the state vector at the reference time and the elapsed time in between. Because this development assumes linearized dynamics, the state transition matrix, denoted  $\Phi(t, t_0)$ , is simply multiplied by the state vector at the reference time,  $\mathbf{x}(t_0)$ .

$$\mathbf{x}(t) = \Phi(t, t_0) \mathbf{x}(t_0) \quad (2.11)$$

As mentioned, the instrument does not directly measure the state vector. Instead, it measures some parameters related to the state vector and includes the ever present errors. In this development, this observation relation is also linear and is expressed as

$$\mathbf{z}_i = \mathbf{H}_i \mathbf{x}(t_i) + \mathbf{e}_i \quad (2.12)$$

By combining the two equations, we see the relationship between the instrument data and the state vector at the reference time.

$$\mathbf{z}_i = \mathbf{H}_i \Phi(t_i, t_0) \mathbf{x}(t_0) + \mathbf{e}_i \quad (2.13)$$

Finally, a covariance matrix,  $\mathbf{Q}_e$ , is now introduced. This is a square matrix composed of the instrument variances for each element of the observation vector as the diagonal elements and the covariances as the off-diagonals. The covariances represent the degree of statistical interdependence between the error of one observation and the error of another. In many applications, these covariances are zero, making the covariance matrix a diagonal matrix.

The following abbreviation is common.

$$\mathbf{T}_i \equiv \mathbf{H}_i \Phi(t_i, t_0) \quad (2.14)$$

Additionally, for  $N$  independent observation vectors, the matrices and vectors can be grouped as follows.

$$\mathbf{Z} \equiv \begin{bmatrix} \mathbf{z}_1 \\ \mathbf{z}_2 \\ \vdots \\ \mathbf{z}_N \end{bmatrix} \quad (2.15)$$

$$\mathbf{T} \equiv \begin{bmatrix} \mathbf{T}_1 \\ \mathbf{T}_2 \\ \vdots \\ \mathbf{T}_N \end{bmatrix}$$

$$\mathbf{Q} \equiv \begin{bmatrix} \mathbf{Q}_1 & 0 & \dots & 0 \\ 0 & \mathbf{Q}_2 & \dots & 0 \\ \vdots & \vdots & \ddots & \vdots \\ 0 & 0 & \dots & \mathbf{Q}_N \end{bmatrix}$$

Using the same method as section 2.5, the following estimate of the state vector,  $\bar{\mathbf{x}}(t_0)$ , results. [20]

$$\bar{\mathbf{x}}(t_0) = (\mathbf{T}^T \mathbf{Q}^{-1} \mathbf{T})^{-1} \mathbf{T}^T \mathbf{Q}^{-1} \mathbf{Z} \quad (2.16)$$

The reliability of this estimate is expressed as the covariance matrix,  $\mathbf{P}_{\bar{\mathbf{x}}}$ . [20]

$$\mathbf{P}_{\bar{\mathbf{x}}} = (\mathbf{T}^T \mathbf{Q}^{-1} \mathbf{T})^{-1} \quad (2.17)$$

**2.5.3 Non-Linear Least Squares.** [20] The non-linear least squares development differs from the linear development in two ways. First, the  $\mathbf{H}$  matrix and the  $\Phi$  matrix are obtained by linearizing about a reference condition. Second, the method produces a correction to a reference state, and must therefore be iterated until this correction is small.

Instead of using a state transition matrix,  $\Phi(t_i, t_0)$ , which converts the state vector at the reference time to a state vector at any other time, its linearization is instead used to convert a small change in the reference state to a small change in the state at another time.

$$\delta \mathbf{x}(t_i) = \Phi(t_i, t_0) \delta \mathbf{x}(t_0) \quad (2.18)$$

Unfortunately, this linearization matrix is denoted the same and is still called the state transition matrix.

A more appropriate term might be state correction transition matrix. The linearization occurs about a reference state. This reference state is obtained (in the orbit determination problem) from an initial orbit

determination. The methods described by Boulet, Herget and Escobal would all be appropriate for this initial reference state.

Instead of the observation relation

$$\mathbf{z}_i = \mathbf{H}_i \mathbf{x}(t_i) + \mathbf{e}_i \quad (2.12)$$

the non-linear relation becomes

$$\mathbf{z}_i = \mathbf{G}_i(\mathbf{x}(t_i)) + \mathbf{e}_i \quad (2.19)$$

This is linearized about the reference state at the observation time as follows.

$$\mathbf{H}_i = \frac{\partial \mathbf{G}_i(\mathbf{x}_{\text{ref}}(t_i))}{\partial \mathbf{x}} \quad (2.20)$$

The  $\mathbf{T}$  matrix and the  $\mathbf{Q}$  matrix are defined as in the linear case and a residual vector is introduced as

$$\mathbf{r}_i = \mathbf{z}_i - \mathbf{G}_i(\mathbf{x}_{\text{ref}}(t_i)) \quad (2.21)$$

The estimate of the state vector is given as [20]

$$\bar{\mathbf{x}} = \bar{\mathbf{x}}_{\text{ref}}(t_0) + \delta \bar{\mathbf{x}}(t_0) \quad (2.22)$$

where

$$\delta \bar{\mathbf{x}}(t_0) = (\mathbf{T}^T \mathbf{Q}^{-1} \mathbf{T})^{-1} \mathbf{T}^T \mathbf{Q}^{-1} \mathbf{r}$$

and the covariance matrix is [20]

$$\mathbf{P}_{\delta \bar{\mathbf{x}}} = (\mathbf{T}^T \mathbf{Q}^{-1} \mathbf{T})^{-1} \quad (2.23)$$

Equations ( 2.22 ) through ( 2.23 ) provide the means of determining the state vector at the reference time, and the associated covariance matrix. However, there is one more important step in the method of least squares. The resulting reference state can be compared to the observation data to determine the set of residuals,  $\mathbf{r}_i$ . These residuals should agree statistically with the instrument's accuracies. For example, if the instrument is known to have a standard deviation of ten meters in one parameter, then approximately 68% of the residuals should be less than ten meters. This check of the data is required in order to show that something has not gone drastically wrong with the estimation algorithm.

2.5.4 *Computer Implementation.* [20] A modification to the above equations allows more efficient computer implementation. Instead of using the large, combined matrices described by equations ( 2.15 ), the individual  $T_i$  and  $Q_i$  matrices and the individual  $z_i$  vector can be used in the following equations. [20]

$$P_{\delta \bar{x}} = \left( \sum_i T_i^T Q_i^{-1} T_i \right)^{-1} \quad ( 2.24 )$$

$$\delta \bar{x} = P_{\delta \bar{x}} \sum_i T_i^T Q_i^{-1} r_i$$

These equations are iterated until  $\delta \bar{x}$  has converged to a small enough value. The criteria for convergence can come from the covariance matrix. If the correction to each element of the state vector is significantly smaller than the square root of the corresponding diagonal element of the covariance matrix, there is no need to continue iterating.

## 2.6 Sequential Estimation

The methods described in section 2.5 are termed batch estimators. They take all of the available data and process it at one time. This is the most accurate means of data reduction but can become cumbersome for certain systems. In the continual process of orbital estimation for a near-Earth satellite, data may be available spanning several decades. It would be too time intensive to attempt to process all of this data to produce the latest orbit estimate. If the epoch time of the estimate is to be kept somewhat current, the dynamics must be integrated from the time of the older data to the current epoch. This can take considerable time and is not entirely accurate since the dynamics model used is never perfectly accurate. Instead, a common practice is to estimate an orbit using the new data since the last orbit estimate along with the results of the previous estimate. Thus, the previous estimate acts like data to the new estimate and the previous covariance matrix acts like an observation covariance matrix. This process is repeated as often as necessary. Thus, each estimate is at a current epoch and the older data is included in the process by including the previous estimate (which was based on the older data). This process of

continually discarding old data and keeping the estimate and covariance matrix is called sequential estimation. The process of sequential estimation using the method of least squares for each estimate is called a Bayes Filter.

One common problem with any sequential estimator is the reducing size of the covariance matrix. Although this seems like a desirable result, it can eventually turn bad. As the amount of data going into the estimate increases, the covariance matrix will eventually become so small that the estimator essentially believes it has achieved perfection. New data is evaluated but its observation covariance matrix will be quite large compared to the covariance of the previous estimate and so the new data is almost completely ignored. If the dynamics were perfectly known, and there were no numerical errors in the implementation, this would be acceptable. However, as mentioned previously, there are actually some influences on the motion of the satellite which cannot be entirely predicted. Effects such as air drag are not entirely predictable because the atmospheric density at any given point is highly unstable. Predictions may be only accurate to an order of magnitude in some cases. Thus, the newer data is necessary to provide a current orbit estimate, and some means of preventing the covariance matrix from shrinking must be implemented. The method used in this thesis is called fading memory. Fading memory involves multiplying the covariance matrix by another matrix, called a  $\beta$ -matrix, whose size is based on the age of the covariance matrix. The  $\beta$ -matrix is a diagonal matrix whose elements are made from the reciprocal of coefficients raised to the power of the number of days between the epoch of the covariance matrix and the epoch of the current estimate. The coefficients are typically less than one and represent the time scale for the accuracy of that particular state vector element.

$$\mathbf{P}_{\text{new}} = \mathbf{P}_{\text{old}} \boldsymbol{\beta}^{-\Delta t} \quad (2.25)$$

Thus, if the  $\beta$  coefficients are 0.933, and the covariance matrix is 10 days old, the covariance elements would be doubled, corresponding to a data half-life of ten days. Different state vector elements can have different  $\beta$  coefficients corresponding to different time scales for the length of validity of the covariance elements.



## *2.7 Summary*

This chapter has described the basics of orbit determination, least squares batch estimation, the Bayes Filter and fading memory. The thesis makes extensive use of the non-linear, multi-dimensional method of least squares. It uses the computer implementation method described in section 2.5.4. The final and most important portion of the thesis uses a Bayes Filter with fading memory in a long-term simulation. The next chapter begins the detailed description of the thesis effort.

### III. Taylor Series Track Compression

#### 3.1 Introduction

This chapter describes the Taylor series method of track compression. It first details the development of the truth model used to generate the various sets of input observation data. It then details how the Taylor series method of track compression was developed using the method of least squares. Finally, it presents the results of the Taylor series track compression portion of the thesis.

**3.1.1 Notation.** Throughout the thesis, bold-faced letters will be used to represent vectors. State vectors are represented as **X**. Position and velocity vectors are represented as **R** and **V**. Components of position and velocity will be represented as

Table 3-1 Notation

position	velocity
$[R_I \quad R_J \quad R_K]^T$	$[V_I \quad V_J \quad V_K]^T$
$[R_X \quad R_Y \quad R_Z]^T$	$[V_X \quad V_Y \quad V_Z]^T$
$[R_1 \quad R_2 \quad R_3]^T$	$[V_1 \quad V_2 \quad V_3]^T$
$[x \quad y \quad z]^T$	

**3.1.2 Units.** To a large extent, canonical units have been used throughout the thesis. Distances are measured in Distance Units (DUs), time is measured in Time Units (TUs), seconds or Julian Days (JD). A DU is defined as the mean equatorial radius of the Earth equal to 6378.137 km [22]. A TU is defined as the time that a satellite in a circular, Keplerian orbit with a semi-major axis of one DU would take to travel a distance of one DU. This is equal to 13.44685115881 minutes [22]. Exceptions to the canonical units standard occur in the time steps used by the numerical integrator and the reporting of observation times.

### 3.2 Truth Model

The truth data is generated using a fourth-order Runge-Kutta numerical integrator. This integrates a set of first-order differential equations of the form

$$\frac{d x}{d t} = f(x) \quad (3.1)$$

The formulas for the standard fourth-order Runge-Kutta integrator are

$$x_{n+1} = x_n + \frac{1}{6} (k_1 + 2 k_2 + 2 k_3 + k_4) \quad (3.2)$$

where  $k_1 = \Delta t f(x_n)$

$$k_2 = \Delta t f\left(x_n + \frac{k_1}{2}\right)$$

$$k_3 = \Delta t f\left(x_n + \frac{k_2}{2}\right)$$

$$k_4 = \Delta t f(x_n + k_3) [1, 11]$$

In this application, the variable of interest is a state vector,  $\mathbf{X}$ , and the differential equation takes the vector form

$$\frac{d \mathbf{X}}{d t} = \mathbf{f}(\mathbf{X}) \quad (3.3)$$

**3.2.1 State Vector.** For the track compression portions of the thesis, the state vector,  $\mathbf{X}$ , is defined as

$$\mathbf{X} \equiv [R_I \quad R_J \quad R_K \quad V_I \quad V_J \quad V_K]^T \quad (3.4)$$

**3.2.2 Equations of Motion.** For the track compression portions, the EOMs are derived from the Earth's geopotential accounting for the  $J_2$  zonal harmonic caused by the Earth's oblateness. Escobal gives this potential,  $\Phi$ , (not to be confused with the state transition matrix with the same symbol), as [5]

$$\Phi = \frac{Gm}{r} \left[ 1 + \frac{R_{\oplus}^2 J_2}{2r^2} (1 - 3 \sin^2 \delta) \right] \quad (3.5)$$

where  $G$  is the gravitational constant

$m$  is the mass of the Earth

$R_{\oplus}$  is the equatorial radius of the Earth

$r$  is the distance from the Earth's center

$J_2 = 1082.28 \pm 0.3 \times 10^{-6}$  (unitless)

$\sin \delta \equiv z/r$

The acceleration due to gravity about a planet is given as the gradient of the potential, or

$$\frac{d^2 \mathbf{R}}{dt^2} = \nabla \Phi \quad (3.6)$$

and these terms are given as

$$\frac{\partial \Phi}{\partial x} = -\frac{Gmx}{r^3} \left[ 1 + \frac{3}{2} \frac{R_{\oplus}^2 J_2}{r^2} (1 - 5 \sin^2 \delta) \right] \quad (3.7)$$

$$\frac{\partial \Phi}{\partial y} = y \left( \frac{1}{x} \frac{\partial \Phi}{\partial x} \right)$$

$$\frac{\partial \Phi}{\partial z} = -\frac{Gmz}{r^3} \left[ 1 + \frac{3}{2} \frac{R_{\oplus}^2 J_2}{r^2} (3 - 5 \sin^2 \delta) \right]$$

Using canonical units allows the substitution  $\mu \equiv Gm = 1$  and  $R_{\oplus} = 1$ . The equations of motion become

$$\dot{\mathbf{X}} = \begin{bmatrix} V_x \\ V_y \\ V_z \\ -\frac{x}{r^3} \left[ 1 + \frac{3}{2} \frac{J_2}{r^2} \left( 1 - 5 \frac{z^2}{r^2} \right) \right] \\ -\frac{y}{r^3} \left[ 1 + \frac{3}{2} \frac{J_2}{r^2} \left( 1 - 5 \frac{z^2}{r^2} \right) \right] \\ -\frac{z}{r^3} \left[ 1 + \frac{3}{2} \frac{J_2}{r^2} \left( 3 - 5 \frac{z^2}{r^2} \right) \right] \end{bmatrix} \quad (3.8)$$

where  $r$  is determined from

$$r = \sqrt{x^2 + y^2 + z^2} \quad (3.9)$$

**3.2.3 Reference Frames.** The truth model tracks the state vector and acceleration components in the Earth-Centered, Inertial (ECI) reference frame. This is sometimes referred to as the IJK frame, as these letters represent the three basis vectors. This frame uses the center of the Earth as its origin, the equatorial plane as the fundamental frame, the vernal equinox as the direction of the first basis vector, and the North pole as the direction of the third vector. The second vector is in the equatorial plane, perpendicular to the first and third vectors in a right-handed sense.

An Earth-Centered, Rotating (ECR) frame is also used. This frame is similar to the ECI frame except that the first basis vector always points out from the center of the Earth through the equator at a longitude of zero degrees (the longitude of Greenwich). To speed generation of observation data, the site position vector is determined once in the ECR frame. The state vector of the satellite is then rotated to the ECR frame at each time step and compared to the site vector to determine visibility. By rotating the state vector through a single, simple rotation about the third axis, the site vector does not need to be recalculated at each time step. It remains constant in the ECR frame.

Finally, the Topocentric-Horizon reference frame is used to determine the range, azimuth and elevation of the satellite as seen from the site. This reference frame has the site as its origin, the local horizon as the fundamental plane, South (in the local horizon) as the first direction, East as the second direction, and straight up (the zenith) as the third. This frame is usually referred to as the SEZ frame owing to the direction of the basis vectors. The SEZ frame allows easy calculation of the range, azimuth and elevation observations which would be reported by the sites.

**3.2.4 Observation Data.** The truth model is used to generate the observation data for use by the Taylor series track compression algorithm. The observation data represents a typical set of observations which a site of the SSN could generate as a satellite passes within its field of view. The radar sites used will be described next.

3.2.4.1 *Radar Locations.* The radar site locations shown in Table 3-2 were used for this thesis. These are the actual SSN locations. [19]

Table 3-2 Radar Sites of the SSN

Station	Latitude (deg)	Longitude (deg)	Altitude (m)
Indi	-4.67174786	55.47782059	560.50
Reef	-7.27003056	72.36999860	-68.375
Guam	13.61518782	144.85604938	218.93
Hula	21.56226524	201.75789406	429.42
Cook	34.82259890	239.49814705	271.53
Pike	38.805943055	255.471532222	1899.42
Boss	42.94782144	288.37343743	203.37
Pogo	76.51536439	291.40114169	147.03
Lion	51.11758338	359.0936545	146.59

The world-wide distribution of these sites is evident from Figure 3-1 below.

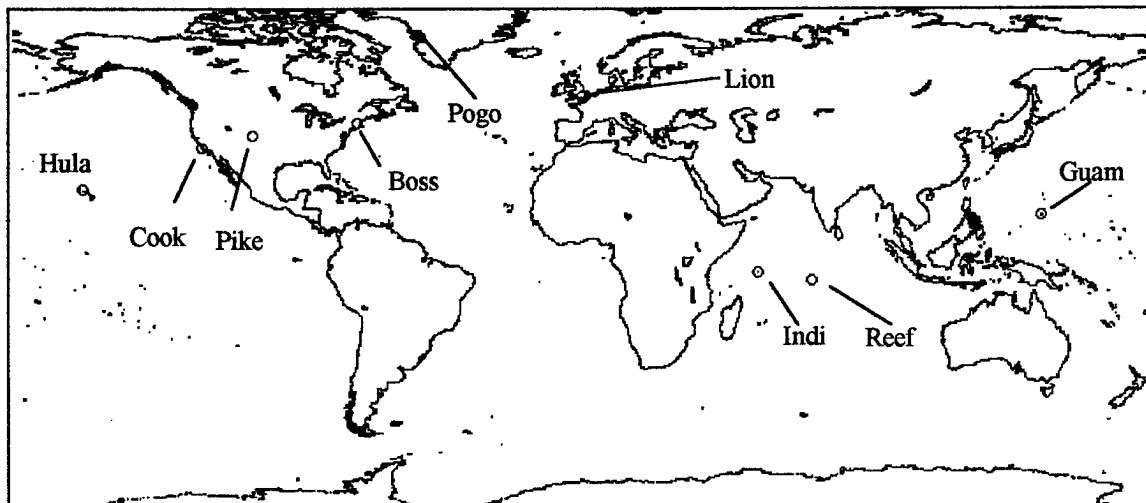


Figure 3-1 Radar Sites of the SSN

3.2.4.2 *Radar Capabilities.* Observation data is generated assuming that all sites have the same type of radar. These radar measure the range, azimuth and elevation of the satellite. The rate of

observations varied for different portions of the thesis. For the track compression development, data rates varied from one observation every five seconds to as high as twelve observations per second.

All radar sites were modeled with the same accuracy. The standard deviations used were 100 meters in range, 0.025 degrees in azimuth and 0.025 degrees in elevation. These are typical SSN accuracies. [19]

**3.2.4.3 ECR Site Vector Calculation.** To calculate the position vector of each site in the ECR frame, one first needs to understand the effects of the Earth's oblateness on latitude, and the distinction between geocentric and geodetic latitudes. As shown in Figure 3-2, geocentric latitude,  $L'$ , is the angle between the equatorial plane and a line from the site to the center of the Earth. Geodetic latitude,  $L$ , is the angle between the equatorial plane and a line through the site and perpendicular to the local horizon. This is what is meant when latitude is typically reported.

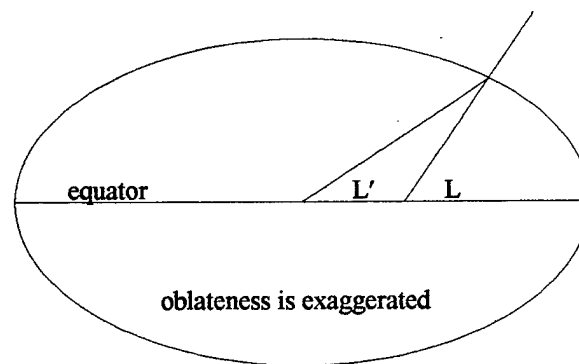


Figure 3-2 Geodetic and Geocentric Latitudes

The latitudes in Table 3-2 are geodetic latitudes. To determine the ECR position vector of a site with geodetic latitude  $L$ , longitude  $\lambda$ , and altitude  $H$ , the following equations are used. [1]

$$\mathbf{R} = \begin{bmatrix} x \cos \lambda \\ x \sin \lambda \\ z \end{bmatrix} \quad (3.10)$$

$$x = \left| \frac{a_e}{\sqrt{1 - e^2 \sin^2 L}} + H \right| \cos L$$

$$z = \left| \frac{a_e(1 - e^2)}{\sqrt{1 - e^2 \sin^2 L}} + H \right| \sin L$$

where  $a_e$  is the mean equatorial radius of the Earth (1 DU)

$e^2$  is the squared eccentricity of the Earth (the amount of oblateness)

From [22]  $e^2 = 0.00669437999013$ .

**3.2.4.4 Observation Geometry.** To predict the measurements, the position vector of the satellite relative to the site is first calculated in ECR coordinates and then rotated into the SEZ frame. The position components of the state vector are used to create the vector of the position of the satellite, relative to the center of the Earth, expressed in ECI coordinates. This vector is then rotated about the third axis by an angle equal to the local sidereal time at Greenwich, resulting in a position vector in ECR coordinates. The position vector of the site is then subtracted from this to leave the position vector of the satellite, relative to the site, expressed in ECR coordinates. This vector is then rotated in a positive direction about the third axis by the longitude of the site, and then in a negative direction about the second axis by the site colatitude, (equal to  $90^\circ$  minus the latitude). This results in a vector representing the position of the satellite, relative to the site, expressed in the topocentric-horizon reference frame. This vector is called RhoSEZ and is abbreviated  $\rho_{SEZ}$ .

Figure 3-3 Observation Geometry, on the next page, shows the topocentric-horizon reference frame and the geometry involved in determining the radar observations.



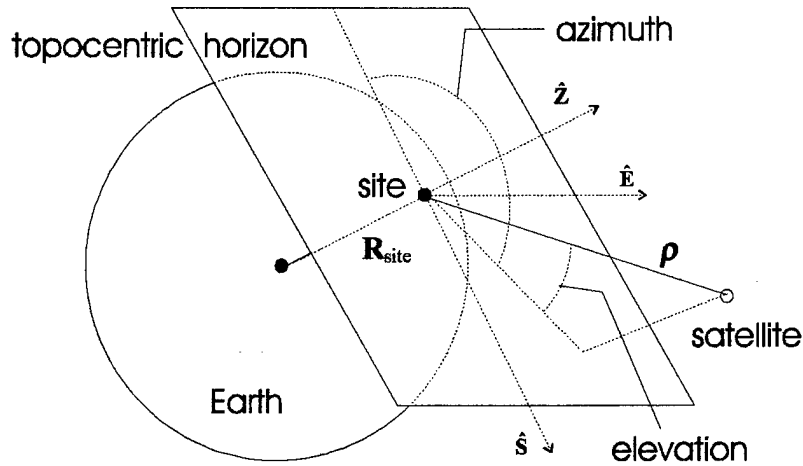


Figure 3-3 Observation Geometry

This figure shows the position vector of the satellite relative to the site. This vector is converted to measurements of range, azimuth and elevation using the following equations.

$$\text{range} = |\rho_{\text{SEZ}}| = \sqrt{\rho_s^2 + \rho_E^2 + \rho_Z^2} \quad (3.11)$$

$$\text{azimuth} = \pi - \tan^{-1} \frac{\rho_E}{\rho_s}$$

$$\text{elevation} = \tan^{-1} \frac{\rho_Z}{\sqrt{\rho_s^2 + \rho_E^2}}$$

**3.2.5 Noise.** Equations ( 3.11 ) provide range, azimuth and elevation data for processing by the track compression algorithms. This is not, however, realistic data. As discussed in chapter two, real data consists of the true portion, and the always present, never separable error, the noise. Observations of the SSN contain contributions from many, very small, error sources. These errors combine to form the reported accuracy of the instrument. According to the Central Limit Theorem (see chapter two), the errors for these measurements follow a Gaussian distribution. This means that the perfect data obtained from equations ( 3.11 ) must be intentionally altered to obtain noisy data. This process occurs by adding the product of a random number and the standard deviation for that type of data. The random number is provided by a routine which determines random numbers of a Gaussian distribution with a mean value of zero and a variance of one. Figure 3-4 shows the distribution of 10,000 of these random numbers.

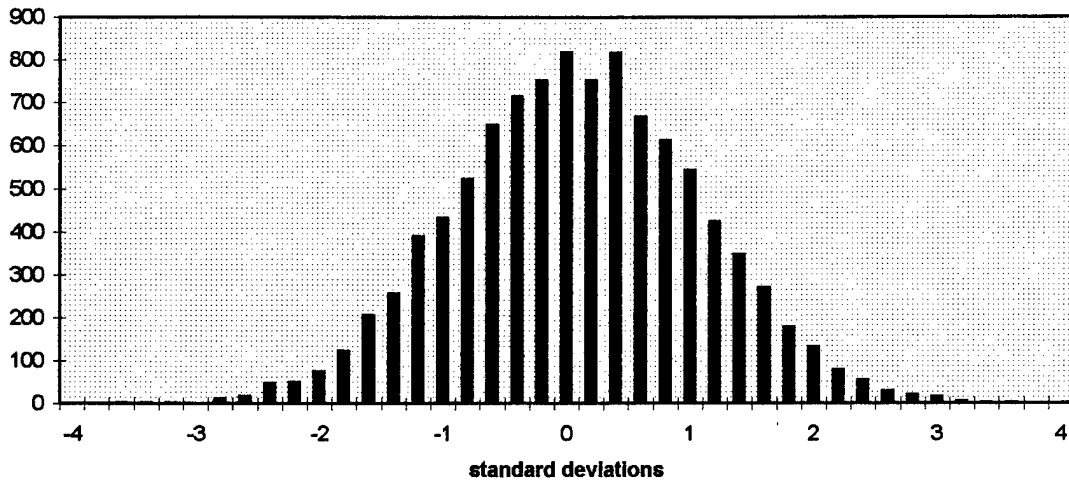


Figure 3-4 Gaussian Random Number Distribution

This error closely resembles a Gauss curve with a variance equal to one. The following three figures show the output of noisy data from a track of 100 observations. Horizontal lines indicate standard deviation intervals on each figure. These show the effect of adding noise to the observations for realism.

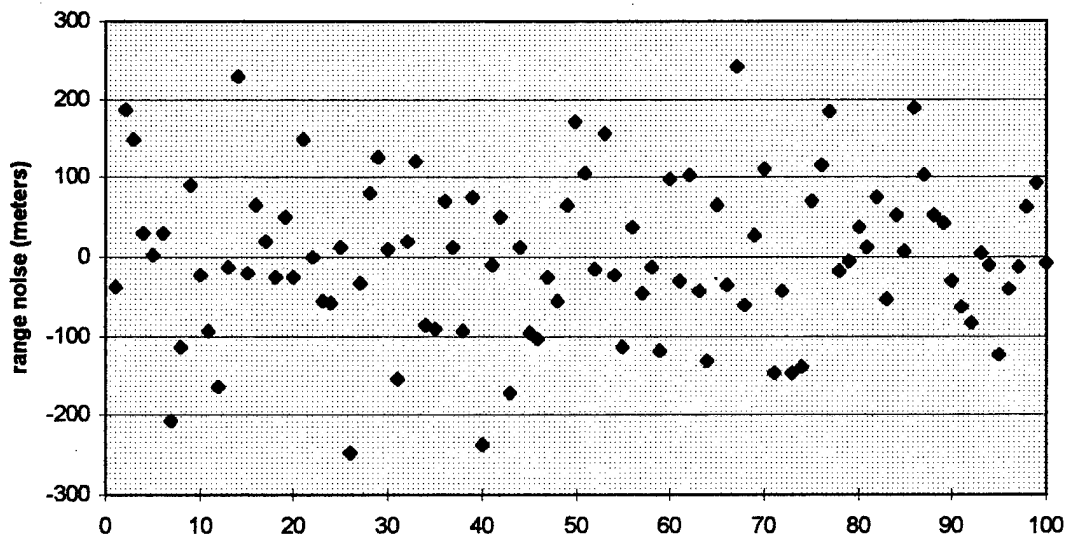


Figure 3-5 Random Range Noise

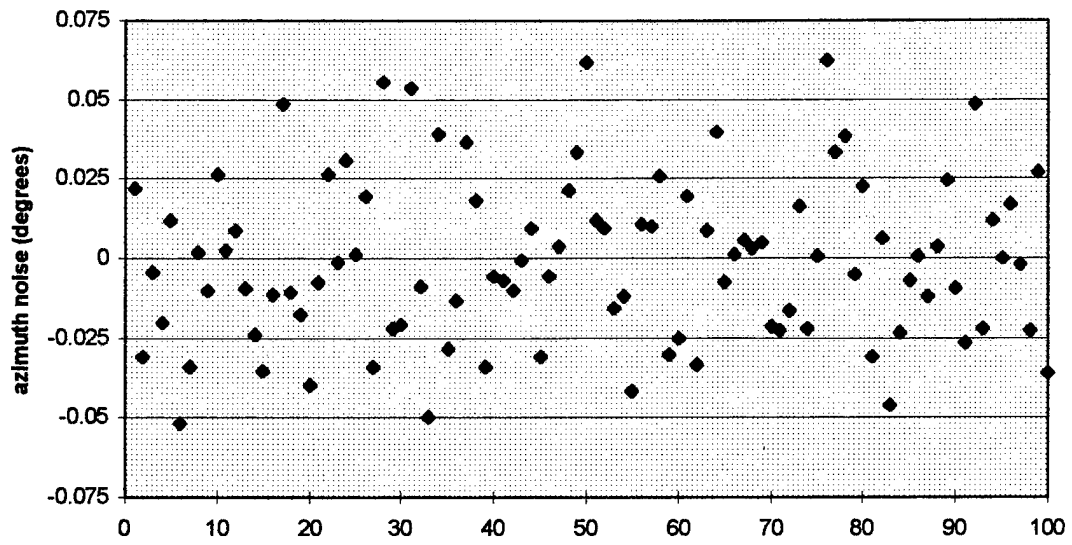


Figure 3-6 Random Azimuth Noise

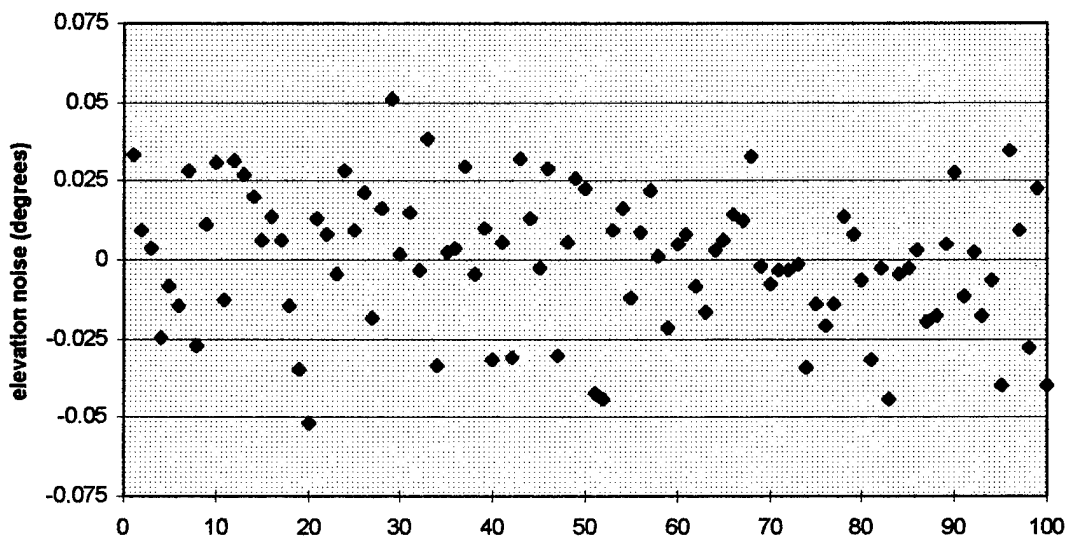


Figure 3-7 Random Elevation Noise

### 3.3 General Description of Track Compression

The two methods of track compression developed in this thesis are based on the use of the multi-dimensional, non-linear least squares algorithm, described in chapter two, to determine a state vector which represents the actual state of the satellite at a particular time. The method also produces the very

important covariance matrix. The algorithm essentially says that if a satellite were at the state computed at the reference time, then it would describe an arc across the sky very close to the arc actually observed by the site. In addition, the covariance matrix describes the accuracy of the estimated state vector.

The state computed at each iteration of the least squares algorithm is called the reference state. The time of this state is the reference time. The trajectory which the satellite would trace if it were actually at the reference state at the reference time is called the reference trajectory. The reference trajectory is used to predict observations to compare with the actual observations to determine the accuracy of the reference state.

This method does not quite determine the satellite's orbit, because it does not provide information about the important drag parameter, the ballistic coefficient. The time scale required for air drag to take effect is too large to be seen during the relatively short arcs observed as one track of data. Also, the information is only based on observations taken on a small piece of the orbit (it excludes input from the opposite side of the orbit). If the data were perfectly accurate, this arc could be extrapolated to completely describe the entire orbit. However, since the information determined by the method is only an estimation, the errors involved in predicting the satellite's position during portions of the orbit far from the arc will be greatly increased. For these reasons, while the process of track compression does produce a six-element state vector which satisfies the classic definition of orbit determination [5], for purposes of this thesis, the actual orbit estimation is not considered to occur until results from multiple tracks are combined (see chapter five).

The two methods both require a dynamics model to predict what observations would be seen if the reference state were the actual state. This dynamics model is used to take a reference state at the reference time and compute the state of the satellite at each observation time. These states are then used to predict the observations. The two methods of track compression developed in the thesis differ in the type of dynamics model used.

### 3.4 Detailed Taylor Series Track Compression Development

The first method of track compression developed for this thesis involves a simplified dynamics model using a Taylor series expansion to determine the position vector of a reference orbit at each observation time. This description disagrees slightly with that of the preceding section. Typically, in the method of non-linear least squares, the entire state is determined at each observation time. In this application, however, only the position need be computed. The observation data do not include any rate information. Thus, the dynamics model does not need to provide the entire state at each time, just the position.

*3.4.1 Initial Reference State.* To implement the non-linear least squares algorithm (see chapter two), a method of determining an initial reference state vector must first be developed. This state must be accurate enough to allow the least squares algorithm to converge. Additionally, the method must be fast to allow for computer-execution thousands of times per day at each site. In this application, the reference state is determined from observation data near the middle of the arc. Specifically, the reference time is determined as the time midway between the first and last observation in the arc. Two observations, one approximately five seconds before the reference time and one approximately five seconds after the reference time are extracted from the data set. Each observation is used to create a position vector at that observation time. This is created in a process exactly reversed from that described in section 3.2.4.4.

A short, second-order arc is then fit between the two vectors; the reference time (very near the middle of the short arc) is used to interpolate along the arc, between the two position vectors, to determine the position vector at the reference time. The velocity vector is determined by assuming a straight line path is traveled between the two position vectors in the (roughly) ten seconds between the two observation times. The position and velocity vectors are combined to create a reference state vector.

More accurate methods of preliminary orbit determination were explored. For instance, Escobal details five different methods of orbit determination from two position vectors and time. In particular, the Gaussian Iteration method is well suited to a time increment of roughly ten seconds. Each of these methods, while more accurate than the arc and line method described above, take considerably longer to

implement. Due to the inaccuracies in the observations, the velocity computed via the arc and line method could contain significant error. Nevertheless, the least squares iteration algorithm has been shown to correct errors in velocity as high as two orders of magnitude in only two iterations. Therefore, even in the worst cases, the arc and line method allows convergence faster than would be possible using a more exact method. It allows rapid reference state calculation from the data arc with sufficient accuracy for least squares convergence in well over 99.9% of the arcs generated.

*3.4.2 Dynamics Model.* After determining an initial reference state, a dynamics model must be used to determine the reference trajectory and the state transition matrix at each observation time. In the Taylor series method of track compression, a Taylor series expansion of the position vector at the reference time is used to allow direct calculation of the position vector at any other time (as opposed to numerical integration). The state transition matrix at an observation time is also directly calculated by taking the partial derivatives of each component of the position vector at the observation time with respect to each component of the reference state.

The Taylor series representation of the position from the reference state is shown below as equation ( 3.12 ).

$$\mathbf{R}(t) = \mathbf{R}(t_0) + \dot{\mathbf{R}}(t_0) \Delta t + \frac{1}{2} \ddot{\mathbf{R}}(t_0) \Delta t^2 + \frac{1}{3!} \dddot{\mathbf{R}}(t_0) \Delta t^3 + \dots \quad (3.12)$$

where  $\mathbf{R}(t_0)$  is the position at the reference time

$\dot{\mathbf{R}}(t_0)$  is the velocity at the reference time

$\ddot{\mathbf{R}}(t_0)$  is the acceleration at the reference time

$\dddot{\mathbf{R}}(t_0)$  is the time rate of change of the acceleration

$\Delta t$  is the time between the observation time,  $t$ , and the reference time,  $t_0$

The position and velocity vectors are contained in the reference state. The acceleration and the acceleration derivatives are obtained from the equations of motion for a satellite.

3.4.2.1 *Order of Terms.* Accelerations resulting from different forces (i.e. different zonal harmonics) are calculated separately and their results are summed. This allows the determination of the relative contribution of each term. Analysis of the contributions is used to determine how many terms are required in order to maintain a desired accuracy in the position vector calculation. Because the accuracy of the expansion decreases as the time interval increases, the track of data must be split up into smaller arcs of data and each arc compressed individually. As more acceleration terms are included in the expansion, the resulting position vectors are more accurate, which allows a track to be split into fewer arcs, but evaluation of the equations takes longer. As the accuracy is decreased, the simpler equations are evaluated faster, but the track must be split up into more arcs, thus requiring the compression scheme to be applied to more arcs. Thus a tradeoff exists between including more terms in the model and splitting the tracks into more arcs.

To determine the number of terms required and the size of each arc, the contribution of each of six terms was graphed as a function of the time interval. These six terms are the first, second and third order two-body terms, first and second order  $J_2$  terms, and the first order  $J_3$  term. This is included as Figure 3-8.

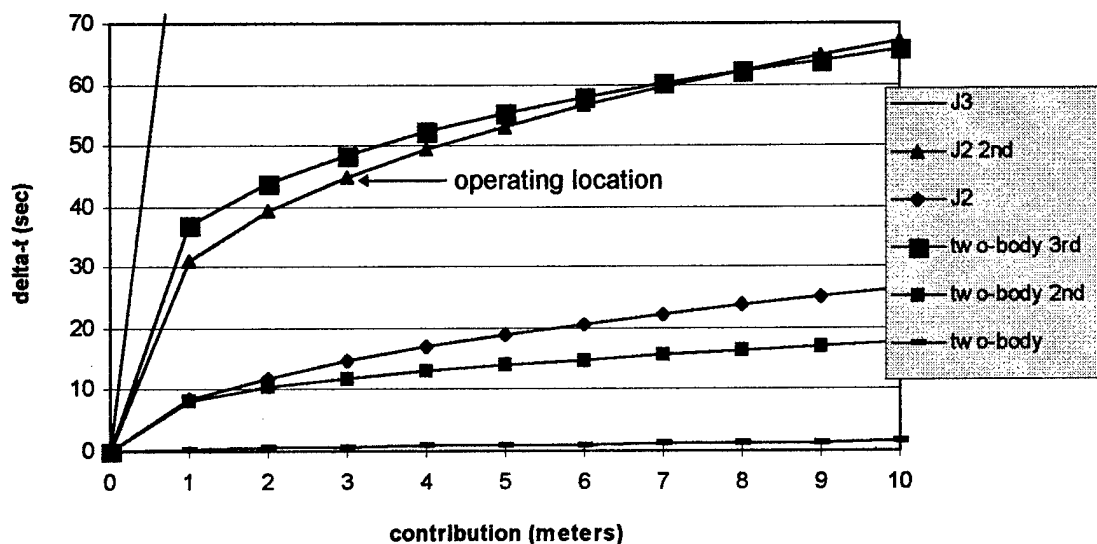


Figure 3-8 Contribution of Taylor Series Terms

Based on this figure, first and second order two-body accelerations and first order  $J_2$  accelerations are included in the equations. This allows for arc lengths of 90 seconds (45 seconds on either side of the reference time) while retaining every term which could contribute more than about three meters to the position of the satellite. Satellites and debris can be more than three meters in size, so including more terms would necessitate accounting for which portion of the satellite body reflected the majority of the radar.

*3.4.2.2 Reference Trajectory.* Using equation ( 3.12 ) and the reference state, the position of the satellite can be directly calculated, with three meter accuracy, at any observation time within 45 seconds of the reference time. This direct calculation avoids the requirement to numerically integrate the equations of motion between observation times. The Taylor series method was originally chosen because it was believed that this would save processing time by eliminating the requirement to numerically integrate a state vector through many small time steps to proceed from one observation to the next. However, as will be discussed in chapter four, this time savings did not occur.

The following is the complete development of the terms of the components of equation ( 3.12 ) in terms of the reference state,  $\mathbf{X}$  . To simplify the presentation of the equations, the following notation will be used.

$$\mathbf{X} = \begin{bmatrix} \mathbf{R} \\ \dots \\ \mathbf{V} \end{bmatrix} = [\mathbf{R}_1 \quad \mathbf{R}_2 \quad \mathbf{R}_3 \quad \mathbf{V}_1 \quad \mathbf{V}_2 \quad \mathbf{V}_3]^T \quad (3.13)$$

$$\mathbf{R}(t_0) = \begin{bmatrix} \mathbf{R}_1 \\ \mathbf{R}_2 \\ \mathbf{R}_3 \end{bmatrix} \quad \dot{\mathbf{R}}(t_0) = \mathbf{V}(t_0) = \begin{bmatrix} \mathbf{V}_1 \\ \mathbf{V}_2 \\ \mathbf{V}_3 \end{bmatrix} \quad (3.14)$$



$$\ddot{\mathbf{R}}(t_0) = \frac{-1}{r^3} \begin{bmatrix} R_1 \\ R_2 \\ R_3 \end{bmatrix} + \frac{-3J_2}{2r^5} \begin{bmatrix} R_1 \left(1 - 5 \frac{R_3^2}{r^2}\right) \\ R_2 \left(1 - 5 \frac{R_3^2}{r^2}\right) \\ R_3 \left(3 - 5 \frac{R_3^2}{r^2}\right) \end{bmatrix}$$

$$\ddot{\mathbf{R}}(t_0) = \frac{1}{r^3} \begin{bmatrix} 3R_1 \frac{\dot{r}}{r} - V_1 \\ 3R_2 \frac{\dot{r}}{r} - V_2 \\ 3R_3 \frac{\dot{r}}{r} - V_3 \end{bmatrix}$$

where  $r = \sqrt{R_1^2 + R_2^2 + R_3^2}$

$$\dot{r} = \frac{d}{dt} r = \frac{R_1 V_1 + R_2 V_2 + R_3 V_3}{r}$$

Combining equations ( 3.12 ) and ( 3.14 ) yields the following final equation for the position of the satellite as a function of the reference state and the time interval between the reference time and the time of the observation,  $\Delta t$ .

$$\mathbf{R} = \begin{bmatrix} R_1 + V_1 \Delta t - \frac{R_1}{2r^3} \Delta t^2 - \frac{3J_2 R_1}{4r^5} \left(1 - 5 \frac{R_3^2}{r^2}\right) \Delta t^2 + \frac{1}{6r^3} \left(\frac{3R_1 \dot{r}}{r} - V_1\right) \Delta t^3 \\ R_2 + V_2 \Delta t - \frac{R_2}{2r^3} \Delta t^2 - \frac{3J_2 R_2}{4r^5} \left(1 - 5 \frac{R_3^2}{r^2}\right) \Delta t^2 + \frac{1}{6r^3} \left(\frac{3R_2 \dot{r}}{r} - V_2\right) \Delta t^3 \\ R_3 + V_3 \Delta t - \frac{R_3}{2r^3} \Delta t^2 - \frac{3J_2 R_3}{4r^5} \left(3 - 5 \frac{R_3^2}{r^2}\right) \Delta t^2 + \frac{1}{6r^3} \left(\frac{3R_3 \dot{r}}{r} - V_3\right) \Delta t^3 \end{bmatrix} \quad (3.15)$$

This equation applies equally for time before the reference time (where  $\Delta t$  is negative) as well as after.

The actual computer code which implements this equation takes advantage of the fact that each term changes only in the time interval when evaluating the position at different observation times. To speed processing, each term is completely evaluated with all but the  $\Delta t$  factor at the beginning of each iteration

of the least squares algorithm. The position vector at each time is then determined by multiplying each term by the appropriate  $\Delta t$  factor and summing. The process of evaluating the reference trajectory consists of determining the position vector at each observation time.

**3.4.2.3 State Transition Matrix.** In addition to a method of computing the reference trajectory, the non-linear least squares algorithm also requires a method of computing the state transition matrix,  $\Phi$ . This is derived from the dynamics model as well. In the Taylor series method, the state transition matrix is developed by taking the partial derivatives of the position vector (from the Taylor series expansion) with respect to the reference state vector.

$$\Phi \equiv \frac{\partial \mathbf{R}(t)}{\partial \mathbf{X}(0)} = \begin{bmatrix} \frac{\partial R_1(t)}{\partial X_1(0)} & \frac{\partial R_1(t)}{\partial X_2(0)} & \frac{\partial R_1(t)}{\partial X_3(0)} & \frac{\partial R_1(t)}{\partial X_4(0)} & \frac{\partial R_1(t)}{\partial X_5(0)} & \frac{\partial R_1(t)}{\partial X_6(0)} \\ \frac{\partial R_2(t)}{\partial X_1(0)} & \frac{\partial R_2(t)}{\partial X_2(0)} & \frac{\partial R_2(t)}{\partial X_3(0)} & \frac{\partial R_2(t)}{\partial X_4(0)} & \frac{\partial R_2(t)}{\partial X_5(0)} & \frac{\partial R_2(t)}{\partial X_6(0)} \\ \frac{\partial R_3(t)}{\partial X_1(0)} & \frac{\partial R_3(t)}{\partial X_2(0)} & \frac{\partial R_3(t)}{\partial X_3(0)} & \frac{\partial R_3(t)}{\partial X_4(0)} & \frac{\partial R_3(t)}{\partial X_5(0)} & \frac{\partial R_3(t)}{\partial X_6(0)} \end{bmatrix} \quad (3.16)$$

where  $\mathbf{R}(t)$  is given by equation ( 3.15 ) and  $\mathbf{X}(0)$  is the state vector which is related to the terms of equation ( 3.16 ) through equation ( 3.13 ). The  $r$  and  $\dot{r}$  terms are each functions of the state, thus the development of this matrix requires multiple uses of the chain rule and becomes quite lengthy. This development is presented in its entirety as Appendix C.

**3.4.3 Observation Relation.** The next step in the least squares algorithm implementation is to determine the observation relation. The observation relation, denoted  $\mathbf{G}$ , is usually a function of the state vector at the observation time. In this case, however, the relation is only a function of the position components of the state. Velocity information is neither provided by the dynamics model nor needed by the observation relation. Therefore, the set of equations comprising the observation relation will only be functions of the position,  $\mathbf{R}(t)$ , and of time.

$$\mathbf{G} = \begin{bmatrix} \text{range}(\mathbf{R}, t) \\ \text{azimuth}(\mathbf{R}, t) \\ \text{elevation}(\mathbf{R}, t) \end{bmatrix} \quad (3.17)$$

The three quantities observed are range, azimuth and elevation. These three quantities are determined by a method similar to that described in section 3.2.4.4 ending with equation ( 3.11 ). The process is detailed in the following three sections.

*3.4.3.1 Determining the RhoIJK Vector.* First, the position vector of the site is subtracted from the position vector of the satellite, with both vectors expressed in the ECI coordinate frame. The resulting vector is called the RhoIJK vector, also denoted  $\rho_{DK}$ . The satellite position vector is obtained in the ECI frame from equation ( 3.15 ). The site position vector in the ECI frame,  $\mathbf{R}_{site}$ , is determined from the site's latitude,  $L$ , longitude,  $\lambda$ , and altitude,  $H$ , and from the observation time (expressed as a Julian Date) using equations very similar to equations ( 3.10 ). [1]

$$\rho_{DK} = \mathbf{R}(t) - \mathbf{R}_{site} \quad (3.18)$$

$$\mathbf{R}_{site} = \begin{bmatrix} x \cos \theta \\ x \sin \theta \\ z \end{bmatrix} \quad (3.19)$$

$$x = \left| \frac{a_e}{\sqrt{1 - e^2 \sin^2 L}} + H \right| \cos L$$

$$z = \left| \frac{a_e(1 - e^2)}{\sqrt{1 - e^2 \sin^2 L}} + H \right| \sin L$$

$$\theta = \text{GST} + \lambda$$

where, as in equation ( 3.10 ),  $a_e$  is the mean equatorial radius of the Earth and  $e^2$  is the squared eccentricity of the Earth. The Greenwich Sidereal Time, GST, is determined from the Julian Date using the following equations. [18]

$$\begin{aligned}
\text{GST} = & 1.75368559 + 628.3319705 \text{ JC} \\
& + 6.770708127 \times 10^{-6} \text{ JC}^2 \\
& + \omega_{\oplus} (\text{JD} - \text{Int}(\text{JD}) - 0.5)
\end{aligned} \tag{3.20}$$

where  $\omega_{\oplus}$  is the rotational rate of the Earth, (6.30038809866574 radians per day) [22]

JD is the Julian Date (not modified)

Int (JD) is the integer portion of the Julian Date

JC is the Julian Century given by the following [18]

$$\text{JC} = \frac{\text{Int}(\text{JD}) + 0.5 - 2451545}{36525} \tag{3.21}$$

Equation ( 3.19 ) gives the ECI position vector of the site. This is subtracted from the satellite's ECI position vector, given by equation ( 3.15 ), yielding the position vector of the satellite relative to the site in the ECI frame, which is RhoIJK.

**3.4.3.2 Determining the RhoSEZ Vector.** The next step in determining the observation relation,  $\mathbf{G}$ , is to calculate the position vector of the satellite relative to the site measured in the Topocentric-Horizon (SEZ) reference frame. This reference frame conversion simply requires two rotations of the RhoIJK vector. This is accomplished via the following rotation matrix.

$$\mathbf{D} = \begin{bmatrix} \cos(\text{LST}) \cos(\text{colat}) & \sin(\text{LST}) \cos(\text{colat}) & -\sin(\text{colat}) \\ -\sin(\text{LST}) & \cos(\text{LST}) & 0 \\ \cos(\text{LST}) \sin(\text{colat}) & \sin(\text{LST}) \sin(\text{colat}) & \cos(\text{colat}) \end{bmatrix} \tag{3.22}$$

where colat is the colatitude of the site, equal to  $90^\circ - L$ . Thus, the RhoSEZ vector is computed from

$$\mathbf{\rho}_{\text{SEZ}} = \mathbf{D} \mathbf{\rho}_{\text{IJK}} \tag{3.23}$$

**3.4.3.3 Final Observation Relation Determination.** The range, azimuth and elevation are then computed from

$$\text{range} = |\mathbf{\rho}_{\text{SEZ}}| = \sqrt{\rho_s^2 + \rho_E^2 + \rho_Z^2} \tag{3.11}$$

$$\text{azimuth} = \pi - \tan^{-1} \frac{\rho_E}{\rho_s}$$

$$\text{elevation} = \tan^{-1} \frac{\rho_z}{\sqrt{\rho_s^2 + \rho_E^2}}$$

Finally, the observation relation,  $\mathbf{G}$ , is obtained by evaluating equations ( 3.18 ) through ( 3.23 ) sequentially, followed by equation ( 3.11 ).

**3.4.4 Observation Matrix.** Once the reference trajectory, state transition matrix and observation relation have all been found, the next step is to determine the observation matrix,  $\mathbf{T}$ . The observation matrix does for the observation relation what the state transition matrix does for the reference trajectory. In fact, it is based in large part on the state transition matrix.  $\mathbf{T}$  essentially tells the algorithm what change in the predicted observation would result from a small change in the reference state,  $\mathbf{X}$ . The observation matrix is defined as

$$\mathbf{T} \equiv \mathbf{H} \Phi \quad (3.24)$$

The matrix  $\mathbf{H}$  gives the change in the observation relation accompanying a change in the state vector at the observation time. The matrix  $\Phi$  gives the change in the state vector at the observation time accompanying a change in the state vector at the reference time. Hence, the two matrices combine to form  $\mathbf{T}$ , which gives the change in the observations at the observation time caused by a change in the reference state vector at the reference time.

$$\mathbf{H} \equiv \frac{\partial \mathbf{G}}{\partial \mathbf{X}(t_i)} \quad (3.25)$$

$$\Phi \equiv \frac{\partial \mathbf{X}(t_i)}{\partial \mathbf{X}(0)}$$

$$\mathbf{T} \equiv \mathbf{H} \Phi = \frac{\partial \mathbf{G}}{\partial \mathbf{X}(t_i)} \frac{\partial \mathbf{X}(t_i)}{\partial \mathbf{X}(0)} \Rightarrow \frac{\partial \mathbf{G}}{\partial \mathbf{X}(0)} \quad (3.26)$$

But in this case the observation relation and state transition matrix both contain only the position components of the state vector, so the relation becomes

$$\mathbf{T} \equiv \mathbf{H} \Phi = \frac{\partial \mathbf{G}}{\partial \mathbf{R}(t_i)} \frac{\partial \mathbf{R}(t_i)}{\partial \mathbf{X}(0)} \Rightarrow \frac{\partial \mathbf{G}}{\partial \mathbf{X}(0)} \quad (3.27)$$

As described by equations ( 3.25 ) and ( 3.27 ), the **H** matrix is taken as the partial derivative of the observation relation with respect to, (in the Taylor series method), the position vector. Thus, the **H** matrix is a three by three matrix consisting of the following partial derivatives.

$$\mathbf{H} = \begin{bmatrix} \frac{\partial \mathbf{G}_1}{\partial \mathbf{R}_1} & \frac{\partial \mathbf{G}_1}{\partial \mathbf{R}_2} & \frac{\partial \mathbf{G}_1}{\partial \mathbf{R}_3} \\ \frac{\partial \mathbf{G}_2}{\partial \mathbf{R}_1} & \frac{\partial \mathbf{G}_2}{\partial \mathbf{R}_2} & \frac{\partial \mathbf{G}_2}{\partial \mathbf{R}_3} \\ \frac{\partial \mathbf{G}_3}{\partial \mathbf{R}_1} & \frac{\partial \mathbf{G}_3}{\partial \mathbf{R}_2} & \frac{\partial \mathbf{G}_3}{\partial \mathbf{R}_3} \end{bmatrix} \quad (3.28)$$

Evaluation of these partial derivatives involves the use of equations ( 3.11 ), ( 3.17 ), ( 3.18 ), ( 3.22 ) and ( 3.23 ) as well as judicious use of the chain rule. Again, this lengthy development will not be presented here. It is contained in its entirety as Appendix D.

**3.4.5 Instrument Covariance Matrix.** The final development for the use of the non-linear least squares algorithm is the instrument covariance matrix, **Q**. The instrument covariance matrix, a diagonal matrix, is obtained from the reported accuracies of the radar sites. The variances, (the square of the instrument's standard deviations), are used as the diagonal elements.

$$\mathbf{Q} = \begin{bmatrix} \sigma_{\text{range}}^2 & 0 & 0 \\ 0 & \sigma_{\text{azimuth}}^2 & 0 \\ 0 & 0 & \sigma_{\text{elevation}}^2 \end{bmatrix} \quad (3.29)$$

The standard deviations used in this thesis are shown on the next page.

$$\sigma_{\text{range}} = 100 \text{ meters} = 1.567856 \times 10^{-5} \text{ DUs}$$

$$\sigma_{\text{azimuth}} = 0.025 \text{ deg} = 4.363323 \times 10^{-4} \text{ rad}$$

$$\sigma_{\text{elevation}} = \sigma_{\text{azimuth}}$$

**3.4.6 Convergence Criteria.** The final step in the application of the least squares algorithm is the decision of a convergence criteria. For the Taylor series method of track compression (and throughout this thesis) the correction applied to the reference state is compared to the diagonal elements of the state covariance matrix, **P**, after each iteration. If the correction to any element of the reference state is larger

than one percent of the square root of the corresponding covariance element, another iteration is accomplished. [20]

*3.4.7 Summary.* To summarize the detailed methodology of the Taylor series method of track compression, a track of data is split into arcs of no more than 90 seconds in length. These arcs are used as observation data for the non-linear least squares algorithm described in chapter two. This algorithm requires the development of a reference trajectory, dynamics model, state transition matrix, observation relation, observation matrix and instrument covariance matrix as well as a decision of the convergence criteria. It is the dynamics model that primarily distinguishes the Taylor series method from the integrator method to be described in chapter four.

The non-linear least squares algorithm is iterated until the convergence criteria is achieved. Once the algorithm has converged to a solution, the residuals are checked to ensure that they are reasonable (see chapter two). The algorithm produces a reference state vector, which represents the state of the satellite at the center of the arc of data, and a covariance matrix, which represents the accuracy of the computed reference state.

### 3.5 Results

This section presents the results of the Taylor series method of track compression portion of the thesis. The results included are a sample of the program output and the first and last pass residuals from track compressions of several different orbits and viewing geometries. The orbital elements used for the first run are shown in Table 3-3.

Table 3-3 Orbit Number One

semi-major axis (DUs)	1.029994
eccentricity	0.003963
inclination (deg)	40.000302
longitude of ascending node (deg)	19.998752
argument of perigee (deg)	358.488511
true anomaly (deg)	46.513560

Radar site LION was used for this first run with observations taken every 0.4 seconds. The satellite was visible for 4 minutes, 37 seconds producing a track of 687 observations which were split into four arcs. Analyzing the residuals shows that each arc was successfully compressed. Figures 3-9 through 3-11 show the residuals from the first pass for each type of data, for the first of the four arcs. These are normalized by dividing by the standard deviations for each type of data. The obvious trends in the data are clear indications that the trajectory evaluated during the first pass is not the optimal trajectory. The residuals of the optimal, converged trajectory should appear as a random series of values with an average near zero and a variance near one. The variance is near one because the residuals are normalized. Approximately 68% of the residuals should be within one standard deviation of the mean.

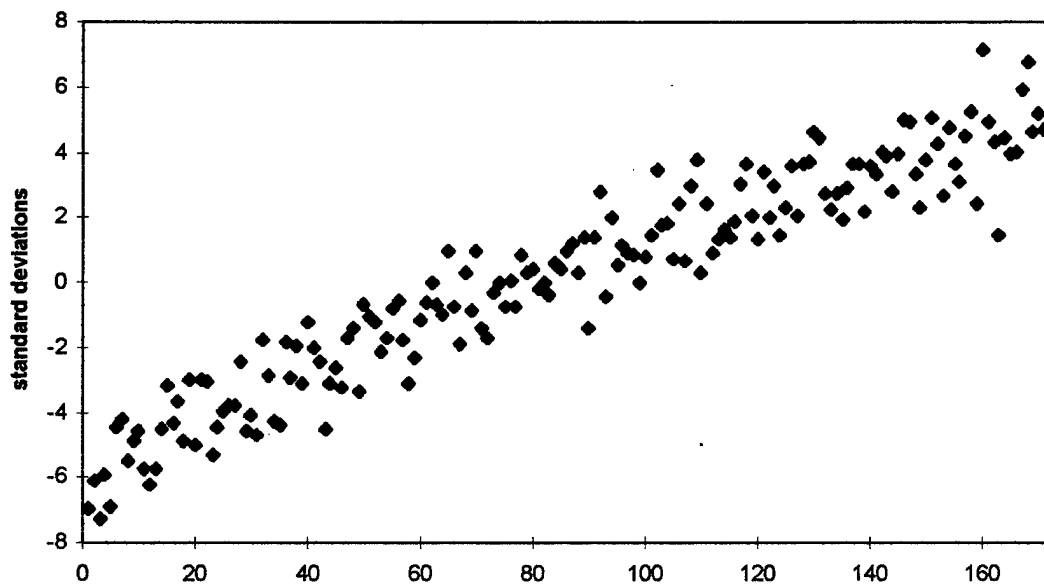


Figure 3-9 First Pass Range Residuals



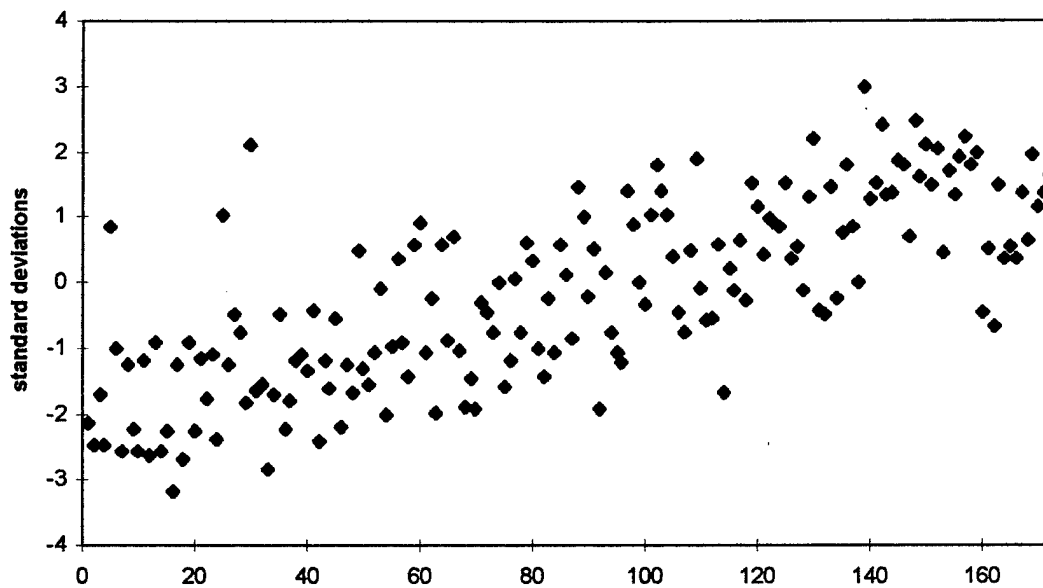


Figure 3-10 First Pass Azimuth Residuals

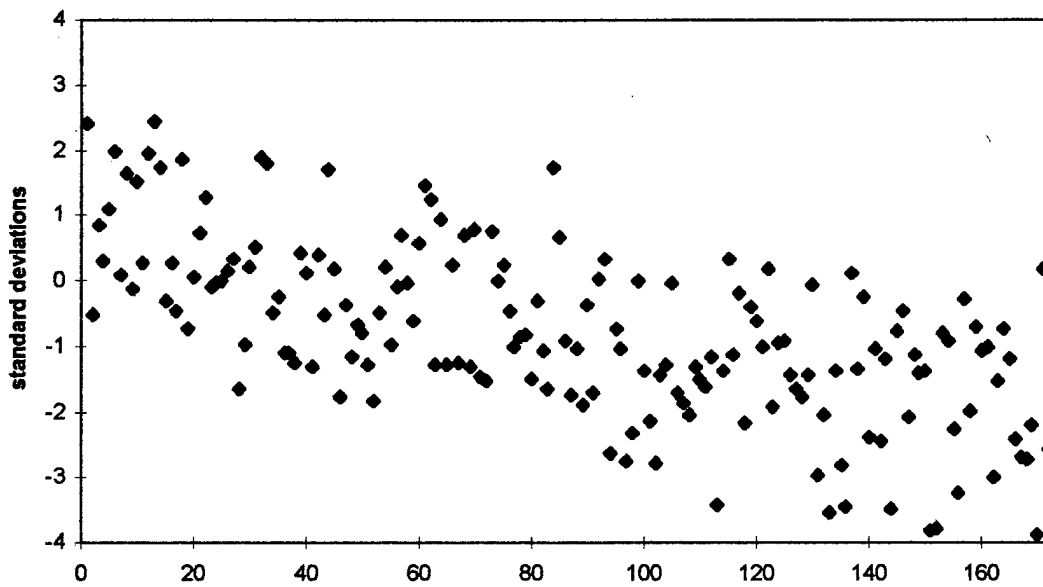


Figure 3-11 First Pass Elevation Residuals

The last pass residuals are shown in Figures 3-12 through 3-14. They show the converged solution, with residuals statistically spread as described previously.

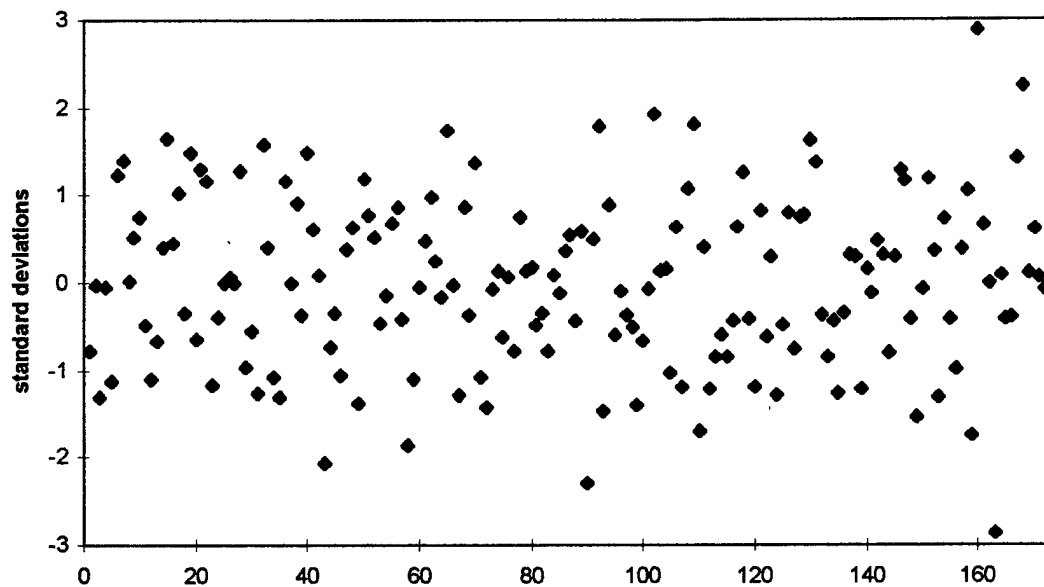


Figure 3-12 Last Pass Range Residuals

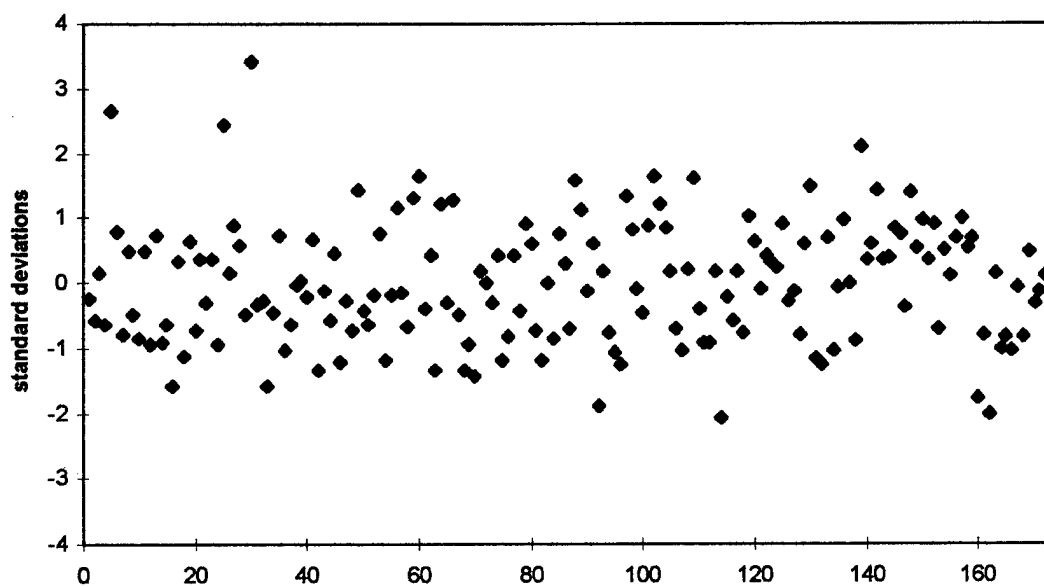


Figure 3-13 Last Pass Azimuth Residuals

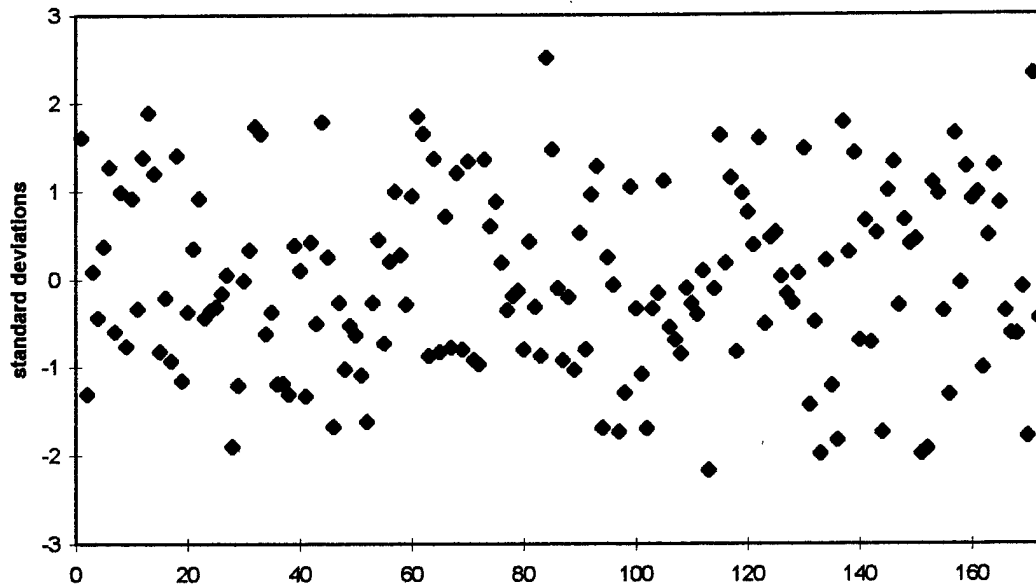


Figure 3-14 Last Pass Elevation Residuals

Similar results appeared for the residuals of the other three arcs. To summarize these results, once the convergence criteria has been achieved, the algorithm calculates the average normalized residual for each type of observation data and the average normalized squared residual. These are recorded and can be used to verify the validity of the converged solution. The following table shows these parameters from this first run. As expected, the average residuals for all three types of data for all four arcs are near zero and the average squared residuals are near one.

Table 3-4 Orbit One Track Compression Results

	range	azimuth	elevation
arc 1 residuals	.00023364	.00000251	.00072454
arc 1 squared residuals	.82982743	.91883676	.98655668
arc 2 residuals	.00028572	.00000180	-.00016240
arc 2 squared residuals	1.02058824	.91098848	.95360661
arc 3 residuals	-.00028598	.00000111	.00004678
arc 3 squared residuals	.94403054	.98764160	1.01218600
arc 4 residuals	-.00028314	.00000415	.00075569
arc 4 squared residuals	.92798399	.86142314	1.03658611

The results in Table 3-4 indicate a successful track compression. The maximum elevation recorded in the data was less than four degrees. This indicates a very low pass in the sky. The second orbit was selected to pass quite high in the sky over the COOK radar site. Its maximum elevation is over 68°. The following shows the second orbit used in the Taylor series method of track compression. It also used a data rate of one observation every 0.4 seconds.

Table 3-5 Orbit Number Two

semi-major axis (DUs)	1.030011
eccentricity	0.003963
inclination (deg)	39.997386
longitude of ascending node (deg)	225.000000
argument of perigee (deg)	358.169601
true anomaly (deg)	46.835123

This orbit is quite similar to orbit one but with the plane rotated to allow it to pass over COOK. This 7 minute, 28 second track of 1111 observations was split into five arcs. Table 3-6 shows the results of the track compression of these five arcs.

Table 3-6 Orbit Two Track Compression Results

	range	azimuth	elevation
arc 1 residuals	-.00003263	-.00000854	-.00012728
arc 1 squared residuals	.88131956	.95627818	.97985336
arc 2 residuals	.00102424	.00001146	-.00019216
arc 2 squared residuals	1.03146837	.85304246	.99571694
arc 3 residuals	-.00343549	.00000031	.01084358
arc 3 squared residuals	.82358193	.96928305	.99036295
arc 4 residuals	.00100726	-.00000616	-.00086904
arc 4 squared residuals	.97109372	1.00082980	1.03648939
arc 5 residuals	-.00002229	-.00000818	-.00020686
arc 5 squared residuals	.95489164	.87828537	.87487937

This table indicates that the high elevation pass also converged successfully. The next step was to apply the Taylor series method of track compression to a higher altitude orbit. For this case, an orbit two Earth radii in size was propagated with COOK taking observations at the same data rate. The satellite passed overhead with more than 82° of elevation.

Table 3-7 Orbit Number Three

semi-major axis (DUs)	2.029923
eccentricity	0.003921
inclination (deg)	39.997902
longitude of ascending node (deg)	225.000684
argument of perigee (deg)	357.730131
true anomaly (deg)	47.272337

The pass lasted 94 minutes producing a track of 13,968 observations split into 63 arcs. All arcs were successfully compressed with valid residuals. All of these residuals were near the desired values of one and zero. Table 3-8 shows the maximum, average and minimum of the 63 average residual and average squared residual results for the range, azimuth and elevation of the 63 arcs.

Table 3-8 Orbit Three Track Compression Results

	maximum	average	minimum
average range residual	0.00003117	-0.00011385	-0.00291641
average squared range residual	1.17498481	0.97460627	0.76891445
average azimuth residual	0.00005437	0.00000135	-0.00004202
average squared azimuth residual	1.20066433	0.97300310	0.78152302
average elevation residual	0.00123700	-0.00018000	-0.00898000
average squared elevation residual	1.19814258	0.98665555	0.75231942

None of these values are too far from the nominal values of zero and one. The final orbit was eccentric with the same semi-major axis. Again, COOK recorded observations at the same data rate.

Table 3-9 Orbit Number Four

semi-major axis (DUs)	2.030040
eccentricity	0.400019
inclination (deg)	39.997573
longitude of ascending node (deg)	225.001504
argument of perigee (deg)	357.731441
true anomaly (deg)	47.270383

This pass lasted 2 hours and 23 minutes. The track consisted of 21,296 observations split into 96 arcs. Table 3-10 presents the residual results in the same manner as for the previous orbit. Again, the values are all reasonable and indicate successful convergence on all arcs.

Table 3-10 Orbit Four Track Compression Results

	maximum	average	minimum
average range residual	0.00004056	-0.00029802	-0.01989010
average squared range residual	1.21929120	0.98029666	0.76489698
average azimuth residual	0.00011469	0.00000372	-0.00004421
average squared azimuth residual	1.16064348	0.96963272	0.76134938
average elevation residual	0.00452605	0.00004444	-0.00474431
average squared elevation residual	1.19675580	0.98611874	0.76251407

### 3.6 Summary

To summarize the results, the Taylor series method of track compression is quite successful at reducing the large tracks of data into manageable state vectors and covariance matrices. The drawback to this method is the large number of arcs that are required for the higher altitude, longer track passes. The large number requires more time to compress and more data to pass to the SCC, undermining the original intent of the thesis. The next portion of the thesis, integrator track compression, was designed to eliminate this problem by allowing a track to be compressed in its entirety, without being split into arcs.

## *IV. Integrator Track Compression*

### *4.1 Introduction*

This chapter details how the integrator method of track compression was developed using the method of least squares. It then presents the results of the integrator track compression portion of the thesis. The notation, units, reference frames and truth model are the same as that described in the Taylor series track compression description in the previous chapter.

### *4.2 Detailed Integrator Track Compression Development*

The integrator method of track compression differs from the Taylor series method primarily in the dynamics model. This model numerically integrates the equations of motion and the equations of variation to determine the state vector and state transition matrix at each observation time, as opposed to directly calculating these as in the Taylor series method.

*4.2.1 Comparison.* The Taylor series method was originally chosen to provide for faster computation. The supposed advantage dealt with the necessity of a numerical integrator to evaluate the state frequently, across small time steps, and thus prevent a direct calculation of the state at a given observation time. However, the savings in time did not manifest itself because the observation times are so closely spaced that a numerical integrator can go directly from one observation time to the next without requiring evaluation across the interval. This fact, coupled with the rather long equations that developed out of the Taylor series method, allowed the numerical integrator to produce state vectors at each observation time at about the same rate as the Taylor series method but with three advantages. The integrator method is more accurate, is easier to modify to account for additional dynamics and, most importantly, does not require the track to be split into arcs. An entire track can be compressed at once, and only one state vector and covariance matrix sent to the SCC.

*4.2.2 Initial Reference State.* The initial reference state for the integrator method is computed in a manner very similar to the Taylor series reference state. The reference state is first calculated using the

arc and line method described in chapter three. The state is then propagated backward to the time of the first observation in the track. The preliminary orbit determination is considered more accurate in the middle of the track, however, the integrator method lends itself to the use of a reference state at the beginning of the track. Therefore, the reference state is calculated at the middle of the track, using the more accurate data, and then propagated to the beginning of the track, to facilitate the integrator dynamics model.

*4.2.3 Dynamics Model.* The dynamics model is the primary difference between the two methods of track compression. The integrator method uses the same fourth-order Runge-Kutta integrator as was described for the truth model in chapter three.

*4.2.3.1 Reference Trajectory.* The reference trajectory is computed by propagating the reference state through each observation time. This propagation requires a set of equations of motion describing the satellite's trajectory. These equations take into account two-body acceleration and the effects of the  $J_2$  geopotential harmonic. They are the same as was used for the truth model.

*4.2.3.2 State Transition Matrix.* The state transition matrix,  $\Phi(t, t_0)$ , is a six by six matrix used to describe the effects of a small change in the reference state on the reference trajectory. As such, it is different for each observation time. Initially, it is the identity matrix,  $\mathbf{I}$ . It changes as the interval between the reference time and the observation time changes. The state transition matrix is computed via the following method. [7, 20]

$$\Phi(t_0, t_0) = \mathbf{I} \quad (4.1)$$

$$\frac{d}{dt} \Phi(t, t_0) = \mathbf{A}(t) \Phi(t, t_0) \quad (4.2)$$

where

$$\mathbf{A}(t) = \nabla_{\mathbf{x}} \mathbf{g}|_{\mathbf{x}_0(t)}$$

and  $\mathbf{g}$  comes from the equations of motion of the state vector,



$$\frac{d}{dt} \mathbf{X} = \mathbf{g}(\mathbf{X}, t)$$

Thus, the components of  $\mathbf{A}(t)$  are evaluated as the partial derivatives of the equations of motion with respect to the state vector. These are known as the equations of variation. Once again, the development of these equations becomes quite lengthy and is presented as Appendix E.

The equations of motion and the equations of variation are integrated together. The equations of motion form a six component vector of equations while the equations of variation form a six by six matrix of equations. Thus the propagator must integrate 42 equations at each time step. This seems quite lengthy, but the equations are not as long as the Taylor series equations and this propagation provides both the reference trajectory and the state transition matrix. Thus, this method is preferable to the Taylor series method.

*4.2.4 Taylor Series Similarities.* The determination of the observation relation, the observation matrix and the instrument covariance matrix is identical to the description contained in the Taylor series development. The convergence criteria is also identical.

*4.2.5 Summary.* To summarize, the integrator method is quite similar to the Taylor series method. The difference lies in the dynamics model where a fourth-order Runge-Kutta integrator is used to numerically integrate the equations of motion and the equations of variation to provide the state vector and the state transition matrix at each observation time. This results in a more accurate state vector derived from the entire track of observations.

### 4.3 Results

This section presents the results of the integrator method of track compression portion of the thesis. The results will be presented in a manner similar to the previous chapter. The same four orbits were used to test the integrator track compression method as were used with the Taylor series method. The first set of orbital elements are reprinted as Table 4-1.

Table 4-1 Orbit Number One

semi-major axis (DUs)	1.029994
eccentricity	0.003963
inclination (deg)	40.000302
longitude of ascending node (deg)	19.998752
argument of perigee (deg)	358.488511
true anomaly (deg)	46.513560

The entire track was compressed into a single state vector and covariance matrix. The first pass normalized residuals are shown in Figures 4-1 through 4-3. Just as in the last chapter, the trends indicate the first pass was not the optimal solution. All three sets of residuals are closer to zero at the middle of the track. This occurs because the reference trajectory used to generate the first set of residuals is constructed from data from the middle of the track.

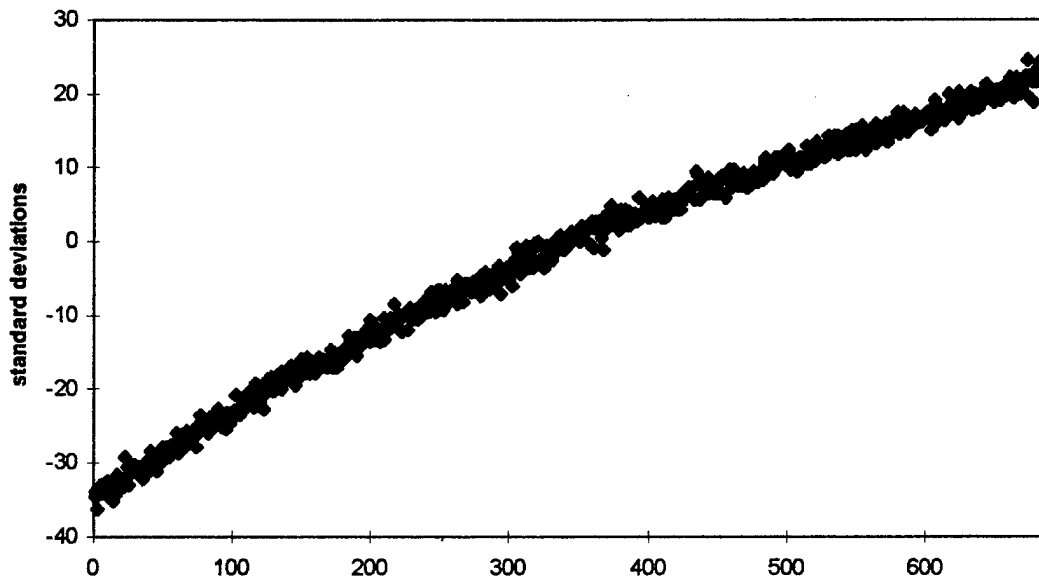


Figure 4-1 First Pass Range Residuals

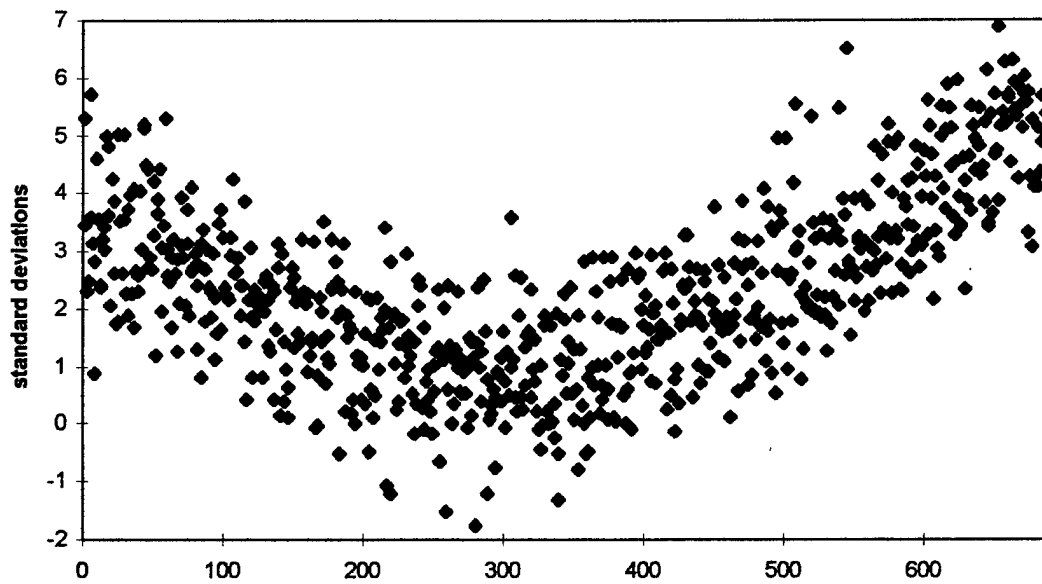


Figure 4-2 First Pass Azimuth Residuals

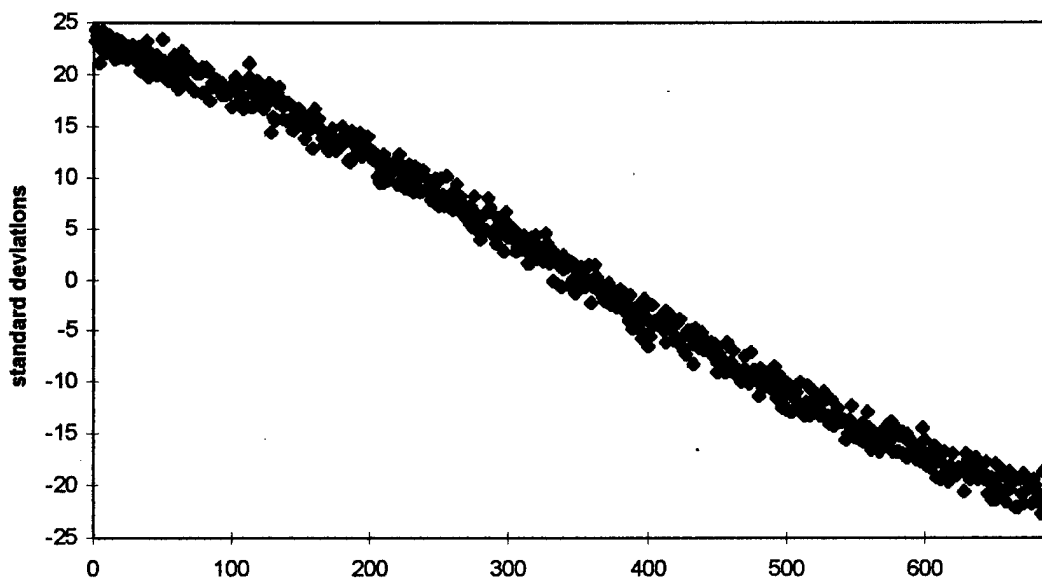


Figure 4-3 First Pass Elevation Residuals

Figures 4-4 through 4-6 show the last pass, converged residuals. As expected, they average near zero and approximately 68% are within one standard deviation of zero.

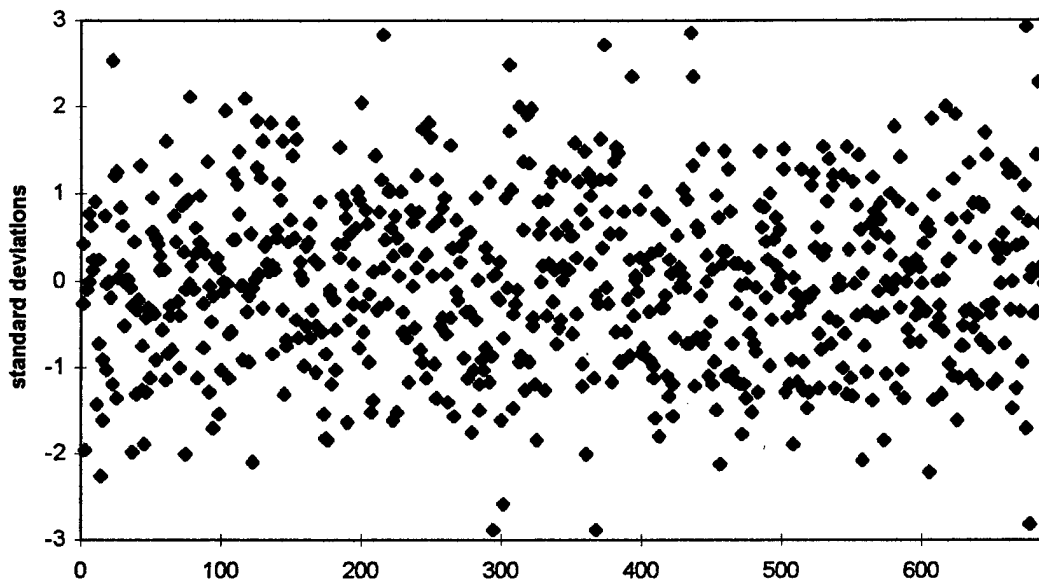


Figure 4-4 Last Pass Range Residuals

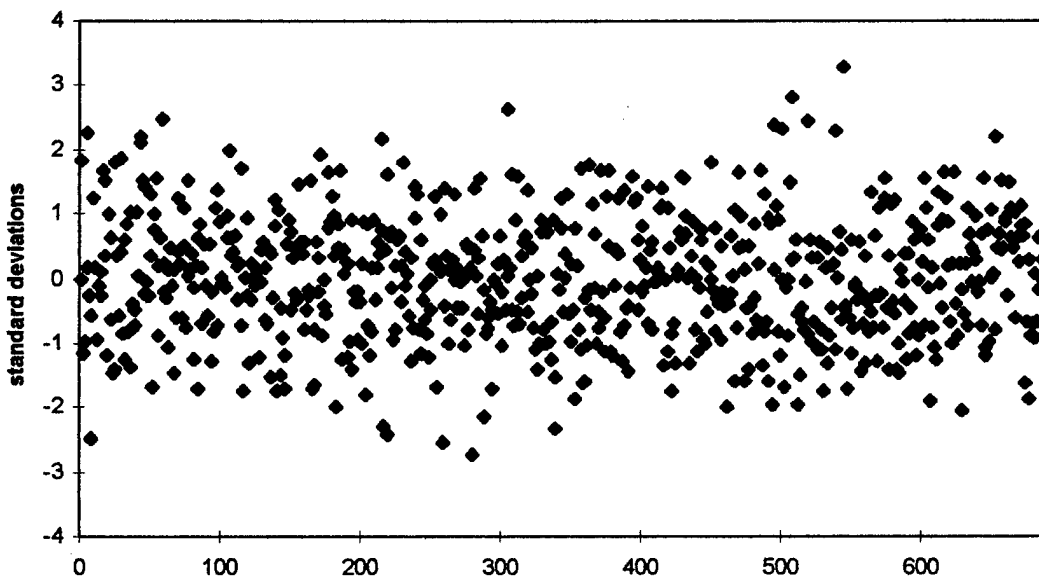


Figure 4-5 Last Pass Azimuth Residuals

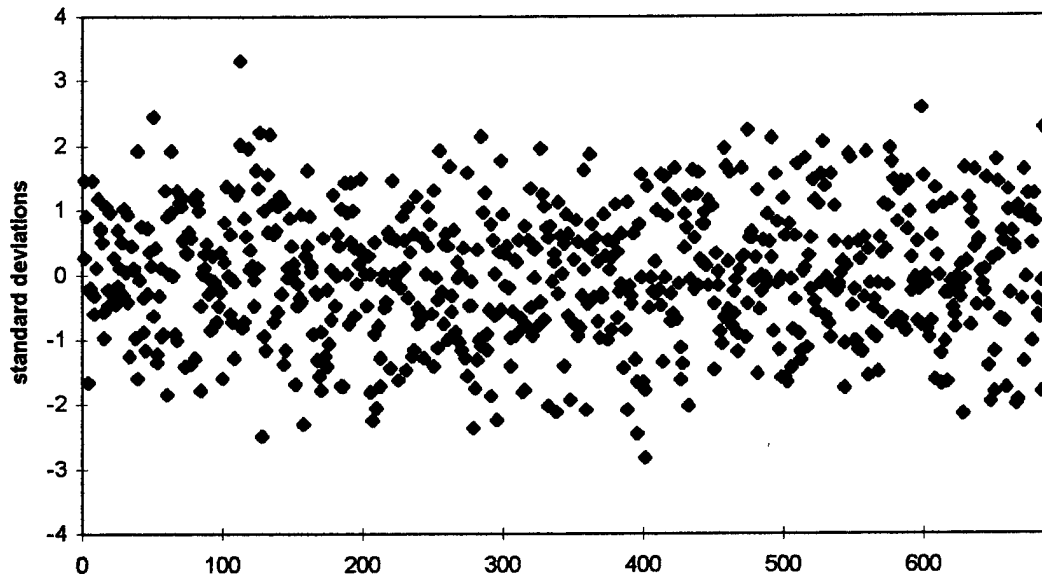


Figure 4-6 Last Pass Elevation Residuals

These figures indicate the compression was successful. The following table shows the average residuals and average squared residuals (normalized) for each data type for the first orbit.

Table 4-2 Orbit One Track Compression Results

	range	azimuth	elevation
residuals	.00056093	.00001764	.00367693
squared residuals	.94139539	.92858585	1.00877648

The following tables complete the results for the integrator method of track compression portion of the thesis. The tables present the last three orbits (the same orbits as the last chapter) and the residual data. They indicate that the integrator method of track compression is also a valid technique for data reduction at the sites. The four cases combine to provide a range of orbit types and viewing angles.

Table 4-3 Orbit Number Two

semi-major axis (DUs)	1.030011
eccentricity	0.003963
inclination (deg)	39.997386
longitude of ascending node (deg)	225.000000
argument of perigee (deg)	358.169601
true anomaly (deg)	46.835123

Table 4-4 Orbit Two Track Compression Results

	range	azimuth	elevation
residuals	-.00651527	.00008277	.02216073
squared residuals	.94371461	.93707563	.98504838

Table 4-5 Orbit Number Three

semi-major axis (DUs)	2.029923
eccentricity	0.003921
inclination (deg)	39.997902
longitude of ascending node (deg)	225.000684
argument of perigee (deg)	357.730131
true anomaly (deg)	47.272337

Table 4-6 Orbit Three Track Compression Results

	range	azimuth	elevation
residuals	-.00122617	.00206993	.03415182
squared residuals	.98469824	.98318182	.99565793

Table 4-7 Orbit Number Four

semi-major axis (DUs)	2.030040
eccentricity	0.400019
inclination (deg)	39.997573
longitude of ascending node (deg)	225.001504
argument of perigee (deg)	357.731441
true anomaly (deg)	47.270383

Table 4-8 Orbit Four Track Compression Results

	range	azimuth	elevation
residuals	-.04312409	.02069728	.12373816
squared residuals	1.02945441	1.00267420	1.02216535

#### 4.4 Summary

The previous results indicate that the integrator method of track compression is as effective as the Taylor series method. Additionally, the integrator method results in one state vector and covariance matrix for a track. This reduces the data required to be sent to and processed by the SCC. Another advantage to the integrator method is the ease with which the dynamics model can be improved. Changing the equations of motion is a relatively simple task. As an example, additional geopotential coefficients and atmospheric drag could be added.

Although the results of the track compression of only four orbits are shown here, many more were actually evaluated for this thesis (for both the integrator and Taylor series methods). The final portion of the thesis involved thousands of orbits and hundreds of thousands of track compressions. About one track per ten thousand produced compression difficulties. This indicates the consistent performance of the integrator method.

## V. *Global Estimate*

### 5.1 *Introduction*

After completion of the two methods of track compression, an obvious question arose. Can the state vectors and associated covariance matrices from multiple compressed tracks be used to provide for an accurate orbit estimate? This would need to be possible if the track compression method is to be implemented by the SCC. To answer this question, the scope of the thesis was extended. This new effort was called *Global Estimate*. This effort involved using the compressed results from multiple tracks from multiple sites around the world as input data to another least squares differential corrector. The application of the least squares algorithm differed from that of the integrator track compression method in several key areas to be discussed in the following sections.

The overall goal of the *Global Estimate* effort was to demonstrate that, if the radar sites of the SSN forwarded data to the SCC in the form of state vectors with covariance matrices, instead of range, azimuth and elevation readings with standard deviations, the SCC could generate accurate orbit estimates in a reasonable period of time. These estimates would have to include ballistic coefficient information.

This chapter details the development of the truth model used to generate the input observation data for the *Global Estimate* portion of the thesis. It then details how the *Global Estimate* process was developed using the method of least squares. The chapter concludes by presenting the *Global Estimate* results.

Canonical units were used for the majority of the *Global Estimate* development. Exceptions to the canonical units standard occur in the time steps used by the numerical integrator and reporting of track compression reference times, as in previous sections, as well as the ballistic coefficient and air density. The ballistic coefficient, denoted  $B^*$ , is measured in units of  $\text{m}^2/\text{kg}$ , while air density is calculated in units of  $\text{kg}/\text{m}^3$ .



## 5.2 Detailed Global Estimate Development

This section describes the detailed development of the equations and matrices used for the *Global Estimate* portion of the thesis. It details the truth model, initial reference state, and estimator development.

**5.2.1 Truth Model.** The truth model used for the *Global Estimate* portion of the thesis is nearly identical to that used for the track compression portions. The difference is the inclusion of air drag using an atmospheric model presented by Regan. [15] The truth model was used to generate the radar site observation data in essentially the same manner as for the two track compression methods. The integrator method of track compression was then used to compress the observation tracks into state vectors and associated covariance matrices. These did not include ballistic coefficient information. The equations of motion for the truth model Runge-Kutta integrator included drag. The equations of motion for the *Global Estimate* dynamics model also included drag, however, the integrator in the track compression dynamics model did not.

**5.2.1.1 State Vector.** For the *Global Estimate* portion, the state vector is extended to allow for the drag calculations. The state includes a term representing half of the ballistic coefficient. The value is only half of the ballistic coefficient simply to save the computer time involved in calculating the acceleration due to drag, which will be shown in the following section to include a factor of  $\frac{1}{2}$ . Thus the seven-component state vector for these portions is defined as

$$\mathbf{X} \equiv \left[ R_I \quad R_J \quad R_K \quad V_I \quad V_J \quad V_K \quad B^*/2 \right]^T \quad (5.1)$$

**5.2.1.2 Equations of Motion.** The equations of motion include the acceleration due to the geopotential as developed in chapter three. Additionally, they include the acceleration due to air drag based on the following equation [9]

$$D = C_D \frac{1}{2} \rho v_r^2 A_f \quad (5.2)$$

where D is the force due to drag

$C_D$  is a dimensionless drag coefficient between one and two [16]

$\rho$  is the local atmospheric density

$v_r$  is the velocity of the spacecraft relative to the local atmosphere

$A_f$  is the exposed, frontal cross-sectional area

By dividing this force by the mass of the satellite,  $m$ , the acceleration due to air drag is shown as

$$\ddot{\mathbf{R}} = -\frac{1}{2} \frac{C_D A_f}{m} \rho v_r^2 \quad (5.3)$$

The ballistic coefficient is now introduced as [21]

$$B^* \equiv \frac{C_D A_f}{m} \quad (5.4)$$

The velocity relative to the local atmosphere is determined by assuming an atmospheric model which rotates with the Earth. Thus the relative velocity is the difference between the satellite's inertial velocity vector and the cross product of the Earth's rotational vector with the satellite's position vector. By combining this with equations ( 5.3 ) and ( 5.4 ), and expressing the result in vector form, the following equation for the acceleration of the satellite due to air drag is obtained

$$\ddot{\mathbf{R}} = -\frac{1}{2} B^* \rho \left| \mathbf{V} - (\boldsymbol{\omega}_\oplus \times \mathbf{R}) \right| \left[ \mathbf{V} - (\boldsymbol{\omega}_\oplus \times \mathbf{R}) \right] \quad (5.5)$$

where  $\boldsymbol{\omega}_\oplus = 0.05883359980154919 \text{ rad/TU } \hat{\mathbf{k}}$  [22].

The satellite-dependent ballistic coefficient is constant and is included as part of the state vector.

Specifically,

$$\mathbf{X}(7) \equiv B^*/2 \quad (5.6)$$

and

$$\dot{\mathbf{X}}(7) = \frac{d}{dt} (B^*/2) = 0$$

Thus, the equations of motion are as shown on the next page.

$$\dot{\mathbf{X}} = \begin{bmatrix} V_I \\ V_J \\ V_K \\ A_{gI} + A_{dI} \\ A_{gJ} + A_{dJ} \\ A_{gK} + A_{dK} \\ 0 \end{bmatrix} \quad (5.7)$$

where  $A_g$  is the acceleration due to gravity given by equation ( 3.8 ) and  $A_d$  is the acceleration due to air drag given by equation ( 5.5 ). The local atmospheric density is determined using an atmospheric model described in Appendix A. [15]

**5.2.1.3 Observation Data.** The same radar sites described in chapter three were used for this portion of the thesis. For this case, however, all sites tracked the satellite whenever it was in view. The sites produced observations at the rate of two per second. The tracks were then compressed using the integrator method of track compression described in chapter four, and the results (state vectors and associated covariance matrices) were used as the input observation data for the *Global Estimate* least squares estimator.

**5.2.2 Initial Reference State.** To start the least squares algorithm, an initial reference state is required. For *Global Estimate*, the first six elements of the initial reference state are taken as the state vector from the first track compression. The seventh element is arbitrarily assigned a value of 0.05. After one iteration, the ballistic coefficient will typically be corrected to a value with at least two digits in agreement with the final, converged value. Thus, the arbitrary nature of this initial value does not hinder the algorithm and convergence is still rapidly achieved.

**5.2.3 Dynamics Model.** The dynamics model used for the estimator is identical to that used by the truth model integrator. The EOMs are the same as equation ( 5.7 ) described in section 5.2.1.2. The development of the state transition matrix requires the evaluation of the  $\mathbf{A}(t)$  matrix. This requires a development similar to that given as Appendix E. The addition of the drag parameter and the

atmospheric model complicate this development. The resulting equations of variation are developed in their entirety in Appendix F.

As in the integrator track compression method, the equations of motion and the equations of variation are integrated simultaneously. Because of the additional component of the state vector, these now constitute 56 first-order differential equations.

**5.2.4 Observation Relation.** The observation relation is considerably simpler in *Global Estimate* than in the previous developments. The input data consists of state vectors containing three position elements and three velocity elements which correspond exactly to the first six components of the *Global Estimate* state vector. The input data gives no direct information about the seventh component, the drag parameter. Thus, the observation relation,  $\mathbf{G}$ , is a direct relation of the first six state vector components.

$$\mathbf{G} = \begin{bmatrix} X_1(t) \\ X_2(t) \\ X_3(t) \\ X_4(t) \\ X_5(t) \\ X_6(t) \end{bmatrix} \quad (5.8)$$

**5.2.5 Observation Matrix.** The observation matrix,  $\mathbf{T}$ , is again given by the following relation.

$$\mathbf{T} \equiv \mathbf{H} \Phi = \frac{\partial \mathbf{G}}{\partial \mathbf{X}(t_i)} \frac{\partial \mathbf{X}(t_i)}{\partial \mathbf{X}(0)} \Rightarrow \frac{\partial \mathbf{G}}{\partial \mathbf{X}(0)} \quad (3.26)$$

Now, however, the  $\mathbf{H}$  matrix is much simpler.

$$\mathbf{H} \equiv \frac{\partial \mathbf{G}}{\partial \mathbf{X}(t_i)} = \begin{bmatrix} 1 & 0 & 0 & 0 & 0 & 0 & 0 \\ 0 & 1 & 0 & 0 & 0 & 0 & 0 \\ 0 & 0 & 1 & 0 & 0 & 0 & 0 \\ 0 & 0 & 0 & 1 & 0 & 0 & 0 \\ 0 & 0 & 0 & 0 & 1 & 0 & 0 \\ 0 & 0 & 0 & 0 & 0 & 1 & 0 \end{bmatrix} \quad (5.9)$$

**5.2.6 Instrument Covariance Matrix.** The instrument covariance matrix changes for each observation, as opposed to the constant  $\mathbf{Q}$  of the track compression sections. The track compression

algorithms produce both a state vector, used as the input data to *Global Estimate*, and a covariance matrix,  $\mathbf{P}$ . This covariance matrix is different for each compressed track and serves as the instrument covariance matrix,  $\mathbf{Q}$ , for *Global Estimate*.

*5.2.7 Convergence Criteria.* The convergence criteria differs from that of the previous chapters only in the number of elements evaluated. The algorithm iterates until each element of the state vector is corrected by less than one percent of the square root of the corresponding diagonal element of the covariance matrix. This time, this includes the seventh diagonal element which corresponds to the ballistic coefficient parameter.

*5.2.8 Summary.* To summarize, the *Global Estimate* effort was aimed at demonstrating the usefulness of the track compression techniques to the overall orbit estimation problem. The project simulated the combination of data forwarded to the SCC by many sites all tracking the same satellite. The same non-linear least squares differential correction algorithm was used for *Global Estimate* as was used for the track compression techniques, but the implementation was considerably different. Most notably, the dynamics model requires propagating 56 equations of variation through several orbits at each iteration, rather than propagating 42 equations through a relatively short arc, as in the integrator method of track compression. The *Global Estimate* development produces a state vector which includes a drag parameter, equal to one-half the ballistic coefficient. This state vector is derived from observations spaced across the satellite's orbit and is therefore considered orbital estimation.

### 5.3 Results

This section presents the results of the *Global Estimate* portion of the thesis. Results from four orbits are included. The first orbit is nearly circular and nearly equatorial. The second is slightly eccentric and retrograde. The third orbit is larger and more eccentric. The fourth orbit is very low with a high ballistic coefficient, resulting in large drag effects. The *Global Estimate* algorithm produces a state vector and covariance matrix at a specified reference time. In all cases, the propagator reported the actual

state vector at this reference time for comparison. These results include the comparison between the *Global Estimate* prediction of the satellite's state and the actual state.

The following table shows the elements of the first orbit.

Table 5-1 Orbit Number One

semi-major axis (DUs)	1.088173
eccentricity	0.000914
inclination (deg)	5.540376
longitude of ascending node (deg)	37.686167
argument of perigee (deg)	69.042996
true anomaly (deg)	254.358992
ballistic coefficient ( $\text{m}^2/\text{kg}$ )	0.033730

This orbit was propagated for 8 hours, 17 minutes, 36 seconds. During this time, 19 tracks of observations were recorded and compressed. After compression, the *Global Estimate* algorithm successfully estimated the satellite's orbit. The following table shows the predicted and actual state vectors, as well as the difference. The state vectors are presented in canonical units (with the exception of the ballistic coefficient). The errors are presented in meters, centimeters per second and square meters per kilogram.

Table 5-2 Orbit One State Vectors

	predicted	actual	error
X-Position (DUs)	0.302786245	0.302786054	1.218 m
Y-Position (DUs)	1.041225660	1.041225678	-0.115 m
Z-Position (DUs)	0.065593099	0.065592718	2.430 m
X-Velocity (DUs/TU)	-0.921111898	-0.921112005	0.085 cm/s
Y-Velocity (DUs/TU)	0.261496070	0.261495883	0.148 cm/s
Z-Velocity (DUs/TU)	0.072230072	0.072230044	0.022 cm/s
B* ( $\text{m}^2/\text{kg}$ )	0.040041509	0.033729594	0.006 $\text{m}^2/\text{kg}$

This shows the accuracy with which *Global Estimate* is able to correctly determine the satellite's orbit. Additionally, the covariance matrix is computed. The square roots of the diagonal elements of the covariance matrix roughly correspond to the three axes of the error ellipsoids. Thus, the first three

diagonals can be used to determine the expected position error, and the next three can be used to determine the expected velocity error. The following table reports these expected errors along with the magnitudes of the actual errors.

Table 5-3 Orbit One Covariance Statistics

	error ellipsoid	actual error
position (m)	3.45	2.72
velocity (cm/s)	3.92	0.17

The second orbit was retrograde. Table 5-4 gives its orbital elements. This was propagated for 6 hours, 19 minutes, 28 seconds. Nineteen tracks were recorded. Tables 5-5 and 5-6 show the results.

Table 5-4 Orbit Number Two

semi-major axis (DUs)	1.160395
eccentricity	0.016347
inclination (deg)	117.685067
longitude of ascending node (deg)	232.270593
argument of perigee (deg)	93.762641
true anomaly (deg)	96.317677
ballistic coefficient ( $\text{m}^2/\text{kg}$ )	0.072933

Table 5-5 Orbit Two State Vectors

	predicted	actual	error
X-Position (DUs)	-0.798729115	-0.798729336	1.410 m
Y-Position (DUs)	-0.469392066	-0.469392202	0.867 m
Z-Position (DUs)	0.676601563	0.676601794	-1.473 m
X-Velocity (DUs/TU)	0.124985690	0.124985946	-0.202 cm/s
Y-Velocity (DUs/TU)	0.699969881	0.699969644	0.187 cm/s
Z-Velocity (DUs/TU)	0.612644198	0.612643960	0.188 cm/s
B* ( $\text{m}^2/\text{kg}$ )	0.077966342	0.072932682	0.005 $\text{m}^2/\text{kg}$

Table 5-6 Orbit Two Covariance Statistics

	error ellipsoid	actual error
position (m)	3.54	2.22
velocity (cm/s)	3.83	0.92

These tables indicate that *Global Estimate* had no problem determining the orbit of this retrograde satellite.

The third orbit attempted was much larger. Its elements are given in Table 5-7.

Table 5-7 Orbit Number Three

semi-major axis (DUs)	2.000000
eccentricity	0.400000
inclination (deg)	28.702842
longitude of ascending node (deg)	75.373285
argument of perigee (deg)	183.806110
true anomaly (deg)	304.719542
ballistic coefficient ( $\text{m}^2/\text{kg}$ )	0.077227

Orbit three was propagated for 4 hours and 48 minutes or one-fifth of a day. There were ten tracks of data recorded and compressed. Tables 5-8 and 5-9 show the results.

Table 5-8 Orbit Three State Vectors

	predicted	actual	error
X-Position (DUs)	1.479112063	1.479112334	-1.730 m
Y-Position (DUs)	-0.208099795	-0.208099705	-0.574 m
Z-Position (DUs)	-0.811761258	-0.811761012	-1.569 m
X-Velocity (DUs/TU)	0.395009244	0.395009444	-0.158 cm/s
Y-Velocity (DUs/TU)	0.713048516	0.713048427	0.070 cm/s
Z-Velocity (DUs/TU)	-0.108714162	-0.108713749	-0.326 cm/s
B* ( $\text{m}^2/\text{kg}$ )	0.061626080	0.077227224	-0.016 $\text{m}^2/\text{kg}$



Table 5-9 Orbit Three Covariance Statistics

	error ellipsoid	actual error
position (m)	4.63	2.41
velocity (cm/s)	2.58	0.37

These tables indicate that *Global Estimate* was also able to successfully estimate the orbit of this higher altitude satellite.

The fourth and final satellite had a lower perigee and a higher ballistic coefficient. These combine to produce a high level of drag on the satellite. Table 5-10 shows the orbital elements for orbit four.

Table 5-10 Orbit Number Four

semi-major axis (DUs)	1.053684
eccentricity	0.019270
inclination (deg)	17.205573
longitude of ascending node (deg)	118.168059
argument of perigee (deg)	250.330578
true anomaly (deg)	307.348639
ballistic coefficient ( $\text{m}^2/\text{kg}$ )	0.128213

Orbit four was propagated for half of a day. There were 31 tracks of data. Tables 5-11 and 5-12 give the results.

Table 5-11 Orbit Four State Vectors

	predicted	actual	error
X-Position (DUs)	-0.007779346	-0.007779829	3.081 m
Y-Position (DUs)	-1.041248918	-1.041248650	1.709 m
Z-Position (DUs)	0.133952657	0.133952453	1.301 m
X-Velocity (DUs/TU)	0.938547552	0.938547812	-0.206 cm/s
Y-Velocity (DUs/TU)	-0.027152032	-0.027152411	0.300 cm/s
Z-Velocity (DUs/TU)	-0.261756518	-0.261756653	0.107 cm/s
B* ( $\text{m}^2/\text{kg}$ )	0.142901590	0.128213036	0.015 $\text{m}^2/\text{kg}$

Table 5-12 Orbit Four Covariance Statistics

	error ellipsoid	actual error
position (m)	3.47	3.76
velocity (cm/s)	3.43	0.38

These tables show that *Global Estimate* was also successful with the high drag case.

#### 5.4 Summary

To summarize, the *Global Estimate* effort produced an algorithm which takes compressed tracks of data and combines them using the non-linear least squares differential correction method to estimate a satellite's orbit. The algorithm was successful at determining the orbits of four case satellites shown in this chapter. Additionally, many thousands of additional orbits were evaluated in the simulation effort, but these results are not included here.

## VI. Simulation

### 6.1 Introduction

After completion of the *Global Estimate* project, another question arose. Could the same method of orbit estimation employed as *Global Estimate* be applied to an entire catalog of satellites? That is, could the sites of the SSN observe the satellites frequently enough, and the SCC process the data quickly enough to keep current an entire catalog of seven to eight thousand objects? The *Global Estimate* project modeled every site in the network tracking a single object every time it was visible. In the real world, such a situation would not exist. Sites have a limited tracking ability so not all satellites will be tracked when the geometry allows. The visible satellites must be prioritized.

To answer these questions, the scope of the thesis was again broadened to include large-catalog simulations. To keep the simulations tractable, 160 satellites (approximately one-fiftieth of AFSPC's catalog) were modeled. The sites of the SSN can typically track 50 objects simultaneously. The simulations modeled sites with the ability to track only one satellite at a time. This way, satellites would be tracked about as frequently as if a full-size catalog was modeled with sites tracking 50 satellites simultaneously. This provides realistic orbit estimation accuracy.

The simulation portion of the thesis was broken down into three phases. The objective of the first phase was to verify the concept of a large-scale simulation and to verify the computer code used. Several different sets of orbits were simulated to observe the response of the orbital estimation process in different altitude regions. The second phase was aimed at increasing the accuracy of the covariance matrices through the use of a fading memory filter. Phase three investigated the orbital estimation performance under conditions of unpredictable solar and atmospheric activity. This chapter describes the development of and the results of the three phases.

## 6.2 Phase One

The simulations of phase one amounted to the propagation of 160 satellites through several days. Radar sites tracked the satellites according to their priority, and compressed the observation tracks into state vectors with covariance matrices. These compressed tracks were used to estimate the orbits multiple (typically five) times daily. The estimates were kept in a catalog, propagated forward in time and used for the prioritization of the next tracking period. Each of the major portions of the simulation is detailed in the following sections.

**6.2.1 Orbits Modeled.** Orbital elements and drag parameters were randomly generated to provide a mix of different types of realistic orbits. The orbits were typically low-Earth, nearly circular orbits. Equations ( 6.1 ) were used to determine the elements. The term *random* signifies a randomly generated number between zero and one. The term *Gaussian* signifies a randomly generated number obeying a Gaussian distribution with an average value of zero and a variance of one. The minimum radius was set at 200 kilometers to prevent the generation of orbits that dipped too far into the atmosphere.

$$R_1 = \frac{\text{Abs}(\text{Gaussian})}{10} + \text{Minimum Radius} \quad (6.1)$$

$$R_2 = \frac{\text{Abs}(\text{Gaussian})}{10} + \text{Minimum Radius}$$

$$A = \frac{R_1 + R_2}{2}$$

$$\text{ecc} = \text{Abs} \left( \frac{R_1 - R_2}{2 A} \right)$$

$$\text{inc} = \text{Mod} \left( \text{Abs}(\text{Gaussian}) \times \frac{\pi}{4}, \pi \right)$$

$$\Omega = \text{random} \times 2\pi$$

$$\omega = \text{random} \times 2\pi$$

$$v = \text{random} \times 2\pi$$

$$B^* = \text{Abs}(0.055 + 0.05 \text{ Gaussian})$$

where A is the semi-major axis

ecc is the eccentricity

inc is the inclination

$\Omega$  is the longitude of the ascending node

$\omega$  is the argument of perigee

v is the true anomaly

B\* is the ballistic coefficient

These formula provide for a range of semi-major axes and eccentricities which do not allow the satellites' orbits to intersect the Earth's surface. They provide a range of inclinations, mostly less than  $45^\circ$  but possibly as high as completely retrograde. The next three elements are all angles randomly distributed between zero and  $360^\circ$ . Finally, the radius and ballistic coefficient formulas were varied to allow the study of different ranges of perturbation effects, but always retained the same basic form as above. The elements of a set of 160 satellites generated from equations ( 6.1 ) and used during a typical simulation are shown in Figures 6-1 through 6-9 and listed in a table as Appendix G.

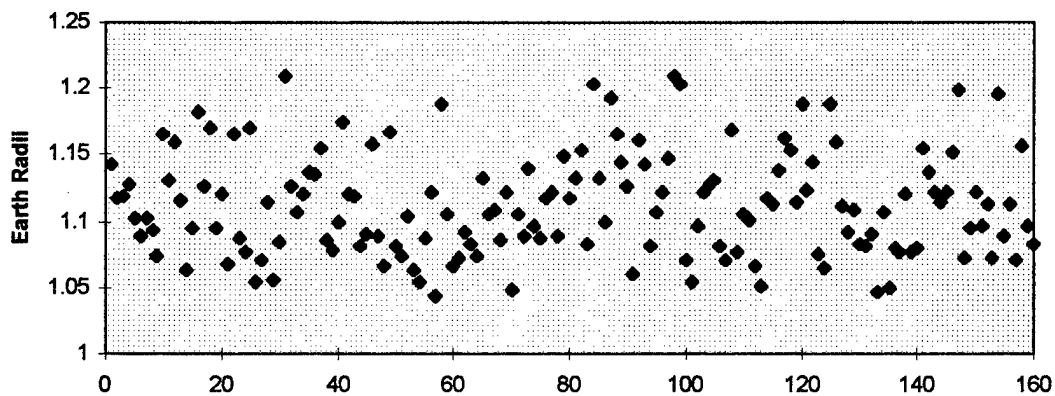


Figure 6-1 Semi-Major Axis

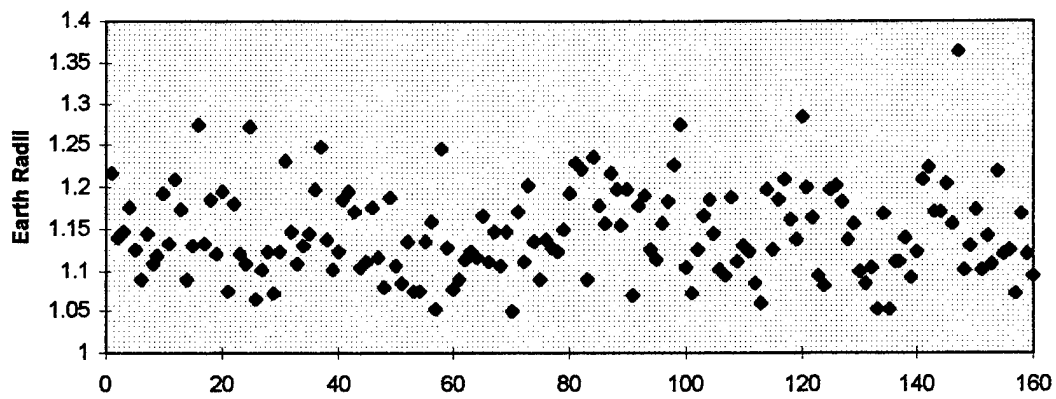


Figure 6-2 Radius of Apogee

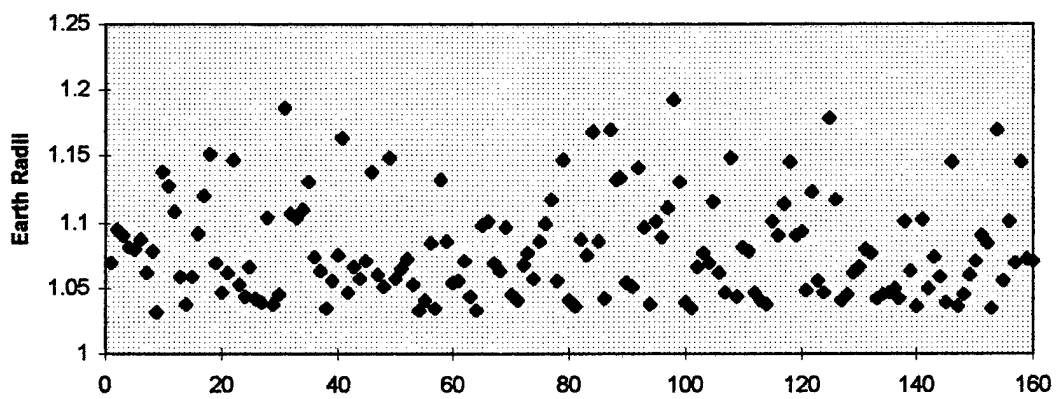


Figure 6-3 Radius of Perigee

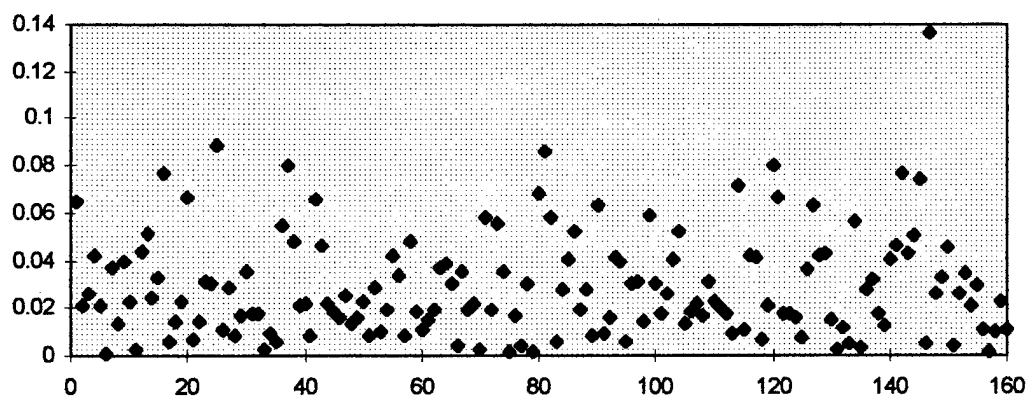


Figure 6-4 Eccentricity

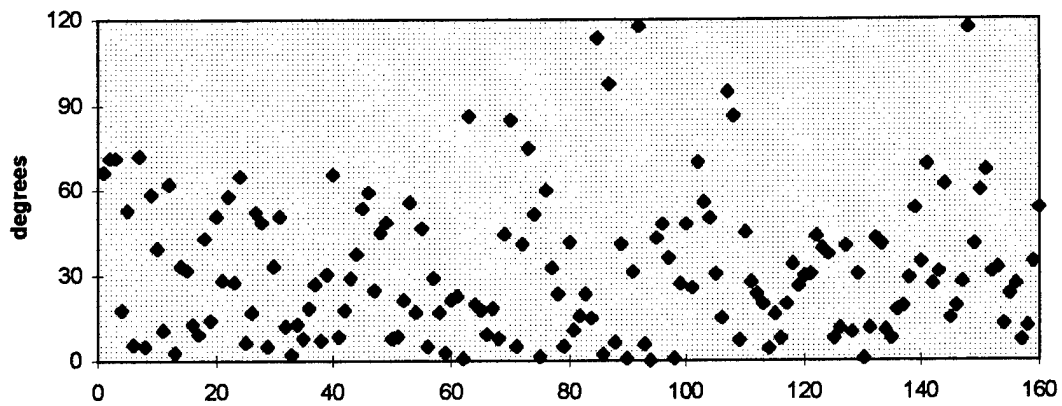


Figure 6-5 Inclination

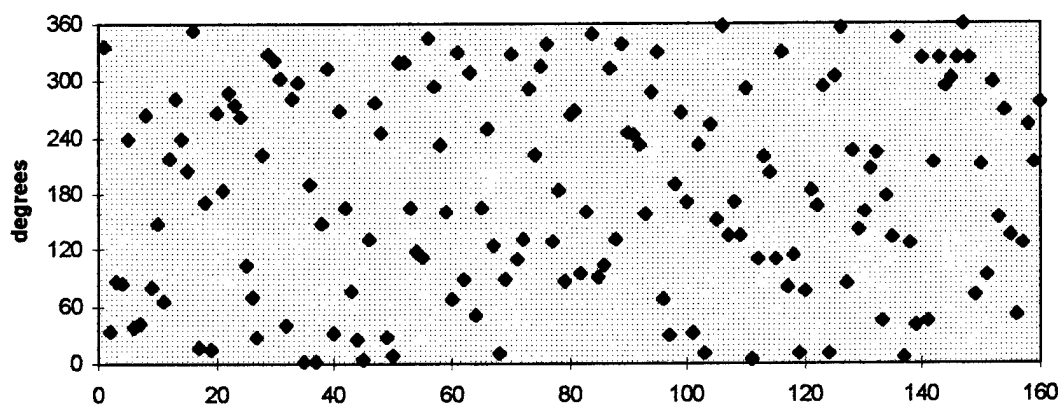


Figure 6-6 Longitude of the Ascending Node

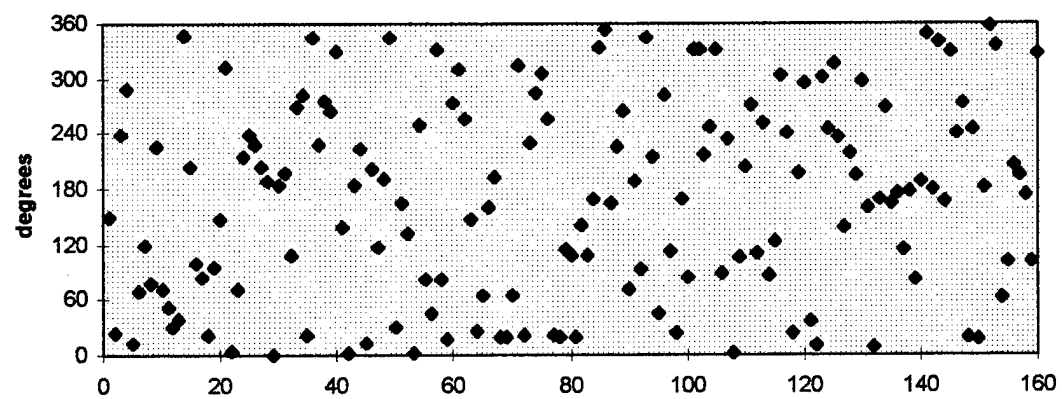


Figure 6-7 Argument of Perigee

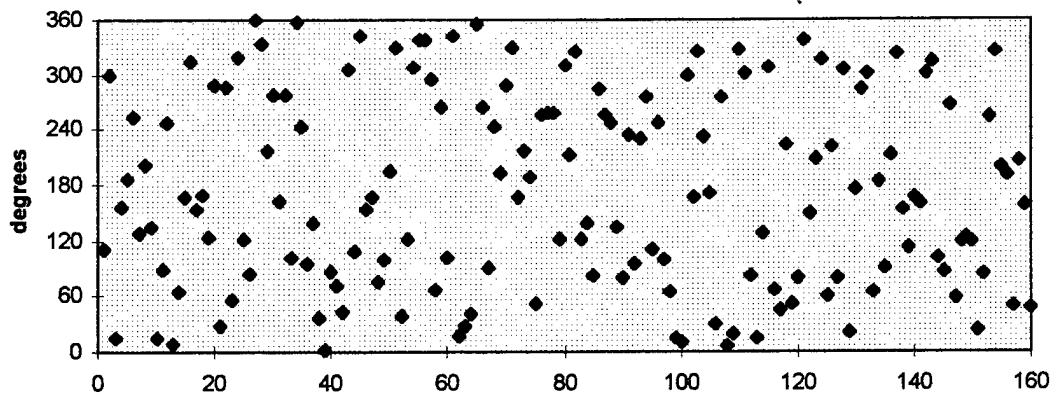


Figure 6-8 True Anomaly

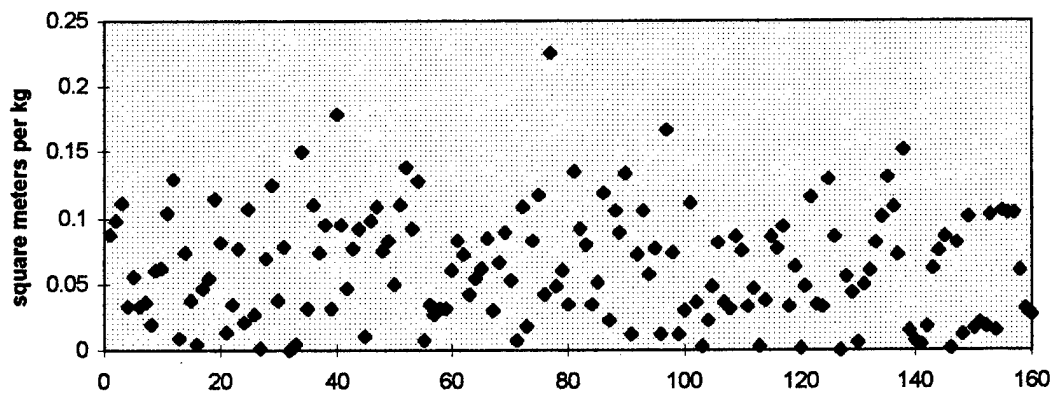


Figure 6-9 Ballistic Coefficient

6.2.2 *Propagation.* After the elements were randomly generated, the corresponding seven-element state vectors were determined using the method described in section 2.5 of Bate, Mueller and White. [1] The satellites' orbits were then propagated through one time period. Usually, this period was one-fifth of a day. In one case, the length was doubled. All 160 satellites in the catalog were propagated simultaneously. The radar sites tracked the satellite in view with the highest priority. The prioritization scheme will be described in section 6.2.8. Observation data was generated using the method described in chapter three.

Additionally, four more zonal harmonics,  $J_3 - J_6$ , were included in the truth model. The development of the equations of motion due to these effects proceeds identically to that of  $J_2$  shown in equations ( 3.6 ) through ( 3.8 ). This lengthy development is provided in Appendix B.



6.2.3 *Track Compression.* Whenever the satellite being actively tracked by a site set (passed below the local horizon of the site) the track compression program was called to compress the observations into the same type of state vector and covariance matrix described previously. The integrator method of track compression was again used for the simulation.

6.2.4 *Global Estimate.* After the propagator had generated observation data for one period, and the track compression subroutine had compressed all of this data into state vectors and covariance matrices, the *Global Estimate* method of orbit estimation was applied to each of the 160 satellites. The results of *Global Estimate* were retained as the catalog. This included the reference time, the seven-element state vector and the 49 by 49 element covariance matrix.

6.2.5 *Bayes Filter.* For the second and subsequent estimations, a slightly different method of orbit determination was required. The method chosen is the Bayes filter described in chapter two. This is identical to the least squares method, except that the results of a previous estimate are used as both the initial reference trajectory and as an observation to be processed. This observation differs from the others only in the level of accuracy and the inclusion of the drag parameter. The Bayes filter produces the same type of state vector and covariance matrix as *Global Estimate*.

The observation matrix for the Bayes filter is different when using the previous estimate as a piece of data. In this case, the matrix is a seven by seven identity matrix. The instrument covariance matrix now becomes the seven by seven covariance matrix of the previous estimate. The state vectors and covariance matrices for the remainder of the data (from the newly compressed tracks) are handled exactly as described in the *Global Estimate* method.

6.2.6 *Update Satellite.* After the *Global Estimate* or Bayes filter method of orbit estimation has been applied to all 160 satellites, the catalog is updated to the end of the propagation cycle. This is required because the two estimation processes provide results for each satellite at the same reference time as each satellite's last track compression. At the end of the estimation portion of the cycle, the propagator is at the end of the cycle time, but the estimates in the catalog are at the various reference times of the track compressions. The update satellite portion propagates the state vector and covariance matrix for

each satellite from its catalog reference time to the same reference time as the simulator, which is the end of the one-fifth day period.

*6.2.7 Truth Catalog Comparison.* Once the catalog of estimates has been propagated to the end of the cycle, it is compared to the truth data. For each satellite, each element of the vector is compared to determine the true error in the prediction. The results of this comparison are the key output desired from the simulation.

*6.2.8 Prioritize.* At the completion of each cycle, the satellites are reprioritized. Each covariance matrix is propagated to the end of the next cycle to determine how big the covariance would become if no estimates occurred during the next cycle. The satellites are rank ordered based primarily on covariance matrix size, but also predicted satellite reentry is taken into account and given high priority. If a satellite's orbit has not been successfully estimated, it is not propagated. Instead, that satellite is also assigned a high priority.

*6.2.9 Output.* The simulator produces several output files at various points of the cycle. A log file is kept which keeps track of when each process is started and stopped, the significant results of some processes and error messages generated during execution. At the end of the propagation phase, the catalog of truth data is recorded. At the end of the estimation phase, the catalog of estimates is recorded. At the end of each cycle, a file is generated recording the differences between the true state vectors and the estimated state vectors. These differences are also normalized by the associated covariance element and recorded. These files combine to provide a detailed record of the simulation.

*6.2.10 Simulation Robustness.* Several pieces of code were specifically modified to prevent program crashes during long-term simulations. The majority of these modifications were designed to prevent the attempted propagation of a satellite through regions of the atmosphere too low to be effectively described by the atmospheric model. These modifications included preventing a compressed track of data from being used as the initial reference trajectory during a *Global Estimate* run if the track of data was too short and hence not of sufficient accuracy. Additionally, ballistic coefficients were checked after each iteration to ensure they were not so far out of range that the satellite would reenter or escape during the

next iteration. After convergence, the resulting ballistic coefficients were again checked against a more stringent window. This prevented such obvious anomalies as negative values. Additionally, code was added which watched for an iteration that was diverging. If three successive corrections to the state vector each increased in magnitude, the estimation was postponed until more data was available (the next cycle). Round-off error occasionally causes a diagonal element of a covariance matrix to become negative. Theoretically, this could never happen, and the elements are assumed positive at several points in the simulation where the square root of the element is needed. To prevent crashes, the diagonal elements were monitored to ensure that no attempt was made to evaluate the square root of a negative covariance element.

By adding code to prevent crashes, and by recording frequent data files for restarting in case it did crash, the simulation code was made quite robust. As a result, simulations can be run spanning several weeks, with no loss of data.

### *6.3 Phase One Results*

The objective of phase one was to verify the integration of the various algorithms used previously in the thesis. Additionally, research objectives included evaluating the effect of varying levels of atmospheric drag on the ability to estimate the orbits of the catalog, and the use of different periods for the propagate-estimate-update cycle. The elements for the first simulation were generated using equations ( 6.1 ). The elements generated are shown in Figures 6-1 through 6-9 and listed as Appendix G. The simulation was run for two days.

The key parameters monitored during each simulation will now be described. First, the number of satellites whose orbits have been estimated is tracked. This parameter is reported as a fraction of the size of the current catalog. The size of the catalog changes with time as some satellites' orbits will decay to reentry. These satellites are then removed from the catalog and their statistics are no longer relevant. The number of satellites removed due to reentry is reported as a percentage of the original size of the catalog. The number of satellites whose positions are predicted within one kilometer of their true

positions is tracked. This parameter is reported both as a fraction of the catalog, and as a fraction of the number of estimated satellites. Obviously, after every satellite in the catalog has been estimated, these two descriptions become identical. Finally, a covariance accuracy parameter is tracked. The covariance matrices computed at each cycle should statistically match the actual estimation accuracies according to the three-dimensional Gaussian probability distributions. This states that approximately 19.9% of the actual error vectors should lie within the one-sigma error ellipsoid reported as the diagonal elements of the covariance matrices. The number of position error vectors that lie within their respective one-sigma error ellipsoids is reported as a fraction of the number of estimated orbits. If the dynamics were perfectly described by all of the estimation algorithms used in the orbit estimation process, then we would expect that this parameter would average around 19.9%. However, since the dynamics used by the truth model are not perfectly modeled by the estimator algorithms (as in real life) the actual errors may be much larger. These five percentages are all plotted at the completion of each cycle. These same parameters are used to show the results of most of the simulations in the thesis. Figure 6-10 shows the results of the first simulation.

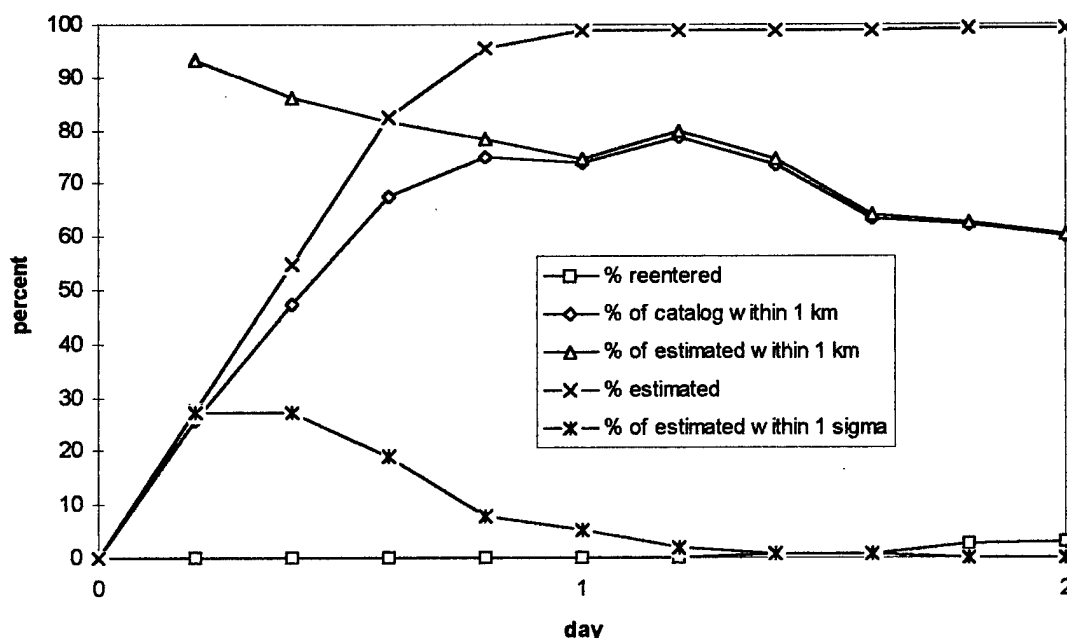


Figure 6-10 Simulation One Results

Over the two-day period, five satellites reentered, all satellites' orbits were estimated, and at one point, nearly 80% of the catalog was estimated within one kilometer. However, the accuracy of the estimations decayed. By the end of the second day of tracking, this parameter was down to 60% and was still falling. Additionally, the covariance matrices computed were far too optimistic. This manifests itself in the decay of the % of estimated within one sigma parameter to zero. Both of these problems are caused by differences in the dynamics of the truth model and the estimator models.

The next set of orbits was generated to observe increased drag effects. The following two figures show the altitudes of perigee and ballistic coefficients used in simulation two.

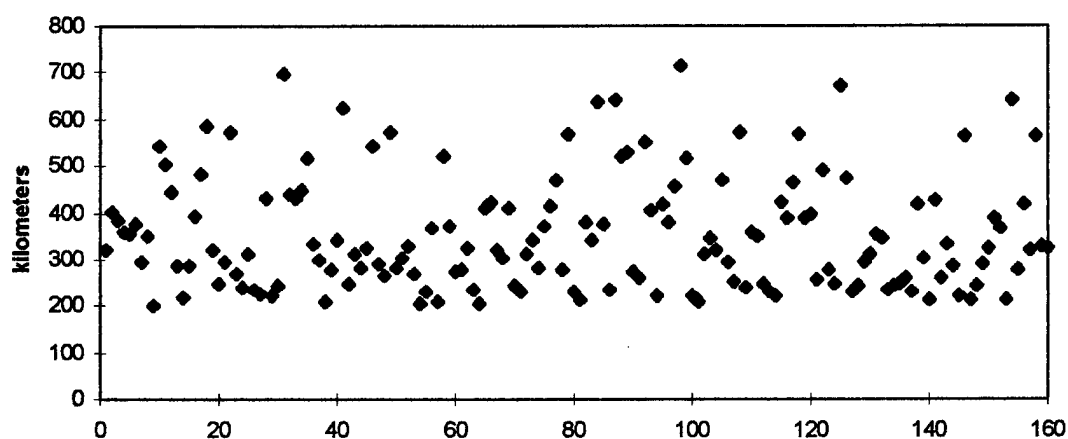


Figure 6-11 Altitude of Perigee -- Simulation Two

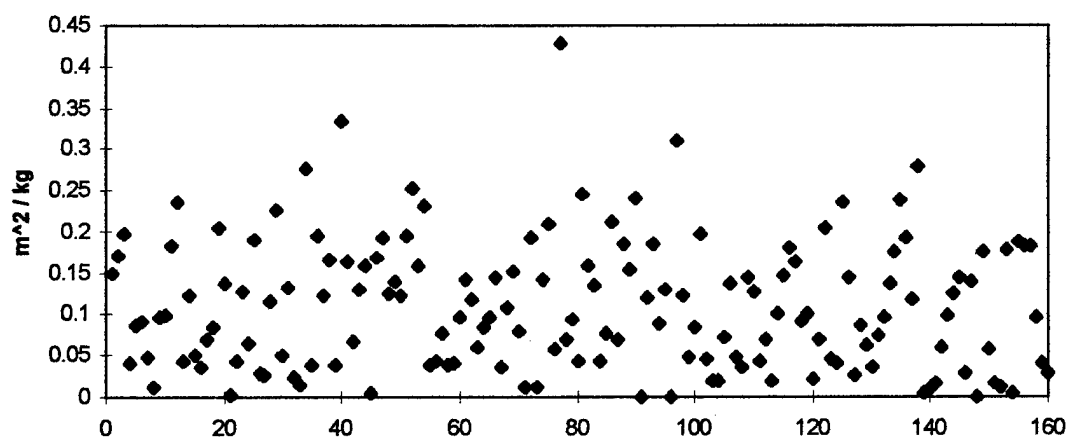


Figure 6-12 Ballistic Coefficient -- Simulation Two

The lower altitudes and increased ballistic coefficients were expected to increase the number of satellites which reentered and decrease the accuracies of the reported covariance matrices. Figure 6-13 shows the actual results observed.

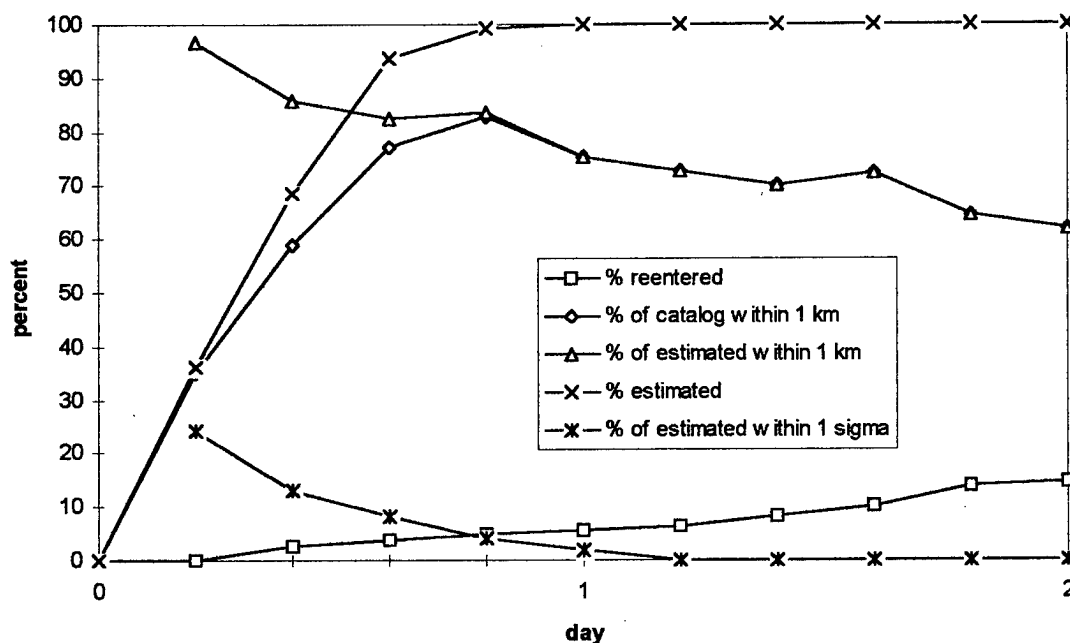


Figure 6-13 Simulation Two Results

As expected, more satellites reentered during the two day period, and the accuracy of the covariance matrices dropped dramatically. The accuracies of the estimates did not change substantially over simulation one, despite the increased drag. This is likely because many of the satellites with more drag have reentered by the end of the second day, thus they are not included in the % *within 1 km* parameters. Also, the lower orbits allow more frequent observation opportunities, which improves the estimations.

The next set of orbits was generated to see the effects of the estimation process for higher altitude satellites. The same ballistic coefficients as simulation one were used. These same ballistic coefficients were used for all other simulations of all three phases as well. The altitudes of perigee are shown in Figure 6-14.

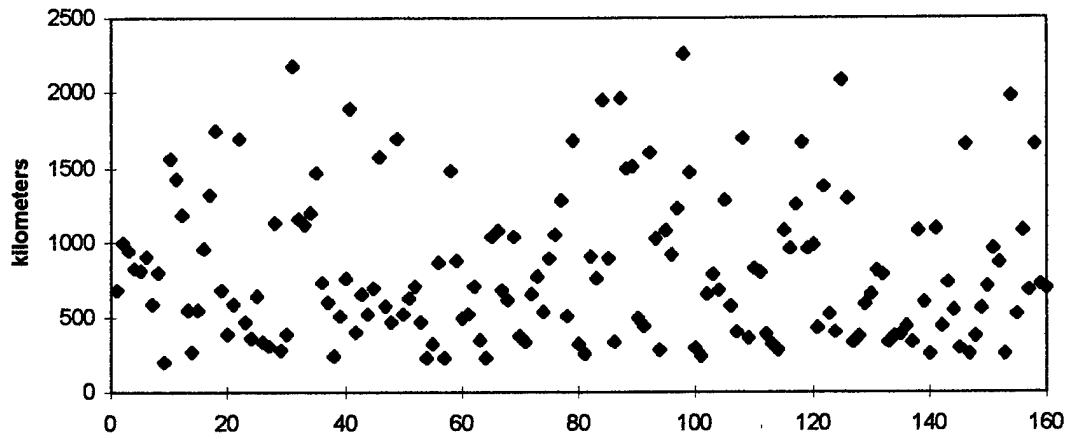


Figure 6-14 Altitude of Perigee -- Simulation Three

This simulation was expected to be less accurate than the previous two, as less frequent tracks of observations are recorded. A decline in reentries was also expected.

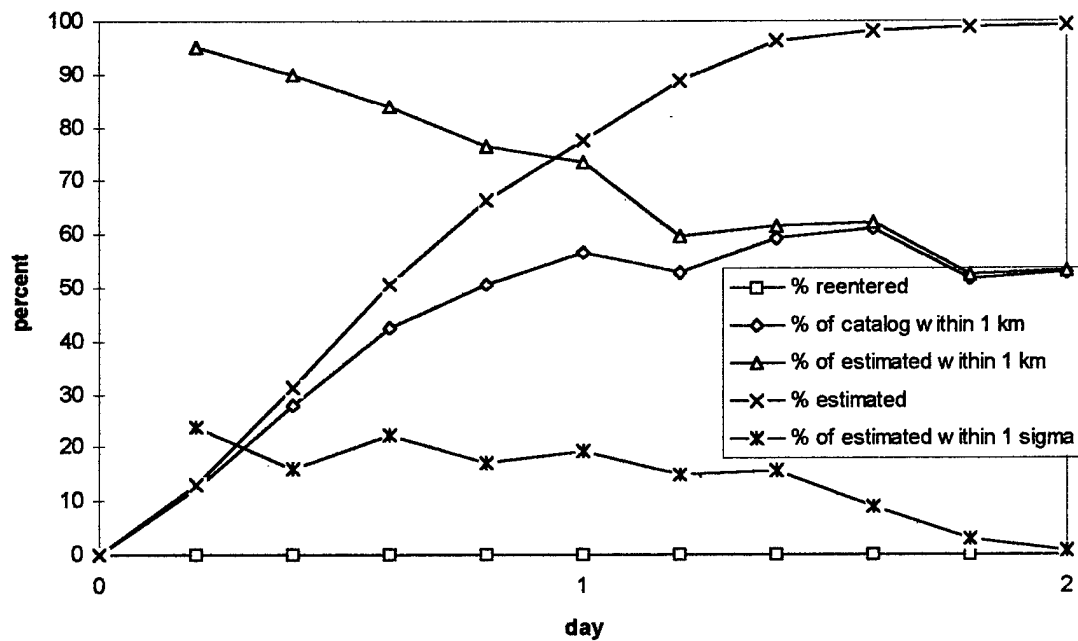


Figure 6-15 Simulation Three Results

During the two day simulation, no satellites reentered, and it took the full two days to estimate every orbit. This is because of the lower frequency of observation tracks. Also, the average accuracy was lower, but not significantly.

The next simulation was designed to show the effect of increased cycle period. Instead of the propagate-estimate-update cycle running over one-fifth day periods, it was extended to two-fifth day periods. All other parameters were the same. Figure 6-16 shows the results.

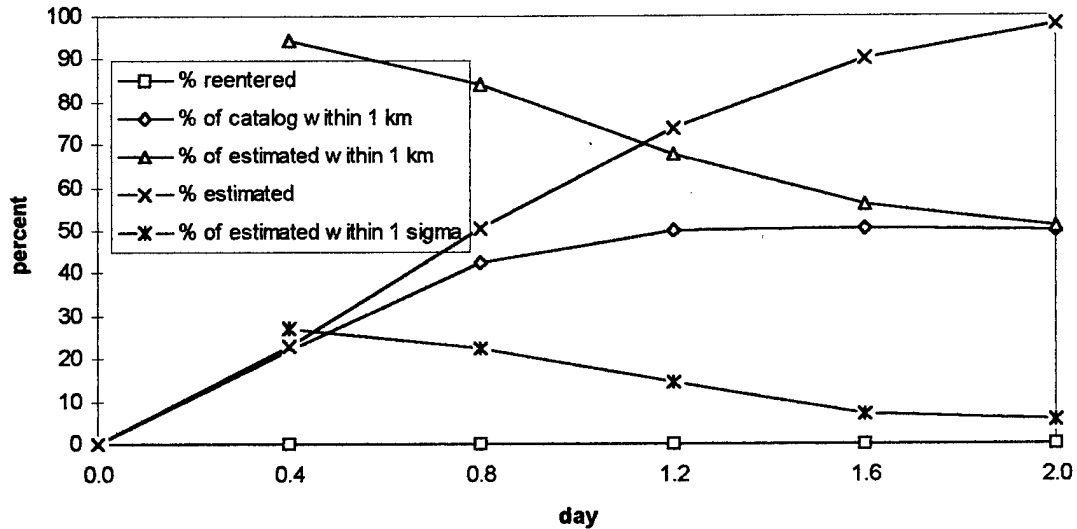


Figure 6-16 Simulation Four Results

The parameter trends are basically the same, indicating that the period is not much of a factor in determining the accuracy of the estimates or of the covariance matrices.

The fifth simulation, the final simulation of phase one, modeled orbits substantially higher than simulations three and four. The size of the orbits stretched to nearly three Earth radii, as shown by the perigee altitudes in Figure 6-17.

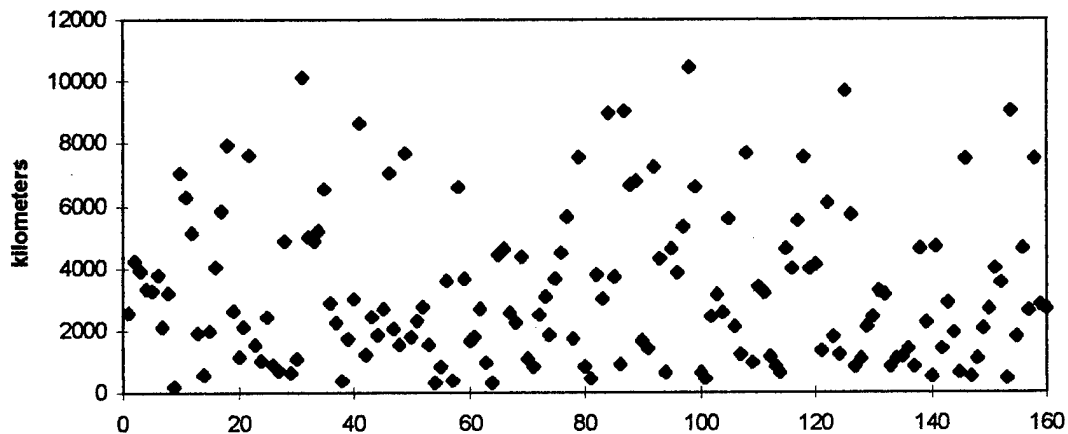


Figure 6-17 Altitude of Perigee -- Simulation Five



Because it took much longer to estimate a substantial portion of the catalog, the simulation was run for three days instead of the usual two. Figure 6-18 shows the results.

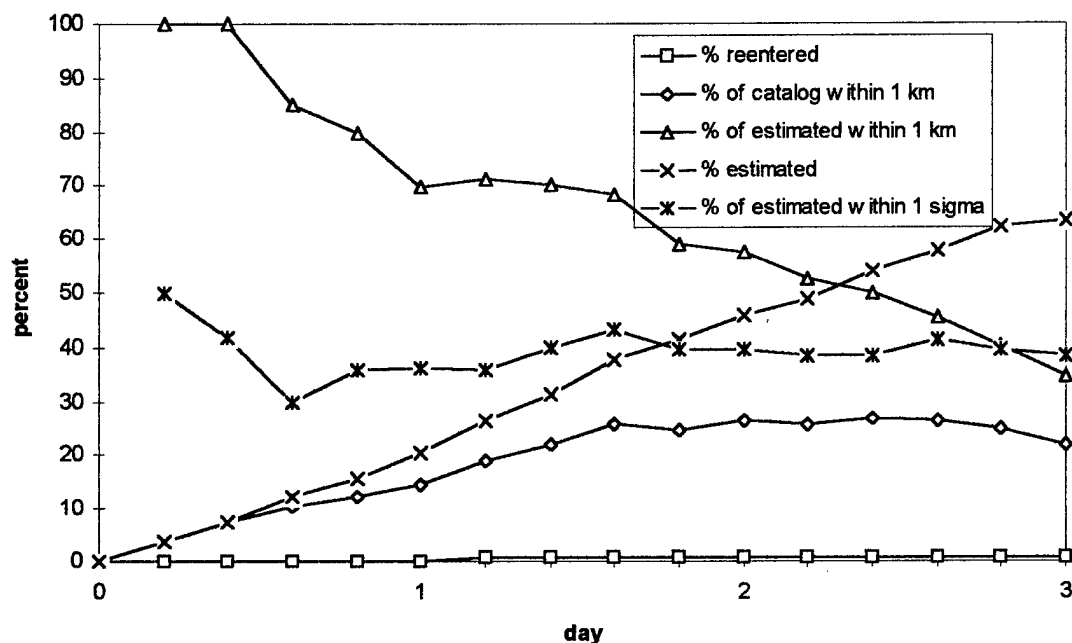


Figure 6-18 Simulation Five Results

After three days, the accuracy of the catalog seemed to have peaked and began a decline, so the simulation was terminated despite having only estimated 101 satellites.

The first phase of the simulation showed that the different software components worked together as expected. The various parameters behaved as expected. Thus, having achieved the objectives of phase one, the next phase was entered.

#### 6.4 Phase Two

The objective of phase two was to increase the accuracy of the covariance matrices. Because the dynamics models of the track compression and orbit estimation algorithms differ from that of the truth model, the actual orbit estimations are not as accurate as reported. This was seen in the majority of the phase one simulations. The covariance matrices must be accurate if they are to be used operationally to provide a confidence level for the estimates. As described in chapter two, a fading memory filter is one way to attack this problem. A fading memory filter allows the estimator to place less weight on older data

and also allows the update portion of the cycle to increase the size of the covariance matrices with time, thus making them more realistic. This requires the determination of a set of coefficients to use as the diagonals of the  $\beta$ -matrix. Phase two of the simulation was devoted to determining the correct values to use for the seven coefficients.

Assumptions were made as to the structure of the  $\beta$ -matrix. The same value was used for the first six coefficients and a value of one was used for the seventh. This amounts to full remembrance of the ballistic coefficient information, and equal remembrance of each of the other state elements.

### 6.5 Phase Two Results

The first value used (for the first six elements) was 0.93. This equates to a data half-life of about nine and one-half days. The same orbital elements and ballistic coefficients used for simulation one were used for all of phase two. The results of simulation six (with  $\beta = 0.93$ ) are shown in Figure 6-19.

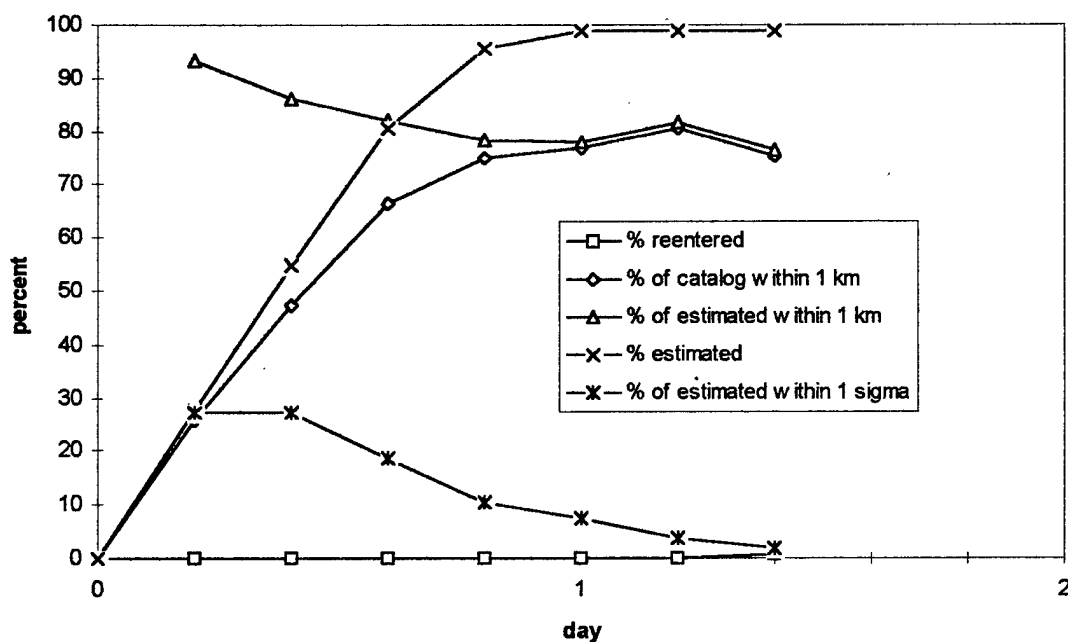


Figure 6-19 Simulation Six Results

After 1.4 days, the simulation was stopped. The figure clearly shows that the value of 0.93 is too large, i.e. a lower value should be used to allow the estimator to reduce the weight of the older data even more.

The next value attempted was 0.90. This corresponds to a data half-life of approximately 6.6 days.

Figure 6-20 shows the results.

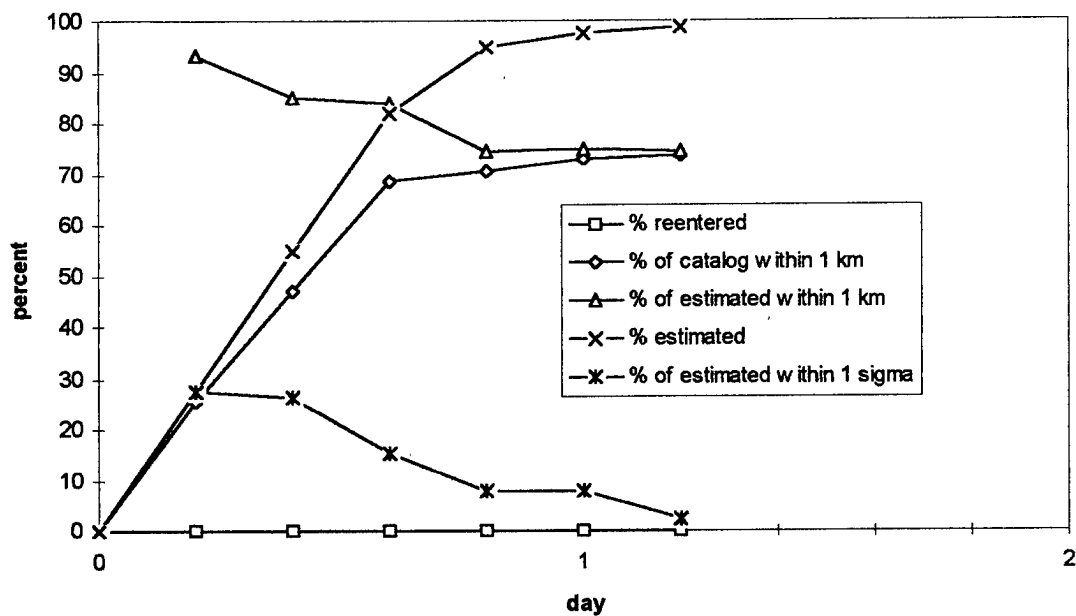


Figure 6-20 Simulation Seven Results

Again, the value of 0.90 is still too high. The third attempt was with a value of 0.85 corresponding to a data half-life of 4.3 days. Figure 6-21 shows these results.

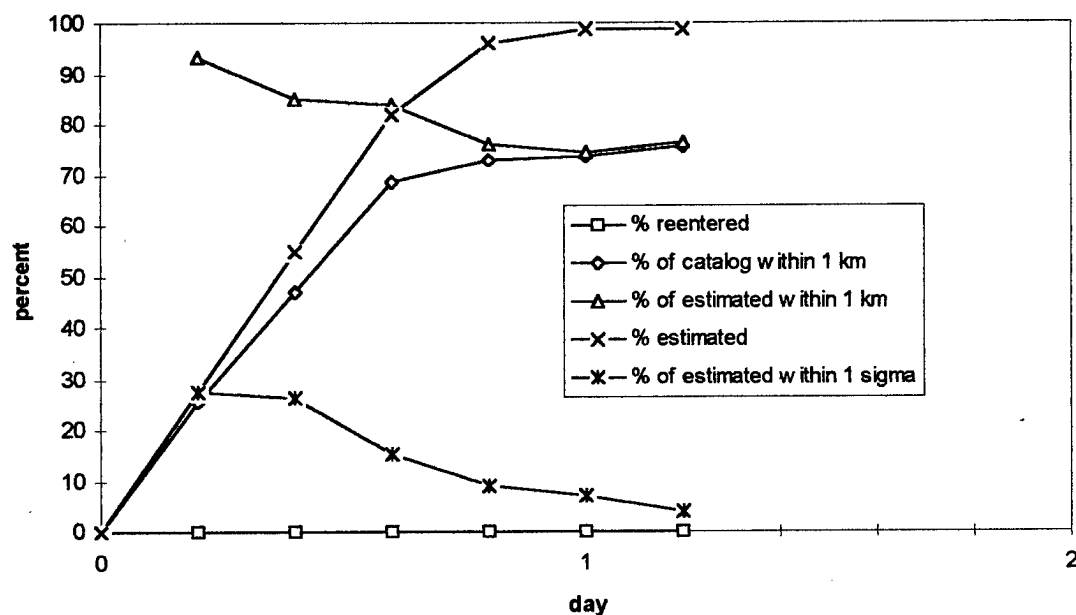


Figure 6-21 Simulation Eight Results

The value of 0.80 was still too high. The next figure shows the results when the value of 0.50 was tried.

This extreme case corresponds to a half-life of only one day.

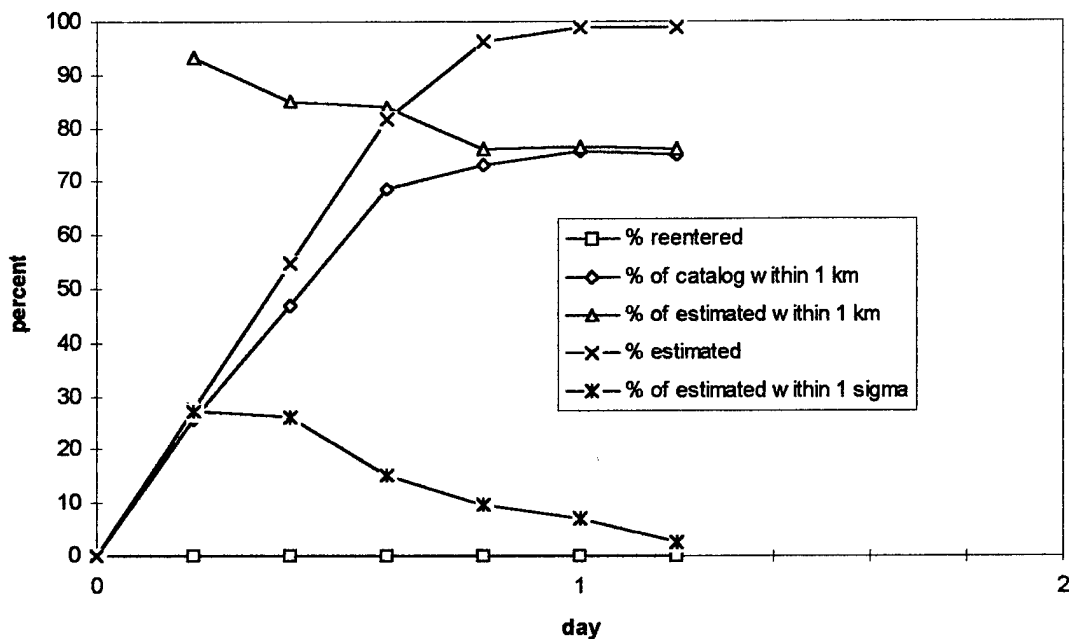


Figure 6-22 Simulation Nine Results

After simulation nine was stopped, a new approach was evidently required. The covariance matrices were far too optimistic, even with an extreme fading memory filter. Additionally, the estimates themselves were not as accurate as expected. The suspected cause of both of these problems was the additional dynamics of the truth model. The estimator should be able to maintain a high degree of accuracy even without all of the dynamics included in the truth model, as long as the additional dynamics do not introduce a systematic error. The truth model can even include a random acceleration to model a stochastic system, and the estimator should still produce good estimates. The suspected problem in this case was the inclusion of the additional zonal harmonics in the truth model. Additional harmonics will cause the orbital period to decrease very slightly. For this estimator, the size of the orbit is being determined so precisely that this small change in period is noticeable. If this were the cause of the problems, then the actual errors would likely lie in the direction of the velocity vectors. To investigate this possibility, the following plots were generated to show the component of each actual error vector, after one day of propagation, resolved along three different axes. The first figure shows the fraction of

each error vector which lies in the direction of the corresponding velocity vector. The second shows the fraction resolved along the radial direction. The third shows the out of plane fraction. These were determined by taking the dot product of each error vector with a unit vector in each of the three directions. Because the orbits are not perfectly circular, the three directions are not orthogonal. Nevertheless, the three figures show a very clear trend.

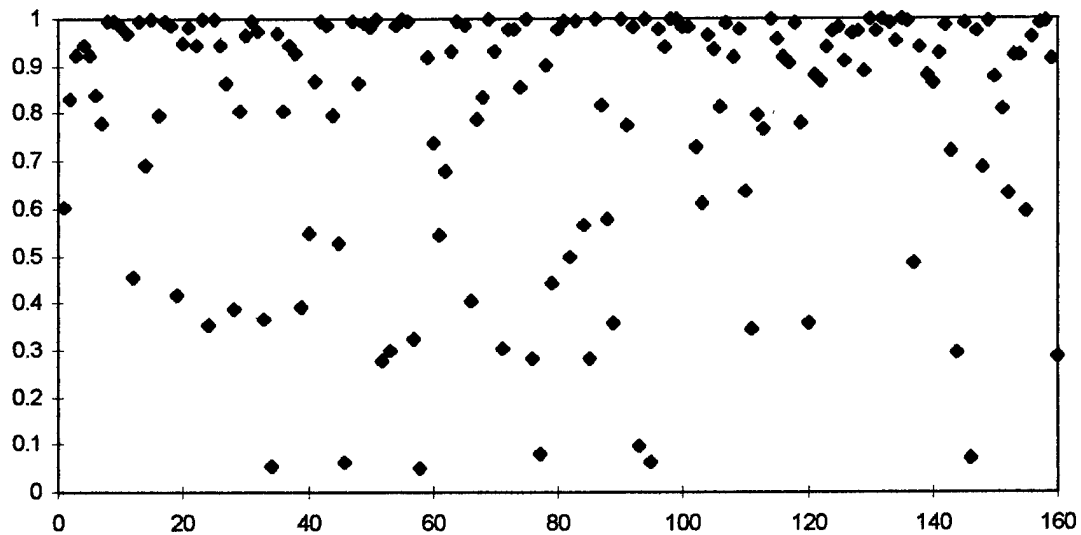


Figure 6-23 In-Track Error Components

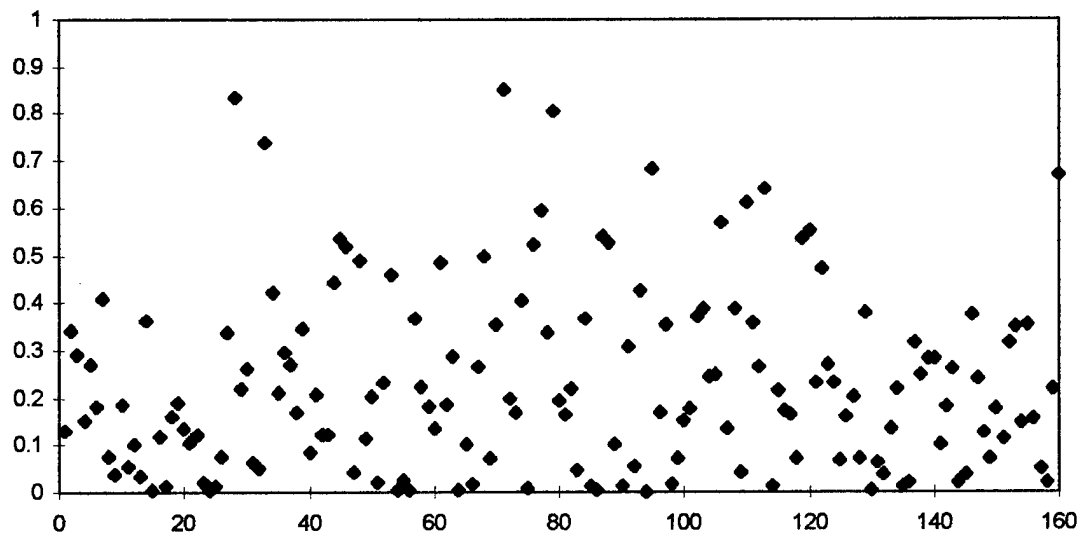


Figure 6-24 Radial Error Components

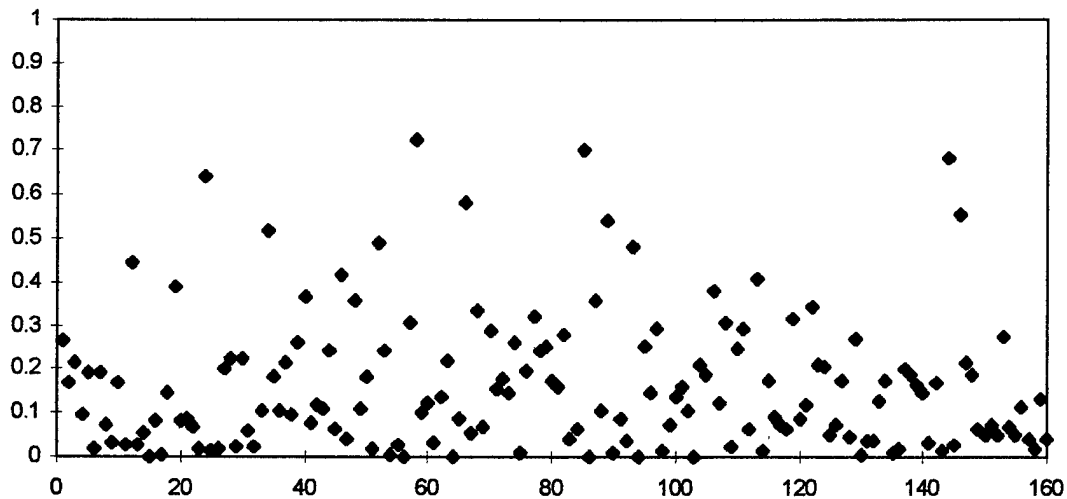


Figure 6-25 Out-of-Plane Error Components

These figures clearly show that the majority of the errors lie in the in-track direction. The vast majority were caused by the satellite's position being estimated behind its actual position. This indicates that the inclusion of the additional zonal harmonics introduced a systematic error into the estimation process. To prove that the zonal harmonics were indeed the source, an additional simulation was completed with the  $\beta$ -coefficient set to one (full remembrance of all elements) and the values for the additional zonal harmonics ( $J_3$ - $J_6$ ) set to zero in the truth model. Figure 6-26 shows these results.

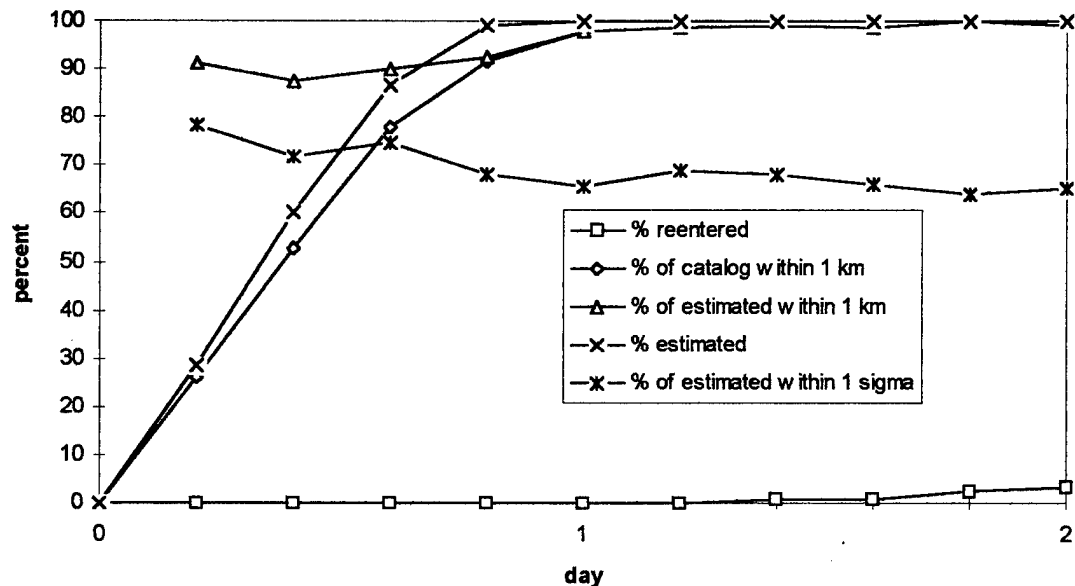


Figure 6-26 Simulation Ten Results

Based on Figure 6-26, it was decided that the estimator was accurate enough to see the effect of the additional harmonics. These harmonics introduced a systematic error. This raised a very important point in the effectiveness of this entire process of orbital estimation. All sources of systematic errors must be determined and included in the estimator dynamics model. For phase three, the zonal harmonic coefficients were left at zero in the truth model to remove their effect. In an operational environment, the estimator model should include a much more accurate geopotential model. In fact, any source of systematic, as opposed to random, error should be included. These are typically deterministic in nature and their inclusion is not particularly difficult. For example, luni-solar effects might become significant in an operational orbit estimator. These effects are easily predicted and would be included in the estimator's dynamics model.

The objective of phase two was to increase the accuracy of the covariance matrices. This objective was achieved, although not through the use of the fading memory filter as expected. Instead, the dynamics of the truth model had to be modified to more closely match those of the estimator. This is not the most desirable situation, however, the effects of the additional zonal harmonics could be included in both models. Since these effects are completely deterministic, they would not significantly change the results.

### *6.6 Phase Three*

The first two phases used an atmospheric model which was identical in both the truth model and the estimator model. In reality, nearly all orbital perturbations can be predicted except for air drag. This is because the atmospheric density varies quite significantly both spatially and temporally. Solar heating, solar flares, geomagnetic storms and local atmospheric weather all affect the local density at any given time. These effects are largely unpredictable, leading to inaccurate atmospheric density models. To model real world effects, phase three of the simulation included a different atmospheric model in the dynamics of the truth model. The estimator dynamics remained the same. This allows for a more

realistic simulation of the actual results which could be expected from the use of the orbital estimation process with real data.

The original atmospheric model described in Appendix A produces a local density based on the altitude and the sea-level atmospheric pressure. By varying the sea-level pressure, slightly different densities are calculated. The variation of this pressure is the basis for the alterations of the atmospheric model of phase three. Three different effects were modeled.

An investigation of more accurate models led to altering the sea-level pressure by  $\pm 25\%$  to allow day-night density variations more in line with actual density profiles. [10, 14] This first effect modeled the atmospheric bulge caused by solar heating on the sunward side of the Earth. This was included in simulation eleven by increasing or decreasing the sea-level pressure by up to 25% depending on where the satellite was relative to the sun. For purposes of the simulation, it only matters that the bulge is in a consistent area relative to the Geocentric-Inertial reference frame. Therefore, the bulge was modeled in the positive direction of the I-axis. The amount of increase or decrease was based on the angle between the satellite's instantaneous position vector and the I-axis. By changing the dynamics of the truth model to provide this 25% variation, the simulation was made more realistic.

Additionally, because the density fluctuates because of other, unpredictable factors, an additional random variation was added. The sea-level pressure was changed by a random percentage following a Gaussian distribution. The standard deviation of this distribution is 5%. The third variation was not included in simulation eleven and will be discussed later.

Finally, because the more realistic atmospheric model was employed, an attempt was also made to generate a catalog of satellites with altitudes which more closely resembled those of the actual catalog. 84% of the objects in the actual catalog are over 800 kilometers in altitude. [4] The equations generating the catalog were modified to provide a distribution with 84% of the semi-major axes over 800 kilometers. The following histogram shows the new distribution of semi-major axes.



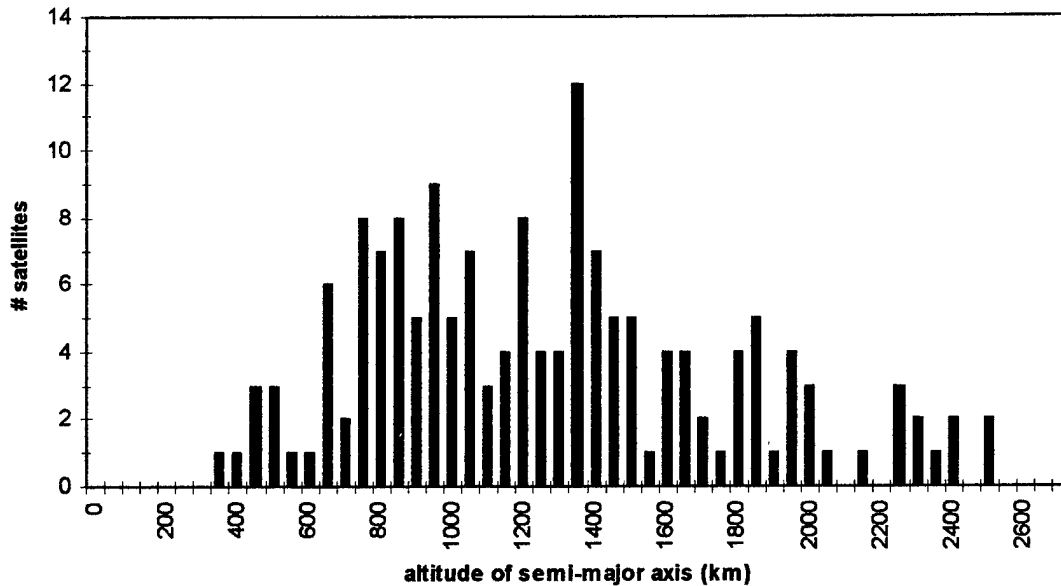


Figure 6-27 Phase Three Altitude Distribution

This distribution was used for all simulations of phase three.

Finally, a number of changes to the estimation algorithm were implemented to make the estimations more accurate. Among these changes was a check of the residuals after the orbit was estimated. If the residuals were unrealistic, the new solution was rejected. Additionally, the number of successive estimation attempt failures, for any reason, for each satellite was tracked. The priority of a given satellite was raised if the algorithm failed to estimate the orbit. This provides more tracks of data for the problem satellite during the next estimation attempt. Finally, if the Bayes filter failed to arrive at an accurate estimate with more than 30 new tracks of data, the previous estimate was dropped and the least squares batch estimator was used to provide a new estimate. If this was not successful, the oldest tracks of data would be dropped, one at a time, until the least squares estimator was successful, or until only 30 tracks of data remained. This prevents outdated data from causing failed estimate attempts when sufficient new data is already available to provide an accurate orbit determination.

### 6.7 Phase Three Results

Figure 6-28 shows the results of simulation eleven. Again, simulation eleven included a  $\pm 25\%$  variation in sea-level pressure representing the sunward bulge in the atmosphere and a random variation

with a Gaussian distribution of  $\pm 5\%$  standard deviation. The orbital elements were chosen to represent a realistic catalog, with 84% of the catalog above 800 kilometers in altitude.

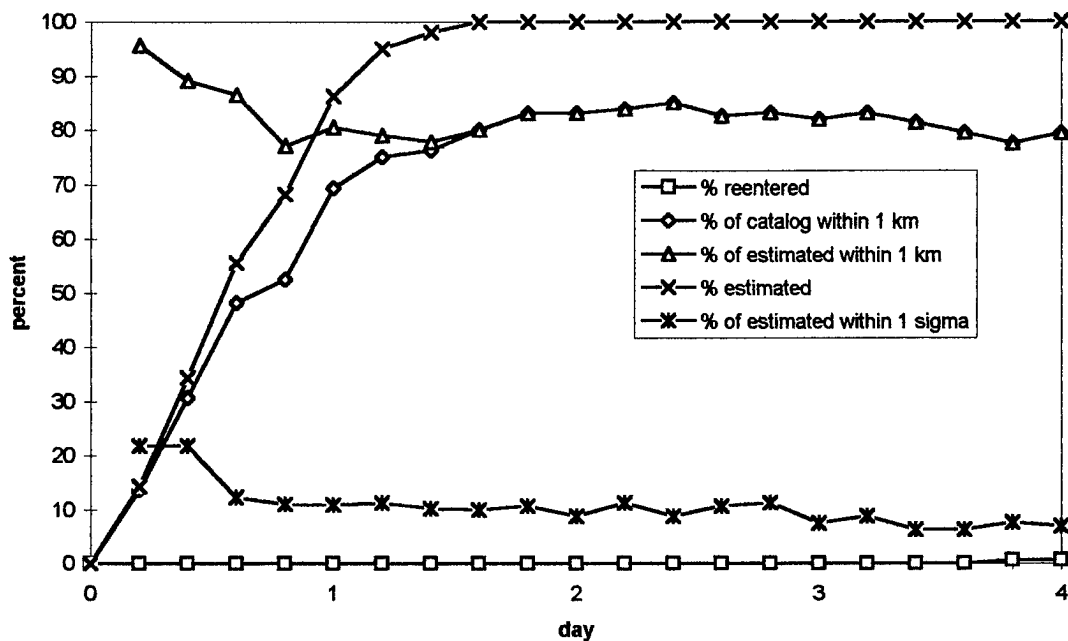


Figure 6-28 Simulation Eleven Results

Comparing this to Figure 6-26 shows that the variation in atmospheric density reduces the accuracy of the estimator. Although the density profile used in this simulation could be made more accurate, the important point is that the profile of the truth model is far more accurate than (and different from) the estimator model. Changing the truth model to make it more realistic would not change the results of the simulation. This figure attests to the fidelity with which the estimator can successfully determine orbits. During the simulation, the average error was as low as two to three kilometers at the end of a propagate-estimate-update cycle. AFSPC currently reports an average error of 12 kilometers as soon as an estimate is made. This indicates the estimator developed in this thesis is far more accurate than that currently operational.

Although Figure 6-28 indicates an improvement in estimation accuracy, the results were further analyzed to try to find a way to improve the accuracy even more. The individual errors of all 160 satellites were plotted as a function of time. Figure 6-29 shows the results for the first 15 satellites.

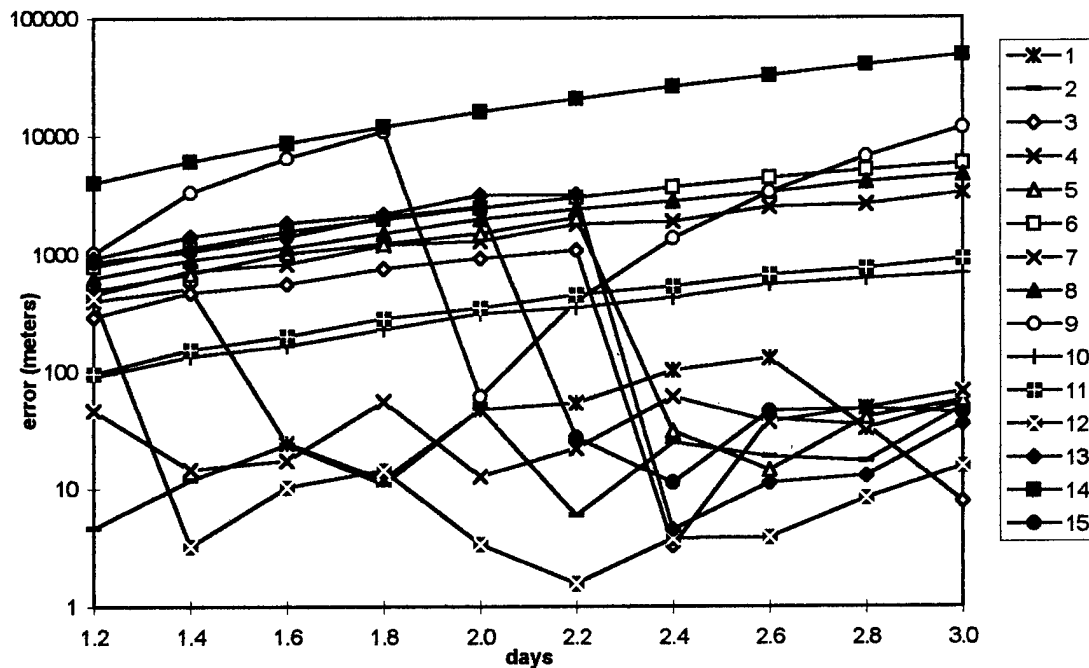


Figure 6-29 Individual Satellite Estimation Errors

A few low-altitude satellites contributed the vast majority of the error at each point in the simulation. Satellites nine and fourteen are two of these low altitude satellites, with altitudes of perigee of 194 and 265 kilometers, respectively. The large errors of these two satellites are obvious in this figure. The higher altitude satellites were estimated with much better accuracy. The accuracy of satellite nine only improved once during the ten cycles shown. This occurred when the orbit was estimated using the least squares batch estimator instead of the sequential Bayes filter. These results indicate that the low altitude satellites are too difficult to estimate because of the differences between the dynamics models of the estimator and the truth model.

To address this problem, a simulation was conducted using only the five satellites with the lowest altitudes of perigee and all nine tracking stations. This provided frequent tracks of data for the estimator. The goal was to see if a higher rate of tracking would allow for more accurate orbit estimation for the low-altitude satellites. This simulation was conducted for 1.4 days and the errors at each point were recorded. Figure 6-30 shows these errors.

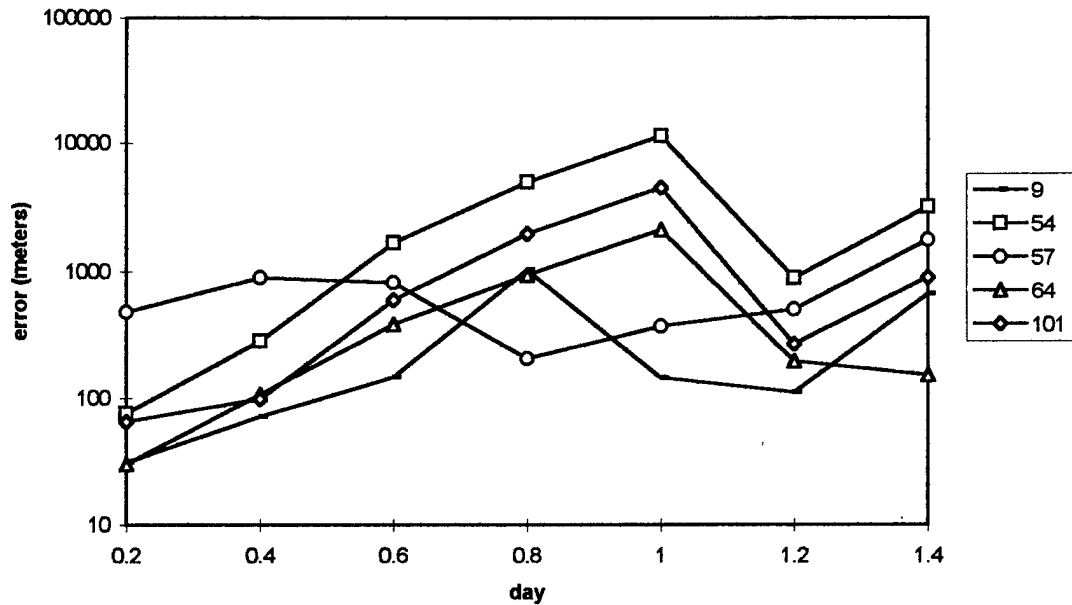


Figure 6-30 Low-Altitude Satellite Errors

This figure shows that, even if the entire tracking network were dedicated to tracking only these five satellites, the errors would still average as high as a kilometer or more. While this seems to indicate that further adjustments to the tracking priority would be futile, another useful fact can be taken from the results. The errors of three of the five satellites dropped dramatically after the 1.2 day cycle. This occurred because these three satellites' orbits were estimated using the least squares batch method instead of the Bayes filter. This indicates that the batch method is better suited to the low altitude satellites, where the changing atmospheric model makes the older data much less reliable.

This analysis was used to adjust the estimator algorithm in two ways. First the prioritization scheme was changed to place a higher priority on satellites with low altitudes of perigee. Second, satellites which have perigee altitudes below 350 kilometers are flagged as low-altitude satellites and their orbits are only estimated using the least squares batch method. These two modifications were aimed at improving the total accuracy of the estimated catalog.

After these modifications were implemented, another simulation was conducted to show the effects. All other parameters of the simulation were identical to simulation eleven. Figure 6-31 shows the results.

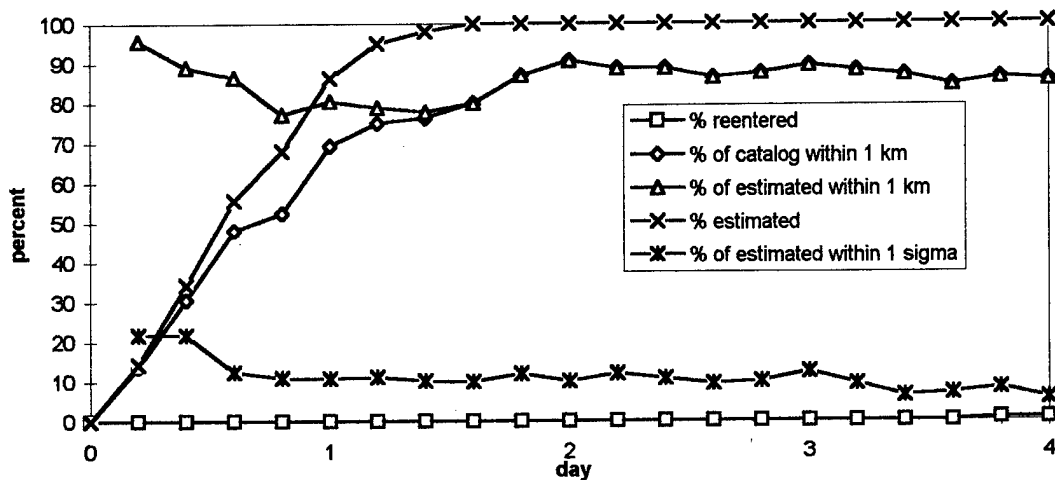


Figure 6-31 Simulation Twelve Results

This figure indicates that the modifications were successful in improving the accuracy of the catalog. Additionally, another set of parameters were tracked for this simulation. The following figure shows the average error and the median error in the catalog at the end of each cycle. The percentage of the catalog accurately estimated within one kilometer is plotted, as in the previous simulations. In this plot, however, the percentage within 100 meters, within ten meters and within one meter are also shown.

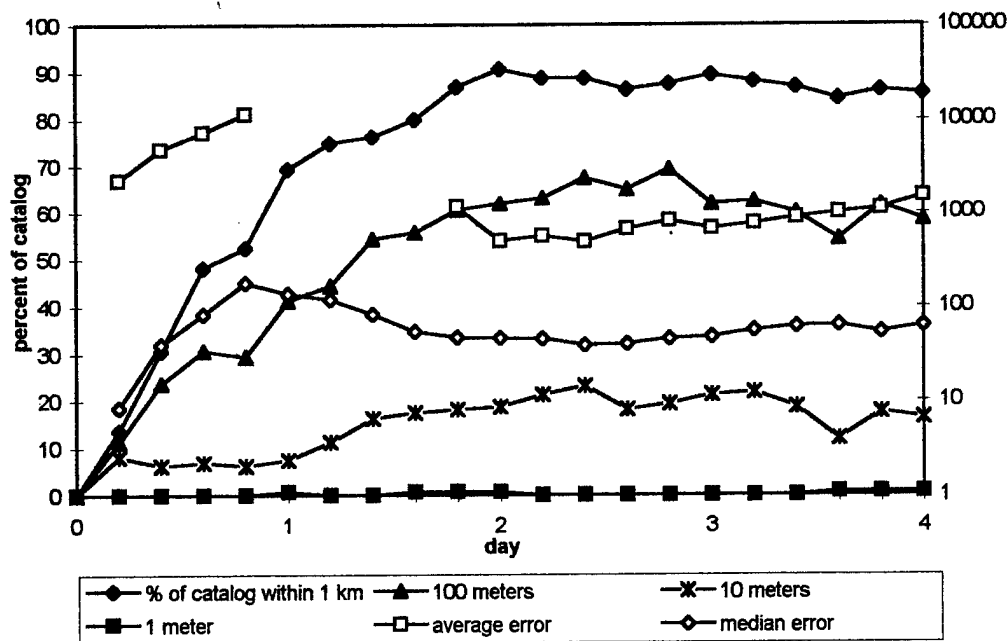


Figure 6-32 Simulation Twelve Error Trends

Figure 6-32 shows the trend in catalog accuracy during the simulation. By the end of the four day simulation, half of the satellites' positions were predicted within 63 meters. This represents a very significant improvement over the current method. Because the results were better with the increased likelihood of batch estimations for low altitude satellites (simulation twelve) over the previous result (simulation eleven), another simulation was conducted to see if increasing the tendency toward batch estimations for all satellites would increase the accuracy further. To investigate this, the algorithm was modified so that the batch method was implemented after any unsuccessful sequential estimation attempt with at least three new tracks of data. Figure 6-33 shows the results of this simulation.

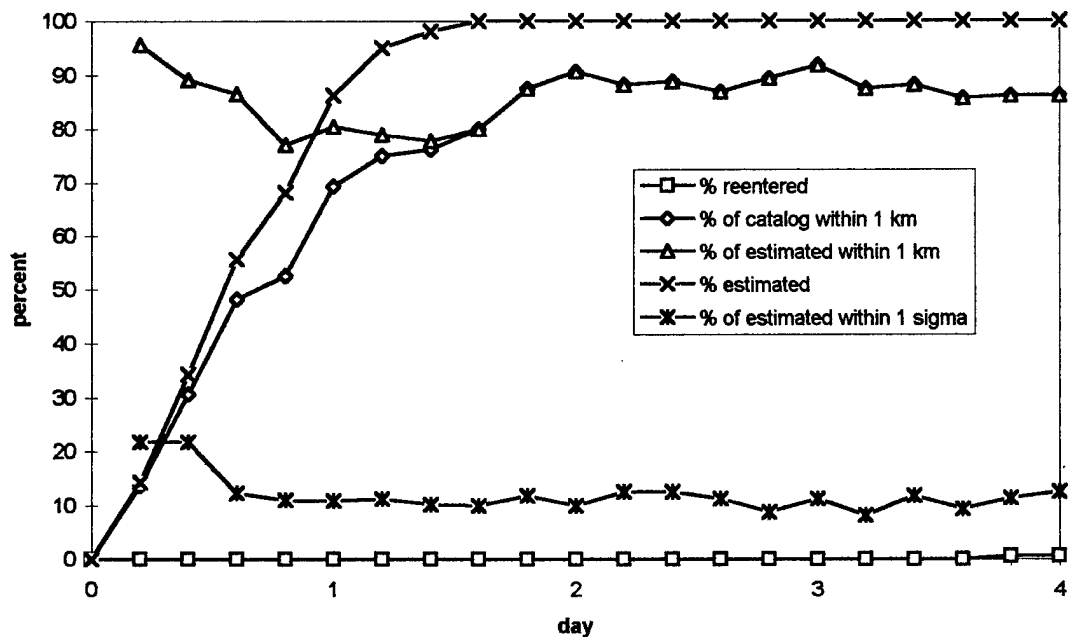


Figure 6-33 Simulation Thirteen Results

The results were better than simulation twelve but only marginally. Nevertheless, this simulation represents the best accuracy obtained during this thesis with a realistic catalog and a realistic truth model. Consistently, more than 85% of the catalog was estimated within one kilometer and the median error averaged less than 50 meters.

The third atmospheric effect modeled is that of a significant solar flare. The effect of this flare on the estimation process was analyzed for the final simulation. Figure 6-34 shows the atmospheric

density profile modeled for this simulation. It includes a day-night variation of  $\pm 25\%$  and a solar flare variation of a factor of two in sea-level pressure.

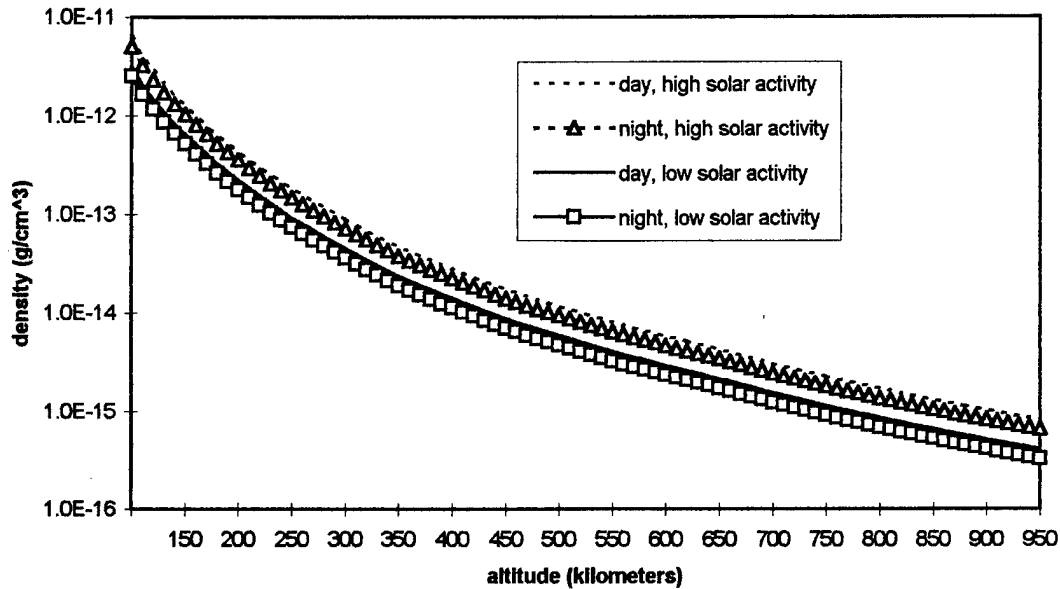


Figure 6-34 Atmospheric Density Variations

As shown above, the day-night variation in sea-level pressure of  $\pm 25\%$  results in a change in density of  $\pm 11\%$  at 200 kilometers. At this same altitude, the increase in sea-level pressure by a factor of two from the solar flare results in an increase in density by a factor of two. To model the flare in the truth model dynamics, the sea-level pressure was instantaneously doubled, and then exponentially returned to normal during the following day. This approximately models the density changes at altitude resulting from a large solar flare.

Simulation fourteen shows what would happen to this estimation process if a solar flare of significant magnitude were to affect an increase in atmospheric density. This scenario is quite plausible and represents a significant obstacle for an estimation algorithm to overcome. A large solar flare will dramatically and unpredictably increase the atmospheric density at a particular altitude. This causes a major increase in atmospheric drag on low-altitude satellites causing large orbital perturbations and even premature reentry. The solar flare began at the end of the second day, and returned to normal near the end of the third day. This simulation was expected to demonstrate the significant impact which a solar flare will have on the estimation accuracy. Figure 6-35 shows the results of this simulation.

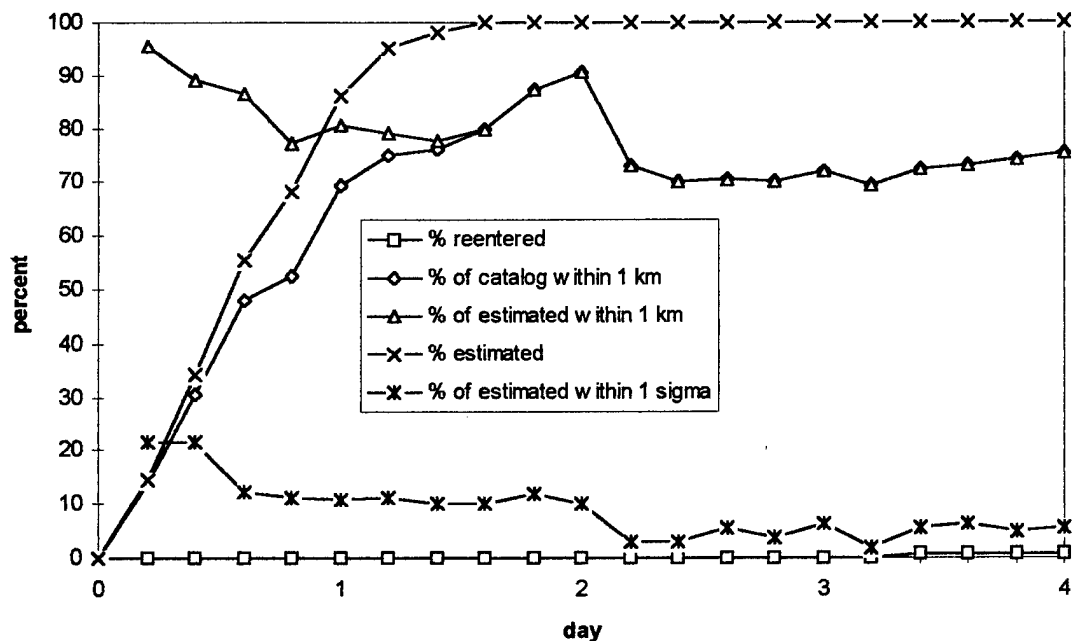


Figure 6-35 Simulation Fourteen Results

As expected, this figure shows that the solar flare dramatically impairs the estimator's ability to accurately predict orbits. Even in this worst case scenario, the track compression/*Global Estimate* process still recovers to outperform the current method.

## 6.8 Summary

In summary, the simulations showed that the track compression/*Global Estimate* method of orbit estimation will work on a full size catalog and that the results are much better than current practice. The results showed that different types of orbits produce a wide variation in accuracies, with low altitude orbits being the most difficult to estimate. This is both because the low altitude dynamics are stronger, meaning that any error will grow quickly, and because the low altitude satellites are subjected to the unpredictable atmosphere, making an estimator's dynamics model less valid.

The results also showed that the covariance matrices are, in general, overly optimistic in the prediction of the amount of error in any estimate. Several attempts were made at making the covariance matrices a better indicator of estimator performance. The application of fading memory coefficients did not significantly improve the results. One simulation which did improve the results placed the *Global*



*Estimate* dynamics model and truth model in perfect agreement. When the more realistic atmospheric effects were added, the covariance accuracies were again optimistic. This is one area which requires further evaluation. A more accurate fading memory matrix with unique values for all elements should be developed. The best values potentially are altitude-specific.

Finally, phase three demonstrated that the track compression/*Global Estimate* method would produce accuracies measured in meters or tens of meters rather than kilometers. The method requires modest computer time. Time trials show that a 133 MHz personal computer running in a Windows environment could handle the real-time processing of approximately 320 to 400 satellites using the algorithm developed in this thesis.

## VII. Conclusions and Recommendations

### 7.1 Summary

This thesis presents two successful methods of compressing tracks of observation data into state vectors and covariance matrices. It also presents an estimator which determines orbits using track compression results as input data and shows the applicability of this process to the satellite tracking mission by simulating its use on large-scale catalogs.

### 7.2 Conclusions

To conclude, the track compression methods were successful. The Taylor series method successfully compressed every arc to which it was applied. Because of the requirement to split each track into multiple arcs, this method was abandoned in favor of the integrator method. The integrator method successfully compressed over one hundred thousand tracks of data taken from thousands of different orbits. This represents a success rate of greater than 99.99%. Additionally, the method showed that the orbits could be determined even though the track compression dynamics model was much less accurate than the truth model. In simulation ten, the track compression dynamics model did not include air drag, yet the orbit estimator was still able to use the track compression results to predict orbit positions within one kilometer for more than 99% of the catalog. This shows that the state vectors and covariance matrices retain enough of the accuracy of the original arcs that a sufficiently accurate orbit estimator can correctly determine orbits with this greatly reduced amount of data.

Additionally, the simulations showed that the *Global Estimate* algorithm would produce a significant improvement in catalog accuracy over current methods. Today, the SCC reports orbit estimations with a one sigma error of twelve kilometers. This indicates that about twenty percent of the orbit determinations are within twelve kilometers. The simulation results indicate that the methods developed in this thesis would result in twenty percent of the orbit predictions within ten to twenty meters.

This represents an improvement of two to three orders of magnitude over the orbit estimation models currently in use by the SCC.

There are also two reasons which indicate that the actual accuracies may be much better than those predicted by the simulations. First, the latest simulations were conducted on a catalog with 84% of the semi-major axes above 800 kilometers. A more accurate catalog would probably have 84% of the altitudes of perigee above 800 kilometers. [4] The estimation process conducted in the latest simulations focused much attention on trying to estimate orbits which were low enough to have significant drag effects. These satellites produce the majority of the error of the catalog. With the actual catalog, most satellites are not nearly as influenced by air drag as those modeled in this thesis. Therefore, the estimator would spend less time trying to estimate the low altitude, difficult satellites and would produce more accurate predictions of the higher altitude satellites.

Secondly, the one sigma accuracy reported by the SCC applies at the instant that a satellite's orbit is determined. This process is called filtering. [7] The one sigma accuracy reported during the simulations is taken at an epoch corresponding to the end time of each cycle. This could be several orbits after the reference time of the orbit determination. This process is called prediction. [7] State prediction is much less accurate in orbital mechanics than filtering because even the best estimate of an orbit will lose accuracy with time. Also, if a limited number of observations are available for a satellite, the epoch of the prediction could be far from the time of the observations, meaning that the estimator is trying to predict where the satellite will be on one side of its orbit based on information from only the opposite side. Both of these reasons point to an improvement potentially greater than the two to three orders of magnitude stated above.

### 7.3 Recommendations

This thesis showed that the use of the track compression/*Global Estimate* method of orbit estimation for the operational satellite tracking mission should be considered. The computational requirements of this new method are modest enough to be implemented by the SCC. It would greatly

improve the accuracy of orbit determinations which would result in a reduced routine radar tracking workload, fewer collision-avoidance maneuvers for manned space flights, more accurate over-flight predictions, faster acquisition for ground-based observation or targeting of satellites and smaller rendezvous fuel budgets.

There are several areas which remain to be investigated. These deal with the operational implementation of the algorithm. First, the long term behavior of the estimator needs to be evaluated. This will require extended computer simulation time. A Monte-Carlo analysis should be conducted to determine appropriate values for each element of the fading memory coefficient matrix. The optimal values for these elements will likely be functions of altitude.

A number of different techniques were employed to increase the reliability of the code. Each of these should be investigated to determine any adverse effects caused by their implementation. These include the exclusion from the estimation process tracks of data which have less than 40 observations and the exclusion of tracks with less than 240 observations from use as the reference trajectory during the estimation process. The ballistic coefficient was carefully monitored during the convergence process. The algorithm had to give a reasonable ballistic coefficient at each iteration, or else it would be stopped. Additionally, the algorithm had to converge on a tighter set of ballistic coefficient criteria. Finally, a check was made at each iteration to see if this parameter was diverging.

During the propagation of the state vector at each iteration of the estimation process, the altitude and energy of the orbit were checked to see if the orbit was being propagated too low into the atmosphere, or if the orbit had escaped. The former would be an indication that the satellite was very near reentry while the latter is a sign of divergence. Additional divergence checks were also used.

The track compression algorithm would give up if it failed to converge within 15 iterations. The same limit was placed on the *Global Estimate* algorithm. The residuals were checked after convergence to see if the result was reasonable. If the algorithm detected that a covariance matrix diagonal element had become negative, it was assumed that this was the result of a numerical precision limitation and that estimate was postponed until more data was available. Also, if an orbit could not be successfully

estimated using the Bayes sequential method, and 30 or more tracks of new data were available, the new data would be fed into a least squares batch estimator. For the last two simulations, this was changed to three or more new tracks of data. If the satellite were flagged as a low altitude satellite, only batch updates were performed.

Finally, the satellites were prioritized in part based on the size of the covariance matrices, but also on the number of successive failed estimation attempts and the altitude of the satellite. All of these methods of modifying the basic theoretical algorithm produced either more robust code, more accurate results or both. The optimal means of implementing each of these modifications should be investigated both to determine if there is a more effective way of modifying the algorithm or if the change adversely affects the process. Some of these may require more processing time than they are worth. The multitude of combinations of the above adjustments makes this optimization study far too time consuming to be attempted in this thesis.

Additional variables which were not investigated significantly in this thesis include varying the length of time for each cycle and estimating orbits using altitude-specific estimation algorithms. Also, a method of prioritizing satellites which looks at which parts of the orbit have not been observed could be considered. Finally, the covariance matrix for each satellite could be propagated along with the state vectors during the observation portion of the cycle, and reprioritized at each time step. This may be a more optimal prioritization scheme. Because the change in the covariance matrix due to new data is only a function of the accuracy of the new data, the covariance matrix could be altered after a new track is compressed even before an estimate is performed. These and many other methods of optimizing the prioritization algorithm could be explored.

By exploring the effects of the robustness modifications, examining potential improvements not investigated in this thesis and by optimizing the prioritization algorithm, the track compression/*Global Estimate* method of orbit estimation can be improved and prepared for operational use.

The results indicate that a significant improvement in estimation accuracy would be seen if AFSPC were to move to this method. The use of this method for the operational satellite tracking mission should be considered.

## Appendix A Atmospheric Model

For the truth model, *Global Estimate* and *Simulate* portions of this thesis, an atmospheric model was required. The model provided the density and density gradient as a function of altitude. The atmospheric model used is taken from Regan. [15] It is derived from a combination of two standard atmospheric models. These models essentially provide a description of the variation of temperature with altitude and the relationship between density and temperature. The models divide the atmosphere into altitude regions called strata. The relationship between temperature and altitude is different for each strata.

The first model, U.S. Standard Atmosphere 1976, provides seven strata between sea-level and 86 km of altitude. Within each of these strata, the temperature either varies linearly with altitude or the strata is isothermal. Above 86 km, four more strata serve to define the atmosphere up to an altitude of 1000 km. One of these regions defines an elliptic variation of temperature with altitude. A second region defines an exponential variation. To keep the model simpler, Regan recommends that, above 86 km a 1962 model be used. This model defines thirteen regions between 86 and 700 km, all with linear temperature-altitude relationships. Attempts were made to prevent the propagation of a satellite into regions of the atmosphere defined by the 1976 model but the code describing these strata was included for the occasion when those altitudes had to be evaluated.

The density,  $\rho$ , for a given altitude is determined from the following two equations

$$\rho = \rho_i \exp \left\{ - \left[ \frac{g_0 (Z - Z_i)}{R T_{Mi}} \right] \left[ 1 - \frac{b}{2} (Z - Z_i) \right] \right\} \quad (A.1)$$

$$\rho = \rho_i \left[ \left( \frac{L_{Zi}}{R T_{Mi}} \right) (Z - Z_i) + 1 \right]^{- \left\{ \left( \frac{g_0}{R L_{Zi}} \right) \left[ \frac{R L_{Zi}}{g_0} + 1 + b \left( \frac{T_{Mi}}{L_{Zi}} - Z_i \right) \right] \right\}} \exp \left\{ \left( \frac{g_0 b}{R L_{Zi}} \right) (Z - Z_i) \right\} \quad (A.2)$$

where  $i$  is the region  
 $\rho_i$  is the density at the base of the region

$g_0$  is the sea-level gravitational acceleration  
 $Z$  is the altitude in kilometers  
 $Z_i$  is the altitude at the base of the region  
 $R$  is the atmospheric gas constant, given by  $R = R^*/M_0$   
 $R^*$  is the universal gas constant  
 $M_0$  is the sea-level molecular weight of air  
 $T_{Mi}$  is the molecular temperature at the base of the region  
 $b = 2 / R_E$   
 $R_E$  is the radius of the Earth  
 $L_{Zi}$  is the thermal lapse rate, the linear constant of variation of temperature for the region

The following table provides the values used for many of these constants.

Table A-1 Atmospheric Constants [15]

$g_0$	9.806 m/s <sup>2</sup>
$R^*$	$8.31432 \times 10^3$ (kg-mole) <sup>-1</sup>
$M_0$	28.964 kg/(kg-mole)
$R_E$	$6.3781 \times 10^6$ m

The values for the different strata are provided in the following two tables.

Table A-2 1976 Standard Atmosphere [15]

layer index	geometric altitude km	molecular temperature K	lapse rate K / km
0	0.0	288.15	-6.5
1	11.0102	216.65	0.0
2	20.0631	216.65	1.0
3	32.1619	228.65	2.8
4	47.3501	270.65	0.0
5	51.4125	270.65	-2.8
6	71.8020	214.65	-2.0
7	86.0	186.946	



Table A-3 1962 Standard Atmosphere [15]

layer index	geometric altitude km	molecular temperature K	lapse rate K / km
7	86.0	186.946	1.6481
8	100.0	210.65	5.0
9	110.0	260.65	10.0
10	120.0	360.65	20.0
11	150.0	960.65	15.0
12	160.0	1110.65	10.0
13	170.0	1210.65	7.0
14	190.0	1350.65	5.0
15	230.0	1550.65	4.0
16	300.0	1830.65	3.3
17	400.0	2160.65	2.6
18	500.0	2420.65	1.7
19	600.0	2590.65	1.1
20	700.0	2700.65	

These two tables, along with equations ( A.1 ) and ( A.2 ) are used to determine the density for a given altitude. Equation ( A.1 ) applies to the isothermal regions (where  $L_{zi} = 0$ ) while equation ( A.2 ) applies to the linear regions.

To determine the density gradient, (the derivative of the density with respect to altitude), equations ( A.1 ) and ( A.2 ) are differentiated. Recognizing that

$$\frac{\partial Z}{\partial r} = \frac{\partial Z}{\partial \text{alt}} = 1$$

leaves

$$\frac{d\rho}{dr} = \frac{\rho_i g_0}{R T_{Mi}} [b(Z - Z_i) - 1] \exp \left\{ - \left[ \frac{g_0 (Z - Z_i)}{R T_{Mi}} \right] \left[ 1 - \frac{b}{2} (Z - Z_i) \right] \right\} \quad (A.3)$$

for the isothermal regions and

$$\begin{aligned} \frac{d\rho}{dr} = \rho_i \left[ \left( \frac{L_{Zi}}{R T_{Mi}} \right) (Z - Z_i) + 1 \right]^{- \left\{ \left( \frac{g_0}{R L_{Zi}} \right) \left[ \frac{R L_{Zi}}{g_0} + 1 + b \left( \frac{T_{Mi}}{L_{Zi}} - Z_i \right) \right] \right\}} \\ \left\{ \frac{g_0 b}{R L_{Zi}} - \frac{\left\{ \left( \frac{g_0}{R L_{Zi}} \right) \left[ \frac{R L_{Zi}}{g_0} + 1 + b \left( \frac{T_{Mi}}{L_{Zi}} - Z_i \right) \right] \right\}}{\left[ \left( \frac{L_{Zi}}{R T_{Mi}} \right) (Z - Z_i) + 1 \right]} \right\} \exp \left\{ \frac{g_0 b}{R L_{Zi}} (Z - Z_i) \right\} \end{aligned} \quad (A.4)$$

for the linear regions.

## Appendix B Geopotential and the Equations of Motion

The purpose of this appendix is to present the oblate Earth model of the geopotential and to develop equations of motion for a satellite under the influence of this potential. These equations of motion were used in the truth model to propagate the satellites' orbits. Since the accelerations due to the Earth's geopotential are only functions of the satellite's position, the following simplified notation will be used

$$\mathbf{R} = \begin{bmatrix} x & y & z \end{bmatrix}^T$$

and the equations of motion will take the form

$$\frac{d^2 \mathbf{R}}{dt^2} = \begin{bmatrix} \frac{d^2 x}{dt^2} \\ \frac{d^2 y}{dt^2} \\ \frac{d^2 z}{dt^2} \end{bmatrix}$$

The geopotential model presented here does not include sectoral or tesseral harmonics.

The aspherical potential of the Earth, modeling zonal harmonics through  $J_6$ , is provided by Escobal as [5]

$$\begin{aligned} \Phi = \frac{Gm}{r} & \left[ 1 + \frac{R_\oplus^2 J_2}{2r^2} (1 - 3 \sin^2 \delta) \right. \\ & + \frac{R_\oplus^3 J_3}{2r^3} (3 - 5 \sin^2 \delta) \sin \delta \\ & - \frac{R_\oplus^4 J_4}{8r^4} (3 - 30 \sin^2 \delta + 35 \sin^4 \delta) \\ & - \frac{R_\oplus^5 J_5}{8r^5} (15 - 70 \sin^2 \delta + 63 \sin^4 \delta) \sin \delta \\ & \left. + \frac{R_\oplus^6 J_6}{16r^6} (5 - 105 \sin^2 \delta + 315 \sin^4 \delta - 231 \sin^6 \delta) \right] \end{aligned} \quad (B.1)$$

where  $G$  is the gravitational constant  
 $m$  is the mass of the Earth  
 $R_{\oplus}$  is the equatorial radius of the Earth  
 $r$  is the distance from the Earth's center  
 $\sin \delta \equiv z/r$   
and the zonal harmonic coefficients are taken from the following table [5]

Table B-1 Coefficients of Gravitational Harmonics

$J_2$	+	1082.28	$\pm 0.3 \times 10^{-6}$
$J_3$	-	2.3	$\pm 0.2 \times 10^{-6}$
$J_4$	-	2.12	$\pm 0.5 \times 10^{-6}$
$J_5$	-	0.2	$\pm 0.1 \times 10^{-6}$
$J_6$	+	1.0	$\pm 0.8 \times 10^{-6}$

Using canonical units allows the substitution  $\mu \equiv Gm = 1$  and  $R_{\oplus} = 1$ . The acceleration due to gravity about a planet is given as the gradient of the potential, or

$$\frac{d^2 \mathbf{R}}{dt^2} = \nabla \Phi \quad (\text{B.2})$$

and these terms are given as

$$\begin{aligned} \frac{\partial \Phi}{\partial x} = -\frac{x}{r^3} & \left[ 1 + \frac{3}{2} \frac{J_2}{r^2} (1 - 5 \sin^2 \delta) \right. \\ & + \frac{5}{2} \frac{J_3}{r^3} (3 - 7 \sin^2 \delta) \sin \delta \\ & - \frac{5}{8} \frac{J_4}{r^4} (3 - 42 \sin^2 \delta + 63 \sin^4 \delta) \\ & - \frac{3}{8} \frac{J_5}{r^5} (35 - 210 \sin^2 \delta + 231 \sin^4 \delta) \sin \delta \\ & \left. + \frac{1}{16} \frac{J_6}{r^6} (35 - 945 \sin^2 \delta + 3465 \sin^4 \delta - 3003 \sin^6 \delta) \right] \end{aligned} \quad (\text{B.3})$$

$$\frac{\partial \Phi}{\partial y} = y \left( \frac{1}{x} \frac{\partial \Phi}{\partial x} \right)$$

$$\begin{aligned}
\frac{\partial \Phi}{\partial z} = & -\frac{z}{r^3} \left[ 1 + \frac{3 J_2}{2 r^2} (3 - 5 \sin^2 \delta) \right. \\
& + \frac{5 J_3}{2 r^3} (6 - 7 \sin^2 \delta) \sin \delta \\
& - \frac{5 J_4}{8 r^4} (15 - 70 \sin^2 \delta + 63 \sin^4 \delta) \\
& - \frac{3 J_5}{8 r^5} (105 - 315 \sin^2 \delta + 231 \sin^4 \delta) \sin \delta \\
& \left. + \frac{1 J_6}{16 r^6} (245 - 2205 \sin^2 \delta + 4851 \sin^4 \delta - 3003 \sin^6 \delta) \right] \\
& + \frac{1}{r^2} \left( \frac{3 J_3}{2 r^3} - \frac{15 J_5}{8 r^5} \right)
\end{aligned}$$

Combining these yields the final equations of motion for a satellite about an oblate planet.

$$\frac{d^2 \mathbf{R}}{dt^2} = \begin{bmatrix} \frac{\partial \Phi}{\partial x} \\ \frac{\partial \Phi}{\partial y} \\ \frac{\partial \Phi}{\partial z} \end{bmatrix} \quad (\text{B.4})$$

## Appendix C Taylor Series Track Compression State Transition Matrix

This appendix presents the state transition matrix,  $\Phi$ , used in the Taylor series method of track compression. The state transition matrix relates a change in the elements of the position vector at time,  $t$ , to a change in the reference state,  $\mathbf{X}$ , at time,  $t_0$ .

$$\Phi \equiv \frac{\partial \mathbf{R}(t)}{\partial \mathbf{X}(0)} \quad (\text{C.1})$$

where the following notation is used

$$\mathbf{R}(t) = \mathbf{R} = \begin{bmatrix} R_1(t) \\ R_2(t) \\ R_3(t) \end{bmatrix} \quad \mathbf{X}(0) = \begin{bmatrix} R_1 \\ R_2 \\ R_3 \\ V_1 \\ V_2 \\ V_3 \end{bmatrix}$$

Using this notation, the state transition matrix becomes.

$$\Phi \equiv \frac{\partial \mathbf{R}(t)}{\partial \mathbf{X}(0)} = \begin{bmatrix} \frac{\partial R_1(t)}{\partial X_1(0)} & \frac{\partial R_1(t)}{\partial X_2(0)} & \frac{\partial R_1(t)}{\partial X_3(0)} & \frac{\partial R_1(t)}{\partial X_4(0)} & \frac{\partial R_1(t)}{\partial X_5(0)} & \frac{\partial R_1(t)}{\partial X_6(0)} \\ \frac{\partial R_2(t)}{\partial X_1(0)} & \frac{\partial R_2(t)}{\partial X_2(0)} & \frac{\partial R_2(t)}{\partial X_3(0)} & \frac{\partial R_2(t)}{\partial X_4(0)} & \frac{\partial R_2(t)}{\partial X_5(0)} & \frac{\partial R_2(t)}{\partial X_6(0)} \\ \frac{\partial R_3(t)}{\partial X_1(0)} & \frac{\partial R_3(t)}{\partial X_2(0)} & \frac{\partial R_3(t)}{\partial X_3(0)} & \frac{\partial R_3(t)}{\partial X_4(0)} & \frac{\partial R_3(t)}{\partial X_5(0)} & \frac{\partial R_3(t)}{\partial X_6(0)} \end{bmatrix} \quad (3.16)$$

To determine these partial derivatives,  $\mathbf{R}(t)$  as a function of  $\mathbf{X}$  must first be written. This function is developed in section 3.4.2.2 as equation ( 3.15 ) and is reprinted on the following page.

$$\mathbf{R} = \begin{bmatrix} R_1 + V_1 \Delta t - \frac{R_1}{2r^3} \Delta t^2 - \frac{3J_2 R_1}{4r^5} \left(1 - 5 \frac{R_3^2}{r^2}\right) \Delta t^2 + \frac{1}{6r^3} \left(\frac{3R_1 \dot{r}}{r} - V_1\right) \Delta t^3 \\ R_2 + V_2 \Delta t - \frac{R_2}{2r^3} \Delta t^2 - \frac{3J_2 R_2}{4r^5} \left(1 - 5 \frac{R_3^2}{r^2}\right) \Delta t^2 + \frac{1}{6r^3} \left(\frac{3R_2 \dot{r}}{r} - V_2\right) \Delta t^3 \\ R_3 + V_3 \Delta t - \frac{R_3}{2r^3} \Delta t^2 - \frac{3J_2 R_3}{4r^5} \left(3 - 5 \frac{R_3^2}{r^2}\right) \Delta t^2 + \frac{1}{6r^3} \left(\frac{3R_3 \dot{r}}{r} - V_3\right) \Delta t^3 \end{bmatrix} \quad (3.15)$$

where  $r = \sqrt{R_1^2 + R_2^2 + R_3^2}$   
 $\dot{r} = \frac{d}{dt} r = \frac{R_1 V_1 + R_2 V_2 + R_3 V_3}{r}$   
 $\Delta t = t - t_0$

$$J_2 = 1082.28 \times 10^{-6}$$

Replacing the individual terms of equation ( 3.15 ) with another shorthand notation will allow the components of the partial derivatives to be developed piecemeal. The equation is reprinted below in the same form to allow an easy understanding of which notation corresponds to each term.

$$\mathbf{R} = \begin{bmatrix} A_x + B_x \Delta t + C_x \Delta t^2 + D_x \Delta t^2 + E_x \Delta t^3 \\ A_y + B_y \Delta t + C_y \Delta t^2 + D_y \Delta t^2 + E_y \Delta t^3 \\ A_z + B_z \Delta t + C_z \Delta t^2 + D_z \Delta t^2 + E_z \Delta t^3 \end{bmatrix} \quad (C.2)$$

As an example, the first partial derivative of equation ( 3.16 ) becomes

$$\frac{\partial R_1(t)}{\partial X_1(0)} = \frac{\partial A_x}{\partial X_1(0)} + \frac{\partial B_x}{\partial X_1(0)} \Delta t + \frac{\partial C_x}{\partial X_1(0)} \Delta t^2 + \frac{\partial D_x}{\partial X_1(0)} \Delta t^2 + \frac{\partial E_x}{\partial X_1(0)} \Delta t^3 \quad (C.3)$$

and is abbreviated

$$\frac{\partial R_1(t)}{\partial X_1(0)} = A_x 1 + B_x 1 \Delta t + C_x 1 \Delta t^2 + D_x 1 \Delta t^2 + E_x 1 \Delta t^3 \quad (C.4)$$

Therefore, determining the eighteen components of equation ( 3.16 ) becomes a process of determining the five partial derivatives of equation ( C.3 ) for each of the eighteen equations which have a form identical to ( C.3 ). These 90 terms are denoted  $A_x 1$  through  $E_z 6$ . These will be much simpler to obtain and describe than if all five terms were evaluated as one. In many cases, they are trivial.

Use of a simplified notation will also be seen in the extensive application of the chain rule. The partial derivatives of certain terms will occur frequently and will not be evaluated each time. Instead, the term will be indicated in the appropriate equation and evaluated below. In the actual computer code, this process occurs in the reverse order. The terms are evaluated and stored beforehand, and then retrieved frequently during the evaluation of the appropriate equations.

The remainder of this appendix is devoted to presenting each of the 90 partial derivatives.

$$A_x 1 = 1 \quad A_x 2 = 0 \quad A_x 3 = 0 \quad A_x 4 = 0 \quad A_x 5 = 0 \quad A_x 6 = 0$$

$$A_y 1 = 0 \quad A_y 2 = 1 \quad A_y 3 = 0 \quad A_y 4 = 0 \quad A_y 5 = 0 \quad A_y 6 = 0$$

$$A_z 1 = 0 \quad A_z 2 = 0 \quad A_z 3 = 1 \quad A_z 4 = 0 \quad A_z 5 = 0 \quad A_z 6 = 0$$

$$B_x 1 = 0 \quad B_x 2 = 0 \quad B_x 3 = 0 \quad B_x 4 = 1 \quad B_x 5 = 0 \quad B_x 6 = 0$$

$$B_y 1 = 0 \quad B_y 2 = 0 \quad B_y 3 = 0 \quad B_y 4 = 0 \quad B_y 5 = 1 \quad B_y 6 = 0$$

$$B_z 1 = 0 \quad B_z 2 = 0 \quad B_z 3 = 0 \quad B_z 4 = 0 \quad B_z 5 = 0 \quad B_z 6 = 1$$

$$C_x 1 = \frac{-1}{2r^3} + \frac{3}{2} \frac{R_1}{r^4} \frac{\partial r}{\partial R_1} \quad C_x 2 = \frac{3}{2} \frac{R_1}{r^4} \frac{\partial r}{\partial R_2} \quad C_x 3 = \frac{3}{2} \frac{R_1}{r^4} \frac{\partial r}{\partial R_3}$$

$$C_x 4 = 0 \quad C_x 5 = 0 \quad C_x 6 = 0$$

$$C_y 1 = \frac{3}{2} \frac{R_2}{r^4} \frac{\partial r}{\partial R_1} \quad C_y 2 = \frac{-1}{2r^3} + \frac{3}{2} \frac{R_2}{r^4} \frac{\partial r}{\partial R_2} \quad C_y 3 = \frac{3}{2} \frac{R_2}{r^4} \frac{\partial r}{\partial R_3}$$

$$C_y 4 = 0 \quad C_y 5 = 0 \quad C_y 6 = 0$$

$$C_z 1 = \frac{3}{2} \frac{R_3}{r^4} \frac{\partial r}{\partial R_1} \quad C_z 2 = \frac{3}{2} \frac{R_3}{r^4} \frac{\partial r}{\partial R_2} \quad C_z 3 = \frac{-1}{2r^3} + \frac{3}{2} \frac{R_3}{r^4} \frac{\partial r}{\partial R_3}$$

$$C_z 4 = 0 \quad C_z 5 = 0 \quad C_z 6 = 0$$

$$D_x 1 = \left( R_1 - 5R_1 \frac{R_3^2}{r^2} \right) \frac{15}{4} \frac{J_2}{r^6} \frac{\partial r}{\partial R_1} - \left( 1 - 5 \frac{R_3^2}{r^2} + 10R_1 \frac{R_3^2}{r^3} \frac{\partial r}{\partial R_1} \right) \frac{3}{4} \frac{J_2}{r^5}$$

$$D_x 2 = \left( R_1 - 5R_1 \frac{R_3^2}{r^2} \right) \frac{15}{4} \frac{J_2}{r^6} \frac{\partial r}{\partial R_2} - \frac{3}{4} \frac{J_2}{r^5} \left( 10R_1 \frac{R_3^2}{r^3} \frac{\partial r}{\partial R_2} \right)$$



$$D_x 3 = \left( R_1 - 5R_1 \frac{R_3^2}{r^2} \right) \frac{15 J_2}{4 r^6} \frac{\partial r}{\partial R_3} - \frac{3 J_2}{4 r^5} \left( 10R_1 \frac{R_3^2}{r^3} \frac{\partial r}{\partial R_3} \right)$$

$$D_x 4 = 0$$

$$D_x 5 = 0$$

$$D_x 6 = 0$$

$$D_y 1 = \left( R_2 - 5R_2 \frac{R_3^2}{r^2} \right) \frac{15 J_2}{4 r^6} \frac{\partial r}{\partial R_1} - \frac{3 J_2}{4 r^5} \left( 10R_2 \frac{R_3^2}{r^3} \frac{\partial r}{\partial R_1} \right)$$

$$D_y 2 = \left( R_2 - 5R_2 \frac{R_3^2}{r^2} \right) \frac{15 J_2}{4 r^6} \frac{\partial r}{\partial R_2} - \left( 1 - 5 \frac{R_3^2}{r^2} + 10R_2 \frac{R_3^2}{r^3} \frac{\partial r}{\partial R_2} \right) \frac{3 J_2}{4 r^5}$$

$$D_y 3 = \left( R_2 - 5R_2 \frac{R_3^2}{r^2} \right) \frac{15 J_2}{4 r^6} \frac{\partial r}{\partial R_3} - \frac{3 J_2}{4 r^5} \left( 10R_2 \frac{R_3^2}{r^3} \frac{\partial r}{\partial R_3} \right)$$

$$D_y 4 = 0$$

$$D_y 5 = 0$$

$$D_y 6 = 0$$

$$D_z 1 = \left( 3R_3 - 5 \frac{R_3^2}{r^2} \right) \frac{15 J_2}{4 r^6} \frac{\partial r}{\partial R_1} - \frac{15 J_2}{2 r^5} \left( \frac{R_3^3}{r^3} \frac{\partial r}{\partial R_1} \right)$$

$$D_z 2 = \left( 3R_3 - 5 \frac{R_3^2}{r^2} \right) \frac{15 J_2}{4 r^6} \frac{\partial r}{\partial R_2} - \frac{15 J_2}{2 r^5} \left( \frac{R_3^3}{r^3} \frac{\partial r}{\partial R_2} \right)$$

$$D_z 3 = \left( 3R_3 - 5 \frac{R_3^2}{r^2} \right) \frac{15 J_2}{4 r^6} \frac{\partial r}{\partial R_3} - \left( 3 - 15 \frac{R_3^2}{r^2} + 10 \frac{R_3^3}{r^3} \frac{\partial r}{\partial R_3} \right) \frac{3 J_2}{4 r^5}$$

$$D_z 4 = 0$$

$$D_z 5 = 0$$

$$D_z 6 = 0$$

$$E_x 1 = \frac{-1}{2r^4} \frac{\partial r}{\partial R_1} \left( 3R_1 \frac{\dot{r}}{r} - V_1 \right) + \frac{1}{6r^3} \left( 3 \frac{\dot{r}}{r} + 3 \frac{R_1}{r} + \frac{\partial \dot{r}}{\partial R_1} - 3R_1 \frac{\dot{r}}{r^2} \frac{\partial r}{\partial R_1} \right)$$

$$E_x 2 = \frac{-1}{2r^4} \frac{\partial r}{\partial R_2} \left( 3R_1 \frac{\dot{r}}{r} - V_1 \right) + \frac{1}{6r^3} \left( 3 \frac{\dot{r}}{r} + 3 \frac{R_1}{r} + \frac{\partial \dot{r}}{\partial R_2} - 3R_1 \frac{\dot{r}}{r^2} \frac{\partial r}{\partial R_2} \right)$$

$$E_x 3 = \frac{-1}{2r^4} \frac{\partial r}{\partial R_3} \left( 3R_1 \frac{\dot{r}}{r} - V_1 \right) + \frac{1}{6r^3} \left( 3 \frac{\dot{r}}{r} + 3 \frac{R_1}{r} + \frac{\partial \dot{r}}{\partial R_3} - 3R_1 \frac{\dot{r}}{r^2} \frac{\partial r}{\partial R_3} \right)$$

$$E_x 4 = \frac{1}{6r^3} \left( 3 \frac{R_1}{r} \frac{\partial \dot{r}}{\partial V_1} - 1 \right)$$

$$E_x 5 = \frac{1}{6r^3} \left( 3 \frac{R_1}{r} \frac{\partial \dot{r}}{\partial V_2} - 1 \right)$$

$$E_x 6 = \frac{1}{6r^3} \left( 3 \frac{R_1}{r} \frac{\partial \dot{r}}{\partial V_3} - 1 \right)$$

$$E_y 1 = \frac{-1}{2r^4} \frac{\partial r}{\partial R_1} \left( 3R_2 \frac{\dot{r}}{r} - V_2 \right) + \frac{1}{6r^3} \left( 3 \frac{\dot{r}}{r} + 3 \frac{R_2}{r} + \frac{\partial \dot{r}}{\partial R_1} - 3R_2 \frac{\dot{r}}{r^2} \frac{\partial r}{\partial R_1} \right)$$

$$E_y 2 = \frac{-1}{2r^4} \frac{\partial r}{\partial R_2} \left( 3R_2 \frac{\dot{r}}{r} - V_2 \right) + \frac{1}{6r^3} \left( 3 \frac{\dot{r}}{r} + 3 \frac{R_2}{r} + \frac{\partial \dot{r}}{\partial R_2} - 3R_2 \frac{\dot{r}}{r^2} \frac{\partial r}{\partial R_2} \right)$$

$$E_y 3 = \frac{-1}{2r^4} \frac{\partial r}{\partial R_3} \left( 3R_2 \frac{\dot{r}}{r} - V_2 \right) + \frac{1}{6r^3} \left( 3 \frac{\dot{r}}{r} + 3 \frac{R_2}{r} + \frac{\partial \dot{r}}{\partial R_3} - 3R_2 \frac{\dot{r}}{r^2} \frac{\partial r}{\partial R_3} \right)$$

$$E_y 4 = \frac{1}{6r^3} \left( 3 \frac{R_2}{r} \frac{\partial \dot{r}}{\partial V_1} - 1 \right)$$

$$E_y 5 = \frac{1}{6r^3} \left( 3 \frac{R_2}{r} \frac{\partial \dot{r}}{\partial V_2} - 1 \right)$$

$$E_y 6 = \frac{1}{6r^3} \left( 3 \frac{R_2}{r} \frac{\partial \dot{r}}{\partial V_3} - 1 \right)$$

$$E_z 1 = \frac{-1}{2r^4} \frac{\partial r}{\partial R_1} \left( 3R_3 \frac{\dot{r}}{r} - V_3 \right) + \frac{1}{6r^3} \left( 3 \frac{\dot{r}}{r} + 3 \frac{R_3}{r} + \frac{\partial \dot{r}}{\partial R_1} - 3R_3 \frac{\dot{r}}{r^2} \frac{\partial r}{\partial R_1} \right)$$

$$E_z 2 = \frac{-1}{2r^4} \frac{\partial r}{\partial R_2} \left( 3R_3 \frac{\dot{r}}{r} - V_3 \right) + \frac{1}{6r^3} \left( 3 \frac{\dot{r}}{r} + 3 \frac{R_3}{r} + \frac{\partial \dot{r}}{\partial R_2} - 3R_3 \frac{\dot{r}}{r^2} \frac{\partial r}{\partial R_2} \right)$$

$$E_z 3 = \frac{-1}{2r^4} \frac{\partial r}{\partial R_3} \left( 3R_3 \frac{\dot{r}}{r} - V_3 \right) + \frac{1}{6r^3} \left( 3 \frac{\dot{r}}{r} + 3 \frac{R_3}{r} + \frac{\partial \dot{r}}{\partial R_3} - 3R_3 \frac{\dot{r}}{r^2} \frac{\partial r}{\partial R_3} \right)$$

$$E_z 4 = \frac{1}{6r^3} \left( 3 \frac{R_3}{r} \frac{\partial \dot{r}}{\partial V_1} - 1 \right)$$

$$E_z 5 = \frac{1}{6r^3} \left( 3 \frac{R_3}{r} \frac{\partial \dot{r}}{\partial V_2} - 1 \right)$$

$$E_z 6 = \frac{1}{6r^3} \left( 3 \frac{R_3}{r} \frac{\partial \dot{r}}{\partial V_3} - 1 \right)$$

where  $r = \sqrt{R_1^2 + R_2^2 + R_3^2}$

$$\frac{\partial r}{\partial R_1} = \frac{R_1}{r} \quad \frac{\partial r}{\partial R_2} = \frac{R_2}{r} \quad \frac{\partial r}{\partial R_3} = \frac{R_3}{r}$$

$$\dot{r} = \frac{d}{dt} r = \frac{R_1 V_1 + R_2 V_2 + R_3 V_3}{r}$$

$$\frac{\partial \dot{r}}{\partial R_1} = \frac{V_1}{r} - \frac{\dot{r} R_1}{r^2} \quad \frac{\partial \dot{r}}{\partial R_2} = \frac{V_2}{r} - \frac{\dot{r} R_2}{r^2} \quad \frac{\partial \dot{r}}{\partial R_3} = \frac{V_3}{r} - \frac{\dot{r} R_3}{r^2}$$

$$\frac{\partial \dot{r}}{\partial V_1} = \frac{R_1}{r} \quad \frac{\partial \dot{r}}{\partial V_2} = \frac{R_2}{r} \quad \frac{\partial \dot{r}}{\partial V_3} = \frac{R_3}{r}$$

Inserting these substitutions into the 90 partial derivatives, inserting these 90 partial derivatives into the eighteen equations of the form ( C.4 ), and finally inserting these eighteen equations into equation ( 3.16 ) yields the final form of the state transition matrix,  $\Phi$ , for the Taylor series method of track compression.

## Appendix D Track Compression $\mathbf{H}$ Matrix

This appendix develops the  $\mathbf{H}$  matrix, described in section 3.4.4.1. This matrix relates the change in the observation relation,  $\mathbf{G}$ , with a change in the position vector,  $\mathbf{R}$ .

$$\mathbf{H} = \begin{bmatrix} \frac{\partial \mathbf{G}_1}{\partial \mathbf{R}_1} & \frac{\partial \mathbf{G}_1}{\partial \mathbf{R}_2} & \frac{\partial \mathbf{G}_1}{\partial \mathbf{R}_3} \\ \frac{\partial \mathbf{G}_2}{\partial \mathbf{R}_1} & \frac{\partial \mathbf{G}_2}{\partial \mathbf{R}_2} & \frac{\partial \mathbf{G}_2}{\partial \mathbf{R}_3} \\ \frac{\partial \mathbf{G}_3}{\partial \mathbf{R}_1} & \frac{\partial \mathbf{G}_3}{\partial \mathbf{R}_2} & \frac{\partial \mathbf{G}_3}{\partial \mathbf{R}_3} \end{bmatrix} \quad (3.28)$$

The observation relation,  $\mathbf{G}$ , is given by the following equations

$$\mathbf{G} = \begin{bmatrix} \text{range}(\mathbf{R}, t) \\ \text{azimuth}(\mathbf{R}, t) \\ \text{elevation}(\mathbf{R}, t) \end{bmatrix} \quad (3.17)$$

$$\text{range} = |\boldsymbol{\rho}_{\text{SEZ}}| = \sqrt{\rho_s^2 + \rho_e^2 + \rho_z^2} \quad (3.11)$$

$$\text{azimuth} = \pi - \tan^{-1} \frac{\rho_e}{\rho_s}$$

$$\text{elevation} = \tan^{-1} \frac{\rho_z}{\sqrt{\rho_s^2 + \rho_e^2}}$$

Because the partial derivative of  $\mathbf{G}$  must be taken with respect to  $\mathbf{R}$ , and  $\mathbf{G}$  is expressed in terms of  $\boldsymbol{\rho}_{\text{SEZ}}$ , the relations between the various terms are used to create a chain of derivatives as follows.

$$\mathbf{H} = \frac{\partial \mathbf{G}}{\partial \mathbf{R}} = \frac{\partial \mathbf{G}}{\partial \boldsymbol{\rho}_{\text{SEZ}}} \frac{\partial \boldsymbol{\rho}_{\text{SEZ}}}{\partial \boldsymbol{\rho}_{\text{IJK}}} \frac{\partial \boldsymbol{\rho}_{\text{IJK}}}{\partial \mathbf{R}} \quad (\text{D.1})$$

where  $\mathbf{G}$  is given in terms of  $\boldsymbol{\rho}_{\text{SEZ}}$  by equations (3.17) and (3.11) above,  $\boldsymbol{\rho}_{\text{SEZ}}$  and  $\boldsymbol{\rho}_{\text{IJK}}$  are related through equation (3.23), and  $\boldsymbol{\rho}_{\text{IJK}}$  and  $\mathbf{R}$  are related through equation (3.18), both on the next page.

$$\rho_{SEZ} = \mathbf{D} \rho_{UK} \quad (3.23)$$

$$\rho_{UK} = \mathbf{R}(t) - \mathbf{R}_{site} \quad (3.18)$$

The three terms of equation ( D.1 ) are now determined in reverse order. From equation ( 3.18 ),

$$\frac{\partial \rho_{UK}}{\partial \mathbf{R}} = \mathbf{I} = \begin{bmatrix} 1 & 0 & 0 \\ 0 & 1 & 0 \\ 0 & 0 & 1 \end{bmatrix} \quad (D.2)$$

From equation ( 3.23 ),

$$\frac{\partial \rho_{SEZ}}{\partial \rho_{UK}} = \mathbf{D} \quad (D.3)$$

where

$$\mathbf{D} = \begin{bmatrix} \cos(\text{LST}) \cos(\text{colat}) & \sin(\text{LST}) \cos(\text{colat}) & -\sin(\text{colat}) \\ -\sin(\text{LST}) & \cos(\text{LST}) & 0 \\ \cos(\text{LST}) \sin(\text{colat}) & \sin(\text{LST}) \sin(\text{colat}) & \cos(\text{colat}) \end{bmatrix} \quad (3.22)$$

The third derivative,  $\frac{\partial \mathbf{G}}{\partial \rho_{SEZ}}$ , will now be developed from equations ( 3.17 ) and ( 3.11 ).

$$\frac{\partial \text{range}}{\partial \rho_s} = \frac{\rho_s}{\sqrt{\rho_s^2 + \rho_E^2 + \rho_Z^2}} \quad (D.4)$$

$$\frac{\partial \text{range}}{\partial \rho_E} = \frac{\rho_E}{\sqrt{\rho_s^2 + \rho_E^2 + \rho_Z^2}}$$

$$\frac{\partial \text{range}}{\partial \rho_s} = \frac{\rho_s}{\sqrt{\rho_s^2 + \rho_E^2 + \rho_Z^2}}$$

$$\frac{\partial \text{azimuth}}{\partial \rho_s} = \frac{-\rho_E \rho_s^{-2}}{1 + \left( \frac{\rho_E}{\rho_s} \right)^2}$$

$$\frac{\partial \text{azimuth}}{\partial \rho_E} = \frac{-1/\rho_s}{1 + \left(\rho_E/\rho_s\right)^2}$$

$$\frac{\partial \text{azimuth}}{\partial \rho_Z} = 0$$

$$\frac{\partial \text{elevation}}{\partial \rho_s} = \frac{-\rho_Z \rho_s (\rho_s^2 + \rho_E^2)^{-1/2}}{\rho_s^2 + \rho_E^2 + \rho_Z^2}$$

$$\frac{\partial \text{elevation}}{\partial \rho_E} = \frac{-\rho_Z \rho_E (\rho_s^2 + \rho_E^2)^{-1/2}}{\rho_s^2 + \rho_E^2 + \rho_Z^2}$$

$$\frac{\partial \text{elevation}}{\partial \rho_Z} = \frac{\sqrt{\rho_s^2 + \rho_E^2}}{(\rho_s^2 + \rho_E^2 + \rho_Z^2)}$$

These nine equations are inserted into the following matrix.

$$\frac{\partial \mathbf{G}}{\partial \mathbf{p}_{\text{SEZ}}} = \begin{bmatrix} \frac{\partial \text{range}}{\partial \rho_s} & \frac{\partial \text{range}}{\partial \rho_E} & \frac{\partial \text{range}}{\partial \rho_Z} \\ \frac{\partial \text{azimuth}}{\partial \rho_s} & \frac{\partial \text{azimuth}}{\partial \rho_E} & \frac{\partial \text{azimuth}}{\partial \rho_Z} \\ \frac{\partial \text{elevation}}{\partial \rho_s} & \frac{\partial \text{elevation}}{\partial \rho_E} & \frac{\partial \text{elevation}}{\partial \rho_Z} \end{bmatrix} \quad (\text{D.5})$$

Equation (D.2), the identity matrix, has no effect on the  $\mathbf{H}$  matrix. When equations (D.4) are inserted into equation (D.5), and then multiplied by equation (D.3), the final form of the  $\mathbf{H}$  matrix results.

$$\mathbf{H} = \frac{\partial \mathbf{G}}{\partial \mathbf{R}} = \begin{bmatrix} \frac{\partial \text{range}}{\partial \rho_s} & \frac{\partial \text{range}}{\partial \rho_E} & \frac{\partial \text{range}}{\partial \rho_Z} \\ \frac{\partial \text{azimuth}}{\partial \rho_s} & \frac{\partial \text{azimuth}}{\partial \rho_E} & \frac{\partial \text{azimuth}}{\partial \rho_Z} \\ \frac{\partial \text{elevation}}{\partial \rho_s} & \frac{\partial \text{elevation}}{\partial \rho_E} & \frac{\partial \text{elevation}}{\partial \rho_Z} \end{bmatrix} \mathbf{D} \quad (\text{D.6})$$

## Appendix E Integrator Track Compression Equations of Variation

This appendix develops the equations describing the 36 elements of the **A** matrix of the equation below. These equations are called the equations of variation. [7]

$$\frac{d}{dt} \Phi(t, t_0) = \mathbf{A}(t) \Phi(t, t_0) \quad (4.2)$$

where

$$\mathbf{A}(t) = \nabla_{\mathbf{x}} \mathbf{g}|_{\mathbf{x}_0(t)}$$

and **g** comes from the equations of motion of the state vector,

$$\frac{d}{dt} \mathbf{X} = \mathbf{g}(\mathbf{X}, t)$$

The 36 element form of the **A** matrix is used for the integrator track compression dynamics model. Therefore, the dynamics do not include air drag and the state vector does not include the ballistic coefficient. The **A** matrix is defined as the partial derivative of the equations of motion with respect to the state vector. Equation ( 3.8 ), below, shows the equations of motion for the six-element state vector.

$$\dot{\mathbf{X}} = \begin{bmatrix} V_x \\ V_y \\ V_z \\ -\frac{x}{r^3} \left[ 1 + \frac{3 J_2}{2 r^2} \left( 1 - 5 \frac{z^2}{r^2} \right) \right] \\ -\frac{y}{r^3} \left[ 1 + \frac{3 J_2}{2 r^2} \left( 1 - 5 \frac{z^2}{r^2} \right) \right] \\ -\frac{z}{r^3} \left[ 1 + \frac{3 J_2}{2 r^2} \left( 3 - 5 \frac{z^2}{r^2} \right) \right] \end{bmatrix} \quad (3.8)$$

where *x*, *y* and *z* are the three components of the position vector,  $V_x$ ,  $V_y$  and  $V_z$  are the three components of the velocity vector and *r* is the magnitude of the position vector.

Differentiating equation ( 3.8 ) with respect to the state vector yields the following 36 components. Three of the three-by-three submatrices are trivial. The remaining nine elements will now be determined individually.

$$\frac{\partial \dot{\mathbf{X}}}{\partial \mathbf{X}} = \begin{bmatrix} 0 & 0 & 0 & 1 & 0 & 0 \\ 0 & 0 & 0 & 0 & 1 & 0 \\ 0 & 0 & 0 & 0 & 0 & 1 \\ \frac{\partial \dot{X}_4}{\partial X_1} & \frac{\partial \dot{X}_4}{\partial X_2} & \frac{\partial \dot{X}_4}{\partial X_3} & 0 & 0 & 0 \\ \frac{\partial \dot{X}_5}{\partial X_1} & \frac{\partial \dot{X}_5}{\partial X_2} & \frac{\partial \dot{X}_5}{\partial X_3} & 0 & 0 & 0 \\ \frac{\partial \dot{X}_6}{\partial X_1} & \frac{\partial \dot{X}_6}{\partial X_2} & \frac{\partial \dot{X}_6}{\partial X_3} & 0 & 0 & 0 \end{bmatrix} \quad (\text{E.1})$$

As in previous developments, application of the chain rule allows a simpler development as well as easier computer coding.

$$\frac{\partial \dot{X}_4}{\partial X_1} = 3 \frac{x^2}{r^5} - \frac{1}{r^3} - \frac{3 J_2}{2 r^5} \left[ 1 + 35 \frac{x^2 z^2}{r^4} - 5 \frac{x^2 + z^2}{r^2} \right] \quad (\text{E.2})$$

$$\frac{\partial \dot{X}_4}{\partial X_2} = 3 \frac{xy}{r^5} + \frac{15 J_2}{2} \frac{xy}{r^7} \left[ 1 - 7 \frac{z^2}{r} \right]$$

$$\frac{\partial \dot{X}_4}{\partial X_3} = 3 \frac{xz}{r^5} + J_2 \frac{xz}{r^7} \left[ 15 + \frac{15}{2} z - \frac{105}{2} \frac{z^2}{r^2} \right]$$

$$\frac{\partial \dot{X}_5}{\partial X_1} = 3 \frac{xy}{r^5} + \frac{15 J_2}{2} \frac{xy}{r^7} \left[ 1 - 7 \frac{z^2}{r} \right]$$

$$\frac{\partial \dot{X}_5}{\partial X_2} = 3 \frac{y^2}{r^5} - \frac{1}{r^3} - \frac{3 J_2}{2 r^5} \left[ 1 + 35 \frac{y^2 z^2}{r^4} - 5 \frac{y^2 + z^2}{r^2} \right]$$

$$\frac{\partial \dot{X}_5}{\partial X_3} = 3 \frac{yz}{r^5} + J_2 \frac{yz}{r^7} \left[ 15 + \frac{15}{2} z - \frac{105}{2} \frac{z^2}{r^2} \right]$$



$$\frac{\partial \dot{X}_6}{\partial X_1} = 3 \frac{xz}{r^5} + \frac{15 J_2}{2} \frac{xz}{r^7} \left[ 1 - 7 \frac{z^2}{r} \right]$$

$$\frac{\partial \dot{X}_6}{\partial X_2} = 3 \frac{yz}{r^5} + \frac{15 J_2}{2} \frac{yz}{r^7} \left[ 1 - 7 \frac{z^2}{r} \right]$$

$$\frac{\partial \dot{X}_6}{\partial X_3} = 3 \frac{z^2}{r^5} - \frac{1}{r^3} - \frac{3 J_2}{2 r^5} \left[ 3 - 30 \frac{z^2}{r^2} + 35 \frac{z^4}{r^4} \right]$$

Inserting equations ( E.2 ) into equation ( E.3 ) yields the final form of the **A** matrix.

## Appendix F Global Estimate Equations of Variation

This appendix develops the equations describing the 49 elements of the **A** matrix of the equation below. These equations are called the equations of variation.

$$\frac{d}{dt} \Phi(t, t_0) = A(t) \Phi(t, t_0) \quad (4.2)$$

where

$$A(t) = \nabla_x g|_{X_0(t)}$$

and **g** comes from the equations of motion of the state vector,

$$\frac{d}{dt} X = g(X, t)$$

The 49 element form of the **A** matrix is used for the Global Estimate and Bayes Filter dynamics models. Therefore, the dynamics include air drag and the state vector includes the ballistic coefficient parameter.

$$X(7) \equiv B^*/2 \quad (5.6)$$

The **A** matrix is defined as the partial derivative of the equations of motion with respect to the state vector. Equation ( F.1 ), below, shows the equations of motion for the seven-element state vector.

$$\dot{X} = \begin{bmatrix} V_x \\ V_y \\ V_z \\ A_{gx} + A_{dx} \\ A_{gy} + A_{dy} \\ A_{gz} + A_{dz} \\ 0 \end{bmatrix} \quad (F.1)$$

where  $V_x$ ,  $V_y$  and  $V_z$  are the three components of the velocity vector,  $A_g$  is the acceleration due to gravity given by equation ( F.2 ) and  $A_d$  is the acceleration due to air drag obtained from equation ( 5.5 ) and given in component form by equation ( F.3 ).

$$\dot{\mathbf{X}}_g = \begin{bmatrix} V_x \\ V_y \\ V_z \\ -\frac{x}{r^3} \left[ 1 + \frac{3}{2} \frac{J_2}{r^2} \left( 1 - 5 \frac{z^2}{r^2} \right) \right] \\ -\frac{y}{r^3} \left[ 1 + \frac{3}{2} \frac{J_2}{r^2} \left( 1 - 5 \frac{z^2}{r^2} \right) \right] \\ -\frac{z}{r^3} \left[ 1 + \frac{3}{2} \frac{J_2}{r^2} \left( 3 - 5 \frac{z^2}{r^2} \right) \right] \\ 0 \end{bmatrix} \quad (\text{F.2})$$

where  $x$ ,  $y$  and  $z$  are the three components of the position vector and  $r$  is the magnitude of the position vector.

$$\dot{\mathbf{X}}_d = \begin{bmatrix} 0 \\ 0 \\ 0 \\ \frac{-\frac{1}{2} B^* \rho (V_x - \omega_{\oplus} y)}{\sqrt{(V_x - \omega_{\oplus} y)^2 + (V_y + \omega_{\oplus} x)^2 + V_z^2}} \\ \frac{-\frac{1}{2} B^* \rho (V_y + \omega_{\oplus} x)}{\sqrt{(V_x - \omega_{\oplus} y)^2 + (V_y + \omega_{\oplus} x)^2 + V_z^2}} \\ \frac{-\frac{1}{2} B^* \rho V_z}{\sqrt{(V_x - \omega_{\oplus} y)^2 + (V_y + \omega_{\oplus} x)^2 + V_z^2}} \\ 0 \end{bmatrix} \quad (\text{F.3})$$

where  $\omega_{\oplus} = 0.05883359980154919 \text{ rad/TU}$  [22] and the local atmospheric density is determined

using the atmospheric model described in Appendix A.

The **A** matrix is formed from the partial derivative of equation ( F.1 ) with respect to the seven-component state vector.

$$\frac{\partial \dot{\mathbf{X}}}{\partial \mathbf{X}} = \begin{bmatrix} 0 & 0 & 0 & 1 & 0 & 0 & 0 \\ 0 & 0 & 0 & 0 & 1 & 0 & 0 \\ 0 & 0 & 0 & 0 & 0 & 1 & 0 \\ \frac{\partial \dot{X}_4}{\partial X_1} & \frac{\partial \dot{X}_4}{\partial X_2} & \frac{\partial \dot{X}_4}{\partial X_3} & \frac{\partial \dot{X}_4}{\partial X_4} & \frac{\partial \dot{X}_4}{\partial X_5} & \frac{\partial \dot{X}_4}{\partial X_6} & \frac{\partial \dot{X}_4}{\partial X_7} \\ \frac{\partial \dot{X}_5}{\partial X_1} & \frac{\partial \dot{X}_5}{\partial X_2} & \frac{\partial \dot{X}_5}{\partial X_3} & \frac{\partial \dot{X}_5}{\partial X_4} & \frac{\partial \dot{X}_5}{\partial X_5} & \frac{\partial \dot{X}_5}{\partial X_6} & \frac{\partial \dot{X}_5}{\partial X_7} \\ \frac{\partial \dot{X}_6}{\partial X_1} & \frac{\partial \dot{X}_6}{\partial X_2} & \frac{\partial \dot{X}_6}{\partial X_3} & \frac{\partial \dot{X}_6}{\partial X_4} & \frac{\partial \dot{X}_6}{\partial X_5} & \frac{\partial \dot{X}_6}{\partial X_6} & \frac{\partial \dot{X}_6}{\partial X_7} \\ 0 & 0 & 0 & 0 & 0 & 0 & 0 \end{bmatrix} \quad (\text{F.4})$$

Of the 49 elements, 28 are trivial. The remaining 21 will now be determined. As in previous instances, use of the chain rule will simplify the notation. Also, the partial derivatives of the acceleration terms due to gravity were determined in Appendix E as equations ( E.2 ). Only the partial derivatives of the acceleration terms due to air drag will be developed here.

$$\begin{aligned} \frac{\partial \dot{X}_{4d}}{\partial X_1} &= -\frac{1}{2} B^* (V_x - \omega_\oplus y) \frac{\partial \rho}{\partial x} \left[ (V_x - \omega_\oplus y)^2 + (V_y + \omega_\oplus x)^2 + V_z^2 \right]^{1/2} \\ &\quad - \frac{1}{2} B^* (V_x - \omega_\oplus y) \frac{\omega_\oplus \rho (V_y + \omega_\oplus x)}{\left[ (V_x - \omega_\oplus y)^2 + (V_y + \omega_\oplus x)^2 + V_z^2 \right]^{1/2}} \end{aligned} \quad (\text{F.5})$$

$$\begin{aligned} \frac{\partial \dot{X}_{4d}}{\partial X_2} &= -\frac{1}{2} B^* \frac{\partial \rho}{\partial x} (V_x - \omega_\oplus y) \left[ (V_x - \omega_\oplus y)^2 + (V_y + \omega_\oplus x)^2 + V_z^2 \right]^{1/2} \\ &\quad + \frac{1}{2} B^* \rho \frac{\omega_\oplus [1 + (V_x - \omega_\oplus y)^2]}{\left[ (V_x - \omega_\oplus y)^2 + (V_y + \omega_\oplus x)^2 + V_z^2 \right]^{1/2}} \end{aligned}$$

$$\frac{\partial \dot{X}_{4d}}{\partial X_3} = -\frac{1}{2} B^* \frac{\partial \rho}{\partial z} (V_x - \omega_\oplus y) \left[ (V_x - \omega_\oplus y)^2 + (V_y + \omega_\oplus x)^2 + V_z^2 \right]^{1/2}$$

$$\frac{\partial \dot{X}_{4d}}{\partial X_4} = -\frac{1}{2} B^* \rho \left[ (V_x - \omega_{\oplus} y)^2 + (V_y + \omega_{\oplus} x)^2 + V_z^2 \right]^{\frac{1}{2}}$$

$$- \frac{1}{2} B^* \rho \frac{(V_x - \omega_{\oplus} y)^2}{\left[ (V_x - \omega_{\oplus} y)^2 + (V_y + \omega_{\oplus} x)^2 + V_z^2 \right]^{\frac{1}{2}}}$$

$$\frac{\partial \dot{X}_{4d}}{\partial X_5} = -\frac{1}{2} B^* \rho \left\{ \frac{(V_x - \omega_{\oplus} y)(V_y + \omega_{\oplus} x)}{\left[ (V_x - \omega_{\oplus} y)^2 + (V_y + \omega_{\oplus} x)^2 + V_z^2 \right]^{\frac{1}{2}}} \right\}$$

$$\frac{\partial \dot{X}_{4d}}{\partial X_6} = -\frac{1}{2} B^* \rho \left\{ \frac{V_z (V_x - \omega_{\oplus} y)}{\left[ (V_x - \omega_{\oplus} y)^2 + (V_y + \omega_{\oplus} x)^2 + V_z^2 \right]^{\frac{1}{2}}} \right\}$$

$$\frac{\partial \dot{X}_{4d}}{\partial X_7} = -\frac{1}{2} \rho \left\{ \frac{(V_x - \omega_{\oplus} y)}{\left[ (V_x - \omega_{\oplus} y)^2 + (V_y + \omega_{\oplus} x)^2 + V_z^2 \right]^{\frac{1}{2}}} \right\}$$

$$\frac{\partial \dot{X}_{5d}}{\partial X_1} = -\frac{1}{2} B^* \frac{\partial \rho}{\partial y} (V_y + \omega_{\oplus} x) \left[ (V_x - \omega_{\oplus} y)^2 + (V_y + \omega_{\oplus} x)^2 + V_z^2 \right]^{\frac{1}{2}}$$

$$+ \frac{1}{2} B^* \rho \frac{\omega_{\oplus} (V_x - \omega_{\oplus} y)(V_y + \omega_{\oplus} x)}{\left[ (V_x - \omega_{\oplus} y)^2 + (V_y + \omega_{\oplus} x)^2 + V_z^2 \right]^{\frac{1}{2}}}$$

$$\frac{\partial \dot{X}_{5d}}{\partial X_2} = -\frac{1}{2} B^* (V_y + \omega_{\oplus} x) \frac{\partial \rho}{\partial y} \left[ (V_x - \omega_{\oplus} y)^2 + (V_y + \omega_{\oplus} x)^2 + V_z^2 \right]^{\frac{1}{2}}$$

$$+ \frac{1}{2} B^* (V_y + \omega_{\oplus} x) \frac{\omega_{\oplus} \rho (V_x - \omega_{\oplus} y)}{\left[ (V_x - \omega_{\oplus} y)^2 + (V_y + \omega_{\oplus} x)^2 + V_z^2 \right]^{\frac{1}{2}}}$$

$$\frac{\partial \dot{X}_{5d}}{\partial X_3} = -\frac{1}{2} B^* \frac{\partial \rho}{\partial z} (V_y + \omega_{\oplus} x) \left[ (V_x - \omega_{\oplus} y)^2 + (V_y + \omega_{\oplus} x)^2 + V_z^2 \right]^{\frac{1}{2}}$$

$$\frac{\partial \dot{X}_{5d}}{\partial X_4} = -\frac{1}{2} B^* \rho \left\{ \frac{(V_x - \omega_{\oplus} y)(V_y + \omega_{\oplus} x)}{\left[ (V_x - \omega_{\oplus} y)^2 + (V_y + \omega_{\oplus} x)^2 + V_z^2 \right]^{1/2}} \right\}$$

$$\begin{aligned} \frac{\partial \dot{X}_{5d}}{\partial X_5} = & -\frac{1}{2} B^* \rho \left[ (V_x - \omega_{\oplus} y)^2 + (V_y + \omega_{\oplus} x)^2 + V_z^2 \right]^{1/2} \\ & - \frac{1}{2} B^* \rho \frac{(V_y + \omega_{\oplus} x)^2}{\left[ (V_x - \omega_{\oplus} y)^2 + (V_y + \omega_{\oplus} x)^2 + V_z^2 \right]^{1/2}} \end{aligned}$$

$$\frac{\partial \dot{X}_{5d}}{\partial X_6} = -\frac{1}{2} B^* \rho \left\{ \frac{V_z (V_y + \omega_{\oplus} x)}{\left[ (V_x - \omega_{\oplus} y)^2 + (V_y + \omega_{\oplus} x)^2 + V_z^2 \right]^{1/2}} \right\}$$

$$\frac{\partial \dot{X}_{5d}}{\partial X_7} = -\frac{1}{2} B^* \rho \left\{ \frac{(V_y + \omega_{\oplus} x)}{\left[ (V_x - \omega_{\oplus} y)^2 + (V_y + \omega_{\oplus} x)^2 + V_z^2 \right]^{1/2}} \right\}$$

$$\begin{aligned} \frac{\partial \dot{X}_{6d}}{\partial X_1} = & -\frac{1}{2} B^* \frac{\partial \rho}{\partial x} V_z \left[ (V_x - \omega_{\oplus} y)^2 + (V_y + \omega_{\oplus} x)^2 + V_z^2 \right]^{1/2} \\ & - \frac{1}{2} B^* \rho (V_y + \omega_{\oplus} x) \frac{\omega_{\oplus} V_z}{\left[ (V_x - \omega_{\oplus} y)^2 + (V_y + \omega_{\oplus} x)^2 + V_z^2 \right]^{1/2}} \end{aligned}$$

$$\begin{aligned} \frac{\partial \dot{X}_{6d}}{\partial X_2} = & -\frac{1}{2} B^* \frac{\partial \rho}{\partial y} V_z \left[ (V_x - \omega_{\oplus} y)^2 + (V_y + \omega_{\oplus} x)^2 + V_z^2 \right]^{1/2} \\ & + \frac{1}{2} B^* \rho (V_x - \omega_{\oplus} y) \frac{\omega_{\oplus} V_z}{\left[ (V_x - \omega_{\oplus} y)^2 + (V_y + \omega_{\oplus} x)^2 + V_z^2 \right]^{1/2}} \end{aligned}$$

$$\frac{\partial \dot{X}_{6d}}{\partial X_3} = -\frac{1}{2} B^* \frac{\partial \rho}{\partial z} V_z \left[ (V_x - \omega_{\oplus} y)^2 + (V_y + \omega_{\oplus} x)^2 + V_z^2 \right]^{1/2}$$

$$\frac{\partial \dot{X}_{6d}}{\partial X_4} = -\frac{1}{2} B^* \rho \frac{V_z (V_x - \omega_{\oplus} y)}{\left[ (V_x - \omega_{\oplus} y)^2 + (V_y + \omega_{\oplus} x)^2 + V_z^2 \right]^{1/2}}$$

$$\frac{\partial \dot{X}_{6d}}{\partial X_5} = -\frac{1}{2} B^* \rho \frac{V_z (V_y + \omega_{\oplus} x)}{\left[ (V_x - \omega_{\oplus} y)^2 + (V_y + \omega_{\oplus} x)^2 + V_z^2 \right]^{1/2}}$$

$$\begin{aligned} \frac{\partial \dot{X}_{6d}}{\partial X_6} = & -\frac{1}{2} B^* \rho \frac{V_z^2}{\left[ (V_x - \omega_{\oplus} y)^2 + (V_y + \omega_{\oplus} x)^2 + V_z^2 \right]^{1/2}} \\ & -\frac{1}{2} B^* \rho \left[ (V_x - \omega_{\oplus} y)^2 + (V_y + \omega_{\oplus} x)^2 + V_z^2 \right]^{1/2} \end{aligned}$$

$$\frac{\partial \dot{X}_{6d}}{\partial X_7} = -\frac{1}{2} \rho V_z \left[ (V_x - \omega_{\oplus} y)^2 + (V_y + \omega_{\oplus} x)^2 + V_z^2 \right]^{1/2}$$

and

$$\frac{\partial \rho}{\partial x} = \frac{\partial \rho}{\partial r} \frac{\partial r}{\partial x} = \frac{\partial \rho}{\partial r} \frac{x}{r} \quad (F.6)$$

$$\frac{\partial \rho}{\partial y} = \frac{\partial \rho}{\partial r} \frac{\partial r}{\partial y} = \frac{\partial \rho}{\partial r} \frac{y}{r}$$

$$\frac{\partial \rho}{\partial z} = \frac{\partial \rho}{\partial r} \frac{\partial r}{\partial z} = \frac{\partial \rho}{\partial r} \frac{z}{r}$$

The atmospheric model provides the gradient of the atmospheric density for use in equations ( F.6 ).

Inserting equations ( E.2 ), and ( F.5 ) into equation ( F.4 ) yields the final form of the **A** matrix.

## Appendix G Orbital Elements

The following table provides the orbital elements for the satellites used in simulation one and simulations six and after. Note it is given as  $B^*$ , not  $B^*/2$ .

Table G-1 Orbital Elements

	axis (DUs)	ecc	apogee (DUs)	perigee (DUs)	inc (deg)	$\Omega$ (deg)	$\omega$ (deg)	$\nu$ (deg)	$B^*$ $m^2/kg$
1	1.1431	0.0649	1.2173	1.0689	66.6670	337.0477	149.2720	111.0444	0.0871
2	1.1176	0.0207	1.1408	1.0944	71.4925	33.6281	24.0132	299.7730	0.0978
3	1.1189	0.0260	1.1480	1.0898	71.1933	87.8515	239.2868	14.8873	0.1107
4	1.1284	0.0422	1.1760	1.0807	17.9057	84.9663	288.6909	157.0855	0.0326
5	1.1023	0.0207	1.1251	1.0795	52.7924	239.9506	13.1372	186.1254	0.0554
6	1.0882	0.0009	1.0892	1.0872	5.5404	37.6862	69.0430	254.3590	0.0337
7	1.1030	0.0374	1.1443	1.0617	72.2489	41.9233	119.3513	128.8672	0.0365
8	1.0933	0.0134	1.1079	1.0786	4.7114	265.1745	77.5812	201.5614	0.0191
9	1.0744	0.0398	1.1171	1.0316	58.5559	81.1987	224.7762	133.9783	0.0605
10	1.1655	0.0231	1.1925	1.1386	39.7510	148.1973	72.3493	14.8886	0.0613
11	1.1305	0.0028	1.1337	1.1273	10.7826	66.0109	51.2450	88.9736	0.1042
12	1.1594	0.0438	1.2101	1.1086	62.3430	218.0545	30.7839	247.9762	0.1302
13	1.1165	0.0516	1.1740	1.0589	2.9282	282.5804	39.1168	8.1137	0.0096
14	1.0627	0.0243	1.0885	1.0369	33.2378	240.0768	346.7636	65.6831	0.0739
15	1.0948	0.0327	1.1306	1.0590	31.5112	206.3120	204.8270	166.3494	0.0378
16	1.1828	0.0771	1.2740	1.0916	13.0270	353.7673	100.4942	314.4835	0.0052
17	1.1267	0.0061	1.1336	1.1198	8.9446	17.8261	84.0984	153.2555	0.0474
18	1.1697	0.0145	1.1866	1.1528	43.1829	171.8751	20.9602	169.0522	0.0548
19	1.0947	0.0230	1.1199	1.0695	13.8640	14.1571	95.0683	123.6986	0.1150
20	1.1209	0.0667	1.1957	1.0461	50.8408	266.5706	147.4709	289.1914	0.0815
21	1.0681	0.0063	1.0749	1.0614	27.9660	183.5601	311.3900	27.5289	0.0142
22	1.1650	0.0143	1.1816	1.1483	58.1834	287.9121	4.4881	285.3072	0.0339
23	1.0869	0.0315	1.1211	1.0526	27.7908	275.2574	71.9475	57.3137	0.0762
24	1.0769	0.0304	1.1096	1.0442	64.8925	262.4626	214.3987	319.7559	0.0203
25	1.1694	0.0884	1.2728	1.0661	6.1776	102.7449	238.3270	121.0557	0.1074
26	1.0541	0.0112	1.0659	1.0423	16.7671	69.6316	227.7882	84.9530	0.0274
27	1.0708	0.0291	1.1020	1.0397	52.3488	28.1130	204.8310	359.6201	0.0012
28	1.1139	0.0084	1.1233	1.1046	49.0407	222.6593	189.3927	333.3271	0.0698
29	1.0553	0.0165	1.0727	1.0379	4.8674	327.9385	0.3699	216.3699	0.1252
30	1.0844	0.0357	1.1232	1.0457	33.3252	320.9543	184.2456	277.3348	0.0372
31	1.2088	0.0181	1.2306	1.1869	50.9498	301.9593	197.2199	163.3539	0.0789
32	1.1266	0.0175	1.1462	1.1069	11.8503	40.0213	108.4510	277.6716	0.0002
33	1.1065	0.0021	1.1089	1.1042	1.9064	281.0339	268.8070	102.5428	0.0050
34	1.1203	0.0096	1.1310	1.1095	12.8023	297.6429	281.1327	356.7522	0.1513
35	1.1373	0.0056	1.1436	1.1310	7.8831	2.4541	20.7305	242.0845	0.0312
36	1.1360	0.0551	1.1986	1.0735	18.4088	189.6166	344.1614	95.7255	0.1098



37	1.1555	0.0801	1.2479	1.0630	26.7252	1.8692	228.3934	138.8889	0.0736
38	1.0863	0.0478	1.1382	1.0344	7.3939	148.0673	274.4587	36.7271	0.0954
39	1.0781	0.0211	1.1009	1.0554	30.0380	314.0126	264.2481	1.7241	0.0323
40	1.0992	0.0217	1.1231	1.0753	65.3707	31.9341	330.4760	86.7126	0.1797
41	1.1745	0.0087	1.1847	1.1642	8.7431	269.2701	138.8004	72.5979	0.0946
42	1.1206	0.0658	1.1944	1.0469	17.7696	164.5883	2.1040	43.9168	0.0466
43	1.1186	0.0465	1.1706	1.0666	28.7028	75.3733	183.8061	304.7195	0.0772
44	1.0808	0.0220	1.1046	1.0570	37.5336	26.2564	223.7465	107.4421	0.0924
45	1.0904	0.0184	1.1105	1.0704	53.9295	4.1245	12.5513	342.3633	0.0102
46	1.1576	0.0161	1.1762	1.1389	59.6470	131.5987	202.4999	153.0539	0.0972
47	1.0882	0.0254	1.1158	1.0605	24.9452	278.1446	117.9650	168.0659	0.1082
48	1.0660	0.0132	1.0800	1.0520	45.4555	245.8460	190.7447	76.6971	0.0755
49	1.1678	0.0164	1.1870	1.1486	48.6396	27.0271	345.1981	99.4496	0.0828
50	1.0816	0.0232	1.1067	1.0566	8.0752	9.2708	29.5075	195.4267	0.0490
51	1.0739	0.0088	1.0833	1.0645	8.2498	319.9620	165.1917	329.4712	0.1095
52	1.1033	0.0287	1.1350	1.0716	20.9109	320.3864	132.8557	39.8585	0.1393
53	1.0633	0.0101	1.0740	1.0526	55.6062	164.4913	1.1809	121.1371	0.0917
54	1.0537	0.0193	1.0740	1.0334	17.2056	118.1681	250.3306	307.3486	0.1282
55	1.0876	0.0425	1.1338	1.0413	46.6057	112.6308	81.9692	337.5289	0.0069
56	1.1219	0.0335	1.1594	1.0843	4.8253	345.4804	46.4249	337.4609	0.0347
57	1.0431	0.0087	1.0522	1.0340	28.9611	294.7578	332.1956	294.3451	0.0264
58	1.1890	0.0478	1.2459	1.1321	17.0618	233.0833	82.9705	67.1935	0.0322
59	1.1060	0.0189	1.1270	1.0851	3.0777	160.0468	16.7335	264.0200	0.0324
60	1.0662	0.0114	1.0783	1.0541	20.9841	68.3871	272.9238	102.8918	0.0608
61	1.0722	0.0148	1.0881	1.0563	22.8532	331.1518	311.0460	341.9078	0.0829
62	1.0917	0.0190	1.1124	1.0709	0.3572	89.2465	255.6719	18.0779	0.0716
63	1.0828	0.0368	1.1226	1.0430	86.2770	309.6474	148.5171	28.7410	0.0424
64	1.0745	0.0385	1.1158	1.0332	19.5698	51.5868	27.0432	40.7247	0.0544
65	1.1324	0.0307	1.1672	1.0976	17.2969	164.5896	65.3758	356.6559	0.0610
66	1.1055	0.0041	1.1100	1.1010	9.2470	250.9242	160.4322	263.8602	0.0846
67	1.1080	0.0352	1.1471	1.0689	18.5225	124.2972	192.4976	92.1080	0.0304
68	1.0851	0.0196	1.1064	1.0639	7.7002	10.6279	20.4620	243.6264	0.0668
69	1.1215	0.0219	1.1460	1.0969	44.3934	88.7568	19.6555	192.5299	0.0881
70	1.0483	0.0029	1.0514	1.0453	84.9628	327.4103	64.8151	287.5925	0.0527
71	1.1059	0.0584	1.1705	1.0414	5.2258	109.9359	314.6927	330.3650	0.0070
72	1.0887	0.0197	1.1101	1.0672	40.8379	130.7821	22.1982	167.3150	0.1092
73	1.1397	0.0554	1.2028	1.0766	74.6453	291.5189	229.0588	216.6272	0.0184
74	1.0958	0.0353	1.1345	1.0571	51.5872	222.3257	283.4561	189.4006	0.0831
75	1.0872	0.0013	1.0886	1.0857	1.2687	316.0793	305.6106	51.4051	0.1176
76	1.1176	0.0169	1.1364	1.0988	59.8006	339.4066	256.8701	256.4840	0.0417
77	1.1216	0.0044	1.1265	1.1167	32.5231	128.4403	21.6407	258.1910	0.2264
78	1.0888	0.0304	1.1219	1.0557	23.1912	183.7182	20.0149	258.2101	0.0475
79	1.1488	0.0013	1.1504	1.1473	5.1364	87.7743	115.6297	122.2167	0.0595
80	1.1176	0.0682	1.1939	1.0413	41.6074	264.9887	109.2273	310.2476	0.0340
81	1.1327	0.0857	1.2298	1.0356	10.3841	269.9463	19.7305	213.0376	0.1358
82	1.1542	0.0578	1.2209	1.0874	15.5084	95.6579	140.3718	325.3227	0.0914
83	1.0823	0.0062	1.0891	1.0756	23.5461	161.4358	109.3949	120.4272	0.0805
84	1.2027	0.0280	1.2365	1.1690	14.8856	348.5631	169.2374	139.1684	0.0341
85	1.1321	0.0405	1.1780	1.0862	113.9529	91.0082	334.7344	83.4499	0.0507
86	1.0996	0.0521	1.1569	1.0423	1.7771	104.1121	353.4131	284.9476	0.1186

87	1.1935	0.0196	1.2170	1.1701	97.4594	313.1902	165.7496	256.9802	0.0227
88	1.1654	0.0280	1.1980	1.1328	6.5821	131.5619	224.9501	247.3834	0.1049
89	1.1443	0.0086	1.1541	1.1345	41.2712	339.0936	265.4069	135.1790	0.0893
90	1.1262	0.0635	1.1977	1.0546	0.3797	245.2991	71.0157	81.0542	0.1334
91	1.0605	0.0094	1.0705	1.0505	31.2140	243.5936	188.2868	234.3808	0.0128
92	1.1604	0.0163	1.1794	1.1414	117.6851	232.2706	93.7626	96.3177	0.0729
93	1.1436	0.0416	1.1911	1.0960	5.8666	159.5464	344.3954	229.5100	0.1051
94	1.0813	0.0400	1.1245	1.0381	0.0022	287.7002	215.2703	274.8106	0.0567
95	1.1067	0.0056	1.1128	1.1005	43.3079	331.2284	44.8839	110.5314	0.0772
96	1.1224	0.0305	1.1566	1.0882	48.1290	68.4842	281.1379	246.7967	0.0127
97	1.1477	0.0310	1.1833	1.1121	35.7073	29.0210	113.5560	99.7578	0.1674
98	1.2096	0.0141	1.2266	1.1925	0.3966	191.1538	24.4558	64.4541	0.0740
99	1.2029	0.0593	1.2743	1.1315	26.5404	266.6083	168.2728	14.3005	0.0121
100	1.0709	0.0302	1.1032	1.0386	48.1287	171.9883	85.4453	11.5818	0.0297
101	1.0538	0.0179	1.0726	1.0349	25.4310	32.1280	332.4195	299.6122	0.1117
102	1.0958	0.0264	1.1248	1.0668	69.5618	233.7671	332.8418	166.0365	0.0356
103	1.1224	0.0401	1.1674	1.0773	55.6960	10.7290	217.5610	325.4053	0.0025
104	1.1276	0.0522	1.1865	1.0688	49.9591	253.2827	247.4279	231.9581	0.0225
105	1.1308	0.0132	1.1457	1.1158	30.2230	152.4164	332.4541	170.3711	0.0482
106	1.0813	0.0188	1.1016	1.0610	14.8885	358.7862	89.2269	30.9728	0.0812
107	1.0705	0.0218	1.0938	1.0472	94.4547	136.4097	234.4521	275.4491	0.0361
108	1.1690	0.0170	1.1889	1.1491	85.9534	171.6882	2.5731	5.7106	0.0309
109	1.0773	0.0312	1.1109	1.0436	7.2121	135.8179	106.7154	19.2707	0.0852
110	1.1061	0.0226	1.1311	1.0811	44.9844	291.2499	202.7720	328.2264	0.0760
111	1.1008	0.0202	1.1231	1.0785	27.7604	3.8539	271.6153	301.1990	0.0336
112	1.0658	0.0181	1.0851	1.0466	23.4795	109.1038	109.9460	81.7455	0.0473
113	1.0509	0.0091	1.0604	1.0413	19.9907	219.9161	252.3158	15.6640	0.0024
114	1.1181	0.0715	1.1981	1.0381	3.9775	203.7216	86.2010	128.6163	0.0380
115	1.1129	0.0108	1.1250	1.1008	16.3236	109.8051	123.6732	307.9787	0.0854
116	1.1386	0.0420	1.1864	1.0908	7.6532	330.9279	302.8739	68.0330	0.0773
117	1.1625	0.0414	1.2106	1.1144	19.6369	80.9530	241.3757	44.9758	0.0938
118	1.1543	0.0067	1.1620	1.1467	33.6641	113.7110	24.3845	222.7081	0.0328
119	1.1143	0.0209	1.1376	1.0909	26.0423	10.1618	197.8516	52.6628	0.0632
120	1.1883	0.0804	1.2838	1.0928	29.7336	76.5465	294.6183	79.5476	0.0021
121	1.1241	0.0669	1.1993	1.0489	30.5566	183.2412	37.4978	337.3095	0.0475
122	1.1439	0.0179	1.1644	1.1234	43.7917	168.0863	11.5554	148.7476	0.1154
123	1.0756	0.0178	1.0947	1.0565	39.7634	295.2121	302.0341	209.2552	0.0352
124	1.0643	0.0163	1.0817	1.0469	37.6206	9.8719	245.5279	317.5474	0.0331
125	1.1884	0.0073	1.1971	1.1797	7.8551	304.8853	317.6330	60.3832	0.1302
126	1.1594	0.0362	1.2014	1.1174	10.9649	355.4257	235.4727	221.0328	0.0852
127	1.1117	0.0633	1.1820	1.0414	40.0884	84.9259	139.4195	80.9178	0.0004
128	1.0913	0.0424	1.1375	1.0450	9.9399	227.0377	218.5376	306.3062	0.0560
129	1.1089	0.0428	1.1564	1.0615	30.3993	142.7481	194.2115	21.0905	0.0432
130	1.0830	0.0152	1.0994	1.0665	0.7952	161.4174	297.1485	175.1806	0.0056
131	1.0820	0.0025	1.0847	1.0793	11.3451	208.4440	159.4780	284.3170	0.0498
132	1.0904	0.0120	1.1034	1.0773	43.1153	225.4374	9.3584	301.2082	0.0601
133	1.0470	0.0050	1.0523	1.0418	40.8066	45.1834	168.5124	64.1536	0.0816
134	1.1073	0.0564	1.1697	1.0449	10.4973	178.5997	268.3389	185.3928	0.1002
135	1.0500	0.0034	1.0536	1.0465	7.7646	134.0814	165.5075	91.9933	0.1311
136	1.0804	0.0281	1.1108	1.0501	17.5372	345.4011	176.1226	213.4373	0.1087

137	1.0767	0.0325	1.1116	1.0417	19.2767	7.2440	115.7458	323.8298	0.0719
138	1.1204	0.0178	1.1403	1.1004	28.7470	127.7574	177.7323	153.7001	0.1522
139	1.0772	0.0130	1.0911	1.0632	53.3772	40.6621	81.9571	113.2743	0.0147
140	1.0792	0.0402	1.1225	1.0358	34.4667	323.8779	188.2705	166.5462	0.0073
141	1.1556	0.0463	1.2091	1.1021	69.0221	44.4787	349.1894	160.4663	0.0042
142	1.1375	0.0771	1.2252	1.0499	26.6041	213.3517	179.6893	302.2099	0.0181
143	1.1218	0.0433	1.1703	1.0732	31.1144	324.0674	339.4078	314.5260	0.0620
144	1.1148	0.0503	1.1709	1.0587	62.0488	295.2839	167.3200	101.5411	0.0752
145	1.1214	0.0740	1.2044	1.0385	14.6222	302.1037	329.3200	87.0761	0.0853
146	1.1514	0.0051	1.1573	1.1456	19.1171	324.8261	241.6786	266.0280	0.0014
147	1.1995	0.1364	1.3631	1.0359	27.8020	359.2972	273.8327	57.9923	0.0820
148	1.0730	0.0260	1.1009	1.0452	117.4477	324.4337	20.0344	119.8746	0.0120
149	1.0955	0.0325	1.1311	1.0599	41.0274	71.2503	245.6208	123.7110	0.1003
150	1.1219	0.0455	1.1730	1.0708	59.7640	212.5951	17.9462	119.6296	0.0159
151	1.0957	0.0045	1.1006	1.0908	66.8090	92.1386	183.1887	23.8586	0.0210
152	1.1130	0.0262	1.1422	1.0839	31.2500	298.2411	358.5847	84.4356	0.0179
153	1.0723	0.0345	1.1093	1.0353	32.3924	153.8931	335.2301	252.7709	0.1017
154	1.1952	0.0208	1.2200	1.1703	12.8923	269.4326	62.0266	325.0776	0.0153
155	1.0884	0.0295	1.1205	1.0563	23.5829	135.6911	102.9380	200.5870	0.1058
156	1.1125	0.0108	1.1245	1.1005	26.7361	50.7552	205.4316	190.9031	0.1036
157	1.0706	0.0015	1.0723	1.0690	7.4065	126.8404	194.7714	49.4995	0.1044
158	1.1573	0.0102	1.1691	1.1455	11.7577	253.5347	173.3257	206.8456	0.0606
159	1.0969	0.0224	1.1215	1.0723	34.7298	214.8044	101.4008	159.2973	0.0324
160	1.0822	0.0111	1.0942	1.0703	53.7359	278.3727	327.3056	48.3476	0.0270

## Appendix H Bibliography Cross Reference

The following table provides a list of each source from the bibliography, the locations in the thesis where it is referenced, and the particular section or page numbers from which the reference is taken.

Table H-1 Bibliography Cross Reference

1	Bate, Mueller and White	Fundamentals of Astrodynamics 3-2 3-6 3-17 6-6 414 98 98 71
2	Boulet, Dan L.	Methods of Orbit Determination for the Microcomputer 2-1 389 413 451
3	Brouwer and Clemence	Methods of Celestial Mechanics 2-7 210
4	Chapman, Suzann	Space Junk, Air Force Magazine 1-1 7-2 39 39
5	Escobal, Pedro R.	Methods of Orbit Determination second edition 2-1 2-2 3-2 3-11 B-1 B-2 272 188 49 3 49 50 187 50 293
6	Gauss, Carl F.	Theory of the Combination of Observations Least Subject to Errors 2-2 2-2 2-2 5 5 13
7	Gelb, Arthur	Applied Optimal Estimation 2-7 7-2 7-2 E-1 58 3 3 58
8	Herget, Paul	The Computation of Orbits 2-1 40 52
9	Hill and Peterson	Mechanics and Thermodynamics of Propulsion second edition 5-2 474
10	Hughes, Peter C.	Spacecraft Attitude Dynamics 6-22 259

11	Kreyszig, Erwin	Advanced Engineering Mathematics seventh edition 3-2 1040									
12	Mendenhall, William	Introduction to Probability and Statistics third edition 2-5 153									
13	Moulton, Forest Ray	An Introduction to Celestial Mechanics second revised edition 2-2 259									
14	NASA	Space and Planetary Environment Criteria Guidelines 6-22 2-12									
15	Regan and Anandakrishnan	Dynamics of Atmospheric Reentry 5-2    5-4    A-1    A-2    A-2    A-3 24    21    24    29    24    26									
16	Roy, A. E.	Orbital Motion third edition 5-3 324									
17	Shchigolev, B. M.	Mathematical Analysis of Observations 2-2 159									
18	Vallado, David	Methods of Astrodynamics: A Computer Approach 3-18    3-18 2    C-1 C-5 C-6									
19	Wasson, Michael S.	Data Reduction with Least Squares Differential Correction Using Equinoctial Elements 3-4    3-6 23    28									
20	Wiesel, William E.	MECH 731, Modern Methods of Orbit Determination 2-2    2-7    2-7    2-9    2-9    2-9    2-10    2-10    2-11    2-11    4-2 59    25    25    63    63    68    70    70    64    72    32 59                                              33									
21	Wiesel, William E.	Spaceflight Dynamics second edition 5-3 85									
22	World Geodetic Survey 1984	US Geological Survey 3-1    3-1    3-7    3-18    5-3    F-2 [16] viii									

## Bibliography

1. Bate, Roger R., Mueller, Donald D., and White, Jerry E. *Fundamentals of Astrodynamics*. New York: Dover Publications, 1971
2. Boulet, Dan L. *Methods of Orbit Determination for the Microcomputer*. Richmond VA: Willman-Bell, 1991.
3. Brouwer, Dirk and Clemence, Gerald M. *Methods of Celestial Mechanics*. New York: Academic Press, 1961.
4. Chapman, Suzann. "Space Junk," *Air Force Magazine*, November 1996.
5. Escobal, Pedro R. *Methods of Orbit Determination* second edition. New York: John Wiley and Sons, 1965.
6. Gauss, Carl F. *Theoria Combinationis Observationum Erroribus Minimis Obnoxiae* (Theory of the Combination of Observations Least Subject to Errors) translated by G. W. Stewart. Philadelphia: Society for Industrial and Applied Mathematics, 1995.
7. Gelb, Arthur. *Applied Optimal Estimation*. Cambridge: The M.I.T. Press, 1974.
8. Herget, Paul. *The Computation of Orbits*. Published by the author, Cincinnati, 1948.
9. Hill, Philip G. and Peterson, Carl R. *Mechanics and Thermodynamics of Propulsion* second edition. Reading MA: Addison-Wesley Publishing Company, 1992.
10. Hughes, Peter C. *Spacecraft Attitude Dynamics*. New York: John Wiley and Sons, 1986.
11. Kreyszig, Erwin. *Advanced Engineering Mathematics* seventh edition. New York: John Wiley and Sons, 1993.
12. Mendenhall, William. *Introduction to Probability and Statistics* third edition. Belmont, CA: Duxbury Press, Wadsworth Publishing Company, 1971
13. Moulton, Forest Ray. *An Introduction to Celestial Mechanics* second revised edition. New York: Dover Publications, 1970.
14. NASA Technical Memorandum 82478. *Space and Planetary Environment Criteria Guidelines for Use in Space Vehicle Development, 1982 Revision (Volume 1)*. George C. Marshall Space Flight Center, Marshall Space Flight Center, Alabama, 1983.
15. Regan, Frank J. and Anandakrishnan, Satya M. *Dynamics of Atmospheric Reentry*. Washington DC: American Institute of Aeronautics and Astronautics, 1993.
16. Roy, A. E. *Orbital Motion* third edition. Great Britain: J. W. Arrowsmith, 1991.
17. Shchigolev, B. M. *Mathematical Analysis of Observations*. London: Iliffe Books, 1965.
18. Vallado, David. *Methods of Astrodynamics: A Computer Approach*. Department handout, US Air Force Academy, Department of Astronautics, March 1992.

19. Wasson, Michael S. *Data Reduction with Least Squares Differential Correction Using Equinoctial Elements*. MS thesis, AFIT/GA/ENY/92D-15. School of Engineering, Air Force Institute of Technology (AU), Wright-Patterson AFB OH, December 1992 (AAJ-4571).
20. Wiesel, William E., Jr. Class handout distributed in MECH 731, Modern Methods of Orbit Determination. School of Engineering, Air Force Institute of Technology (AU), Wright-Patterson AFB OH, April 1997.
21. Wiesel, William E., Jr. *Spaceflight Dynamics* second edition. New York: The McGraw-Hill Companies, 1997.
22. *World Geodetic Survey 1984*. US Geological Survey. 1984.

## *Vita*

Captain Vince Chioma was born in [REDACTED] He graduated from Cocoa Beach High School in 1987. After attending the Florida Institute of Technology and the New Mexico Military Institute, he graduated from the United States Air Force Academy in 1992 with a Bachelor of Science degree in Astronautical Engineering and Space Operations.

He was assigned to Laughlin Air Force Base and then to Patrick Air Force Base where he worked as a logistics manager and test manager for the United States Nuclear Detonation Detection System User Segment Integrated Product Team. In 1995 and 1996 he planned and conducted the acceptance test of the Ground Nuclear Detonation Detection System Terminal.

In May of 1996 he entered the Graduate School of Engineering of the Air Force Institute of Technology, Wright-Patterson Air Force Base, Ohio.

Permanent Address: [REDACTED]



<b>REPORT DOCUMENTATION PAGE</b>			Form Approved OMB No. 0704-0188	
Public reporting burden for this collection of information is estimated to average 1 hour per response, including the time for reviewing instructions, searching existing data sources, gathering and maintaining the data needed, and completing and reviewing the collection of information. Send comments regarding this burden estimate or any other aspect of this collection of information, including suggestions for reducing this burden, to Washington Headquarters Services, Directorate for Information Operations and Reports, 1215 Jefferson Davis Highway, Suite 1204, Arlington, VA 22202-4302, and to the Office of Management and Budget, Paperwork Reduction Project (0704-0188), Washington, DC 20503.				
1. AGENCY USE ONLY (Leave blank)		2. REPORT DATE December 1997		3. REPORT TYPE AND DATES COVERED Master's Thesis
4. TITLE AND SUBTITLE ORBIT ESTIMATION USING TRACK COMPRESSION AND LEAST SQUARES DIFFERENTIAL CORRECTION			5. FUNDING NUMBERS	
6. AUTHOR(S) Vincent J. Chioma, Captain, USAF				
7. PERFORMING ORGANIZATION NAME(S) AND ADDRESS(ES) Air Force Institute of Technology 2750 P Street WPAFB OH 45433-7765			8. PERFORMING ORGANIZATION REPORT NUMBER AFIT/GA/ENY/97D-1	
9. SPONSORING/MONITORING AGENCY NAME(S) AND ADDRESS(ES) Col Salvatore Alfano Deputy Chief Scientist, Space Command HQ USSPACECOM/AN 250 S. Peterson Rd. Ste. 116 Peterson AFB, CO 80914-3180			10. SPONSORING/MONITORING AGENCY REPORT NUMBER  A	
11. SUPPLEMENTARY NOTES				
12a. DISTRIBUTION / AVAILABILITY STATEMENT  Approved for public release; distribution unlimited			12b. DISTRIBUTION CODE	
13. ABSTRACT (Maximum 200 words) This thesis develops two methods of compressing a track of radar observations of a satellite into a single state vector and associated covariance matrix, and a method of estimating orbits using results from multiple tracks. The track compression uses least squares differential correction to determine a state vector at the central observation time. The resulting state vectors and covariance matrices are then used to estimate the satellite's orbit, also using least squares differential correction. Numerical integration using two-body, $J_2$ and an atmospheric drag model is used to represent the dynamics. This orbit estimation produces a state vector which includes the ballistic coefficient, as well as an associated covariance matrix. Finally, a one-fiftieth scale demonstration of the full AFSPC catalog of satellites and debris is conducted to demonstrate the improvement in accuracy over current practice which results. The truth model includes $J_2$ zonal harmonic effects and an atmospheric drag model. This demonstration shows that the orbits of 90% of the entire catalog of objects can be estimated with sufficient accuracy to allow position determination within one kilometer after only two days of tracking. Within four days, most satellite positions are determined within fifty meters.				
14. SUBJECT TERMS Orbit Determination, Least Squares, Maximum Likelihood Estimation Artificial Satellites, Trajectories, Track Compression			15. NUMBER OF PAGES 153	
			16. PRICE CODE	
17. SECURITY CLASSIFICATION Unclassified	18. SECURITY CLASSIFICATION Unclassified	19. SECURITY CLASSIFICATION Unclassified	20. LIMITATION OF ABSTRACT UL	